Fall 2008

Design of atmospheric pressure plasma CVD process for deposition of silicon nitride thin films using dielectric barrier discharge

Shunfu Hu
University of New Hampshire, Durham

DESIGN OF ATMOSPHERIC PRESSURE PLASMA CVD PROCESS FOR DEPOSITION OF SILICON NITRIDE THIN FILMS USING DIELECTRIC BARRIER DISCHARGE

BY

SHUNFU HU

University of New Hampshire, 2007

THESIS

Master of Science

in

Materials Science

September, 2008

This thesis has been examined and approved.

Carmela Amato-Wierda

Thesis Director

Carmela Amato-Wierda,

Professor of Material Science

Olof Echt,

Professor of Physics

James Krzanowski,

Professor of Mechanical Engineering

ACKNOWLEDGEMENTS

I would like to thank GT Solar, Inc. and the New Hampshire Industrial Research Center (NHIRC) for their financial support. I owe a debt of gratitude to many other people for making this possible. Especially thanks to Dr. Carmela Amato-Wierda.

TABLE OF CONTENTS

ACKNOWLEDGEMENTS iii
LIST OF TABLES iv
LIST OF FIGURES vii
ABSTRACT xii

CHAPTER **PAGE**

CHAPTER I 1
INTRODUCTION 1
Solar Cell Industry 1
LITERATURE REVIEW 2
Solar Cell 2
P-N Junction 3
Single Crystal Silicon 4
Mechanism of Solar Cell 4
Anti-Reflection Layer 5
CHAPTER II 10
LITERATURE REVIEW 10
Properties of Silicon Nitride 10
Chemical Vapor Deposition Approach of Silicon Nitride Films 12
Thermal Chemical Vapor Deposition of Silicon Nitride 14
Plasma Enhanced CVD Deposition for Silicon Nitride 15
Chemistry of PECVD Silicon Nitride 16
PLASMA THEORY 19
Plasma Physics 19
Glow Discharge 20
Dielectric Barrier Discharge 21
APPLICATIONS OF DIELECTRIC BARRIER DISCHARGE 23
Ozone Generation 23
Dielectric Barrier Discharge Excimer Lamps 24

Surface Treatment 25
Thin Film Deposition 26

CHAPTER III 28

EXPERIMENT METHODS 28

Apparatus 29
Gas Delivery 29
Exhaust 32
Electrical Power 32
Plasma Power Measurement 34

MATERIALS 37

Substrates 37
Process Precursors 37
Silane Safety 37
Dielectric Barrier Materials 38
Reactor Chamber Configuration 39

PROCEDURES 39

Sample Preparation 39
Reactor Preparation 40
Film Deposition Runs 40

THIN FILM ANALYSIS 42

Analysis of Deposited Thin Films 42
X-Ray Photoelectron Spectroscopy 43
Fourier Transform Infrared Spectroscopy 43

CHAPTER IV 46

RESULTS AND DISCUSSION 46

Film Composition as a Function of Temperature 46
Film Composition as a Function of Residence Time 59
Film Composition as a Function of Argon dilution 65
Film Composition as a Function of Stoichiometry 70
Film Composition as a Function of Frequency 80
Film Composition as a Function of Nitrogen Precursor 89
Film Composition as a Function of Varied H_2 Flow Rate with SiH_4/Ar AndAmmonia 96
Composition as a Function of Constant H_2 Flow Rate with Varied SiH_4/Ar and Ammonia Ratios Film 111

CHAPTER V 117

CONCLUSION 117

Film Composition as a Function of Temperature 117
Film Composition as a Function of Residence Time..... 118
Film Composition as a Function of Argon dilution 119
Film Composition as a Function of Stoichiometry..... 120
Film Composition as a Function of Frequency..... 121
Film Composition as a Function of Nitrogen Precursor 123
Film Composition as a Function of Varied H_2 Flow Rate with SiH_4/Ar And Ammonia 124

LITERATURE CITED..... 126

LIST OF TABLES

Table Page

Table 1. Properties of Bulk Silicon Nitride 11
Table 2. DBD Deposited Silicon Nitride Characteristic FTIR Peaks 45
Table 3. Deposition Parameters in the Film Composition as a Function of Temperature 46
Table 4. Constant Film Composition and Onset of Constant Composition as a Function of Temperature 51
Table 5. Constant Film Composition and Onset of Constant Composition as a Function of Total Flow Rate 61
Table 6. Conditions of Film Composition as a Function of Argon Dilution .. 65
Table 7. Constant Film Composition and Onset of Constant Composition in Film Composition as a Function of Argon Dilution Series 69
Table 8. Conditions of Film Composition as a Function of Stoichiometry ... 71
Table 9. Constant Film Composition and Onset of Constant Composition in Film Composition as a Function of Stoichiometry series 76
Table 10. Parameters of Film Composition as a Function of Frequency 81
Table 11. Constant Film Composition and Onset of Constant Composition of Films in Film Composition as a Function of Frequency Series 88
Table 12. Parameters of Film Composition as a Function of Nitrogen Precursor 89
Table 13. Constant Film Composition and Onset of Constant Composition as a Function of Ratio of N_2:SiH_4 96
Table 14. Parameters of Gas Precursors in the Film Composition as a Function of Varied H_2 Flow Rate with SiH_4/Ar And Ammonia 97
Table 15. Constant Film Composition and Onset of Constant Composition of Films in Film Composition as a Function of Varied H2 Flow Rate with SiH4/Ar and Ammonia 110
Table 16. Parameters of Precursors in Film Composition as a Function of Varied H_2 Flow Rate with SiH_4/Ar And Nitrogen 111
Table 17. Constant Film Composition and Onset of Constant Composition of Films in Constant H2 Flow Rate with Varied Silane/Argon and Ammonia Ratios Series 116

LIST OF FIGURES

Figure Page

Figure 1. Oil Prices, 1994-2006. 2
Figure 2. Typical P-N Junction Solar Cell. 4
Figure 3. High Efficiency Commercial Single Crystal Silicon Solar Cell 5
Figure 4. Antireflection Coatings For Reducing The Intensity of Reflected Light. 6
Figure 5. Silicon Nitride Structure 10
Figure 6. Silicon Nitride Structure. 10
Figure 7. Basic Chemical Vapor Deposition Steps 14
Figure 8. Schematic of Glow Discharge. 21
Figure 9. Principle Configuration of Vd 23
Figure 10. Principle Configuration of Sd 23
Figure 11. First Type of Injector. 30
Figure 12. Second Type of Injector. 30
Figure 13. Schematic of Gas Delivery System. 31
Figure 14. Schematics of Electrical Circuit 33
Figure 15. Diagram of the System Circuit for Plasma Measurement. 35
Figure 16. Typical Voltage and Current Waveforms of Plasma. 36
Figure 17. XPS Spectrum of Surface Survey of Silicon Nitride Film deposited at 300 °C.. 47
Figure 18. Depth Profile of 200 °C Film in Film Composition as a Function of Temperature Series.. 48
Figure 19. Depth Profile of 300 °C Film in Film Composition as a Function of Temperature Series.. 48
Figure 20. Depth Profile of 350 °C Film in Film Composition as a Function of Temperature Series. 49
Figure 21. FTIR Spectrum of Film at 200°C in Film Composition as a Function of Temperature Series 51
Figure 22. FTIR Spectrum of Film at 300°C in Film Composition as a Function of Temperature Series 52
Figure 23. FTIR Spectrum of Film at 350°C in Film Composition as a Function of Temperature Series 52
Figure 24. Si-N, Si-H and N-H Peak Area Versus Substrate Temperature 53
Figure 25. Si-N Peak Frequency Versus Substrate Temperature. 55
Figure 26. Film Deposition Rate (Å/s) Versus Substrate Temperature 56

Figure 27. Sem Picture of Silicon Nitride Film Deposited at 200 °C with Control Condition 57
Figure 28. Sem Picture of Silicon Nitride Film Deposited at 300 °C with Control Condition. 58
Figure 29. Sem Picture of Silicon Nitride Film Deposited at 350 °C with Control Condition 58
Figure 30. The XPS Depth Profile of Deposited Film at 500 sccm total flow rate. 59
Figure 31 The XPS Depth Profile of Deposited Film at 1000 sccm total flow rate 60
Figure 32. The XPS Depth Profile of Deposited Film at 1500 sccm total flow rate. 60
Figure 33. FTIR Spectrum of Film at 500 Sccm Total Flow Rate in Film Composition as a Function of Residence Time Series. 62
Figure 34. FTIR Spectrum of Film at 1000 Sccm Total Flow Rate in Film Composition as a Function of Residence Time Series. 62
Figure 35. FTIR Spectrum of Film at 1500 Sccm Total Flow Rate in Film Composition as a Function of Residence Time Series. 63
Figure 36. Peak Ratio Versus Residence Times of Control Condition. 63
Figure 37. Deposition Rate (Å/s) Versus Times of Control Condition Residence Time. 64
Figure 38. Depth Profile of Film Composition as a Function of Argon Dilution Argon=0 Sccm. 66
Figure 39. Depth Profile of Film Composition as a Function of Argon Dilution Argon=200 Sccm 66
Figure40. Depth Profile of Film Composition as a Function of Argon Dilution Argon=400 Sccm 67
Figure 41. Depth Profile of Film Composition as a Function of Argon Dilution Argon=800 Sccm 67
Figure 42. Depth Profile of Film Composition as a Function of Argon Dilution Argon=1000 Sccm. 68
Figure 43. Deposition Rate (Å) Versus Argon Flow Rate (Sccm). 70
Figure 44. Depth Profile of Film Composition as a Function of Stoichiometry with NH_3 Flow Rate= 50 sccm 72
Figure 45. Depth Profile of Film Composition as a Function of Stoichiometry with NH_3 Flow Rate= 100 sccm 72
Figure 46. Depth Profile of Film Composition as a Function of Stoichiometry with NH_3 Flow Rate= 200 sccm 73
Figure 47. Depth Profile of Film Composition as a Function of Stoichiometry with NH_3 Flow Rate= 400 Sccm. 73
Figure 48. Depth Profile of Film Composition as a Function of Stoichiometry with NH_3 Flow Rate= 600 sccm 74
Figure 49. Deposition Rate of Film Composition as a Function of Stoichiometry. 76

Figure 50. FTIR Spectrum of Film with 50 sccm of NH_3 Flow Rate in Film Composition as a Function of Stoichiometry Series 77
Figure 51. FTIR Spectrum of Film with 100 sccm of NH_3 Flow Rate in Film Composition as a Function of Stoichiometry Series 78
Figure 52. FTIR Spectrum of Film with 200 sccm of NH_3 Flow Rate in Film Composition as a Function of Stoichiometry Series 78
Figure 53. FTIR Spectrum of Film with 400 sccm of NH_3 Flow Rate in Film Composition as a Function of Stoichiometry Series 79
Figure 54. FTIR Spectrum of Film with 600 sccm of NH_3 Flow Rate in Film Composition as a Function of Stoichiometry Series 79
Figure 55. The Si-H and N-H (S) to Si-N Peak Area Ratio 80
Figure 56. Deposition Rate Versus The Frequency 82
Figure 57. FTIR Spectrum of Film at 1K Hz Frequency in Film Composition as a Function of Frequency Series 83
Figure 58. FTIR Spectrum of Film at 1.5K Hz Frequency in Film Composition as a Function of Frequency Series 84
Figure 59. FTIR Spectrum of Film at 2K Hz Frequency in Film Composition as a Function of Frequency Series 84
Figure 60. FTIR Spectrum of Film at 3K Hz Frequency in Film Composition as a Function of Frequency Series 85
Figure 61. FTIR Peak Ratios of Film Composition as a Function of Frequency 85
Figure 62. Xps Depth Profile of Film Composition as a Function of Frequency at Frequency 1 k Hz 86
Figure 63. Xps Depth Profile of Film Composition as a Function of Frequency at Frequency 1.5k Hz 87
Figure 64. Xps Depth Profile of Film Composition as a Function of Frequency at Frequency 3k Hz. 87
Figure 65. FTIR Absorbance Spectrums with Ammonia And Nitrogen. 90
Figure 66. FTIR Spectrum of Film with N_2=500 sccm in Film Composition using Nitrogen as Precursor. 91
Figure 67. FTIR Spectrum of Film with N_2=600 sccm in Film Composition using Nitrogen as Precursor. 91
Figure 68. FTIR Spectrum of Film with N_2=800 sccm in Film Composition using Nitrogen as Precursor. 92
Figure 69. FTIR Si-H/Si-N Peak Ratio of Film Composition as a Function of Nitrogen Precursor. 92
Figure 70. Film Deposition Rate of Film Composition as a Function of Nitrogen Precursor. 93
Figure 71. Depth Profile of Film Composition as a Function of Nitrogen Precursor With N_2:SiH_4 =50:1. 94
Figure 72. Depth Profile of Film Composition as a Function of Nitrogen Precursor With N_2:SiH_4 =75:1. 94

Figure 73. Depth Profile of Film Composition as a Function of Nitrogen Precursor With N_2:SiH_4 =200:1. 95
Figure 74. FTIR Spectrums With Utility of Silane/Argon And Silane/Hydrogen 98
Figure 75. FTIR Spectrum of Film at H_2=0 sccm in Film Composition with Varied H_2 Flow Rate with SiH_4/Ar and Ammonia 99
Figure 76. FTIR Spectrum of Film at H_2=15 sccm in Film Composition with Varied H_2 Flow Rate with SiH_4/Ar and Ammonia 100
Figure 77. FTIR Spectrum of Film at H_2=50 sccm in Film Composition with Varied H_2 Flow Rate with SiH_4/Ar and Ammonia 100
Figure 78. FTIR Spectrum of Film at H_2=100 sccm in Film Composition with Varied H_2 Flow Rate with SiH_4/Ar and Ammonia 101
Figure 79. FTIR Spectrum of Film at H_2=200 sccm in Film Composition with Varied H_2 Flow Rate with SiH_4/Ar and Ammonia 101
Figure 80. FTIR Spectrum of Film at H_2=300 sccm in Film Composition with Varied H_2 Flow Rate with SiH_4/Ar and Ammonia 102
Figure 81. FTIR Spectrum of Film at H_2=700 sccm in Film Composition with Varied H_2 Flow Rate with SiH_4/Ar and Ammonia 102
Figure 82. FTIR Spectrum Peak Ratio Of Film Composition as a Function of Varied H_2 Flow Rate with SiH_4/Ar and Ammonia 103
Figure 83. Deposition Rate of Film Composition as a Function of Varied H2 Flow Rate with SiH_4/Ar and Ammonia. 104
Figure 84. Xps Depth Profile of Film Composition as a Function of Varied H_2 Flow Rate with SiH_4/Ar and Ammonia with H_2=0 sccm. 105
Figure 85. Xps Depth Profile of Film Composition as a Function of Varied H_2 Flow Rate with SiH_4/Ar and Ammonia with H_2=15 sccm. 106
Figure86. Xps Depth Profile of Film Composition as a Function of Varied H_2 Flow Rate with SiH_4/Ar and Ammonia with H_2=50 sccm. 106
Figure 87. Xps Depth Profile of Film Composition as a Function of Varied H_2 Flow Rate with SiH_4/Ar and Ammonia with H_2=100 sccm. 107
Figure 88. Xps Depth Profile of Film Composition as a Function of Varied H_2 Flow Rate with SiH_4/Ar and Ammonia with H_2=200 sccm. 107
Figure 89. Xps Depth Profile of Film Composition as a Function of Varied H_2 Flow Rate with SiH_4/Ar and Ammonia with H_2=300 sccm. 108
Figure 90. Xps Depth Profile with Ratio of Silane to Ammonia=1:5. 112
Figure 91. Xps Depth Profile with Ratio of Silane to Ammonia=1:10. 113
Figure 92. Xps Depth Profile with Ratio of Silane to Ammonia=1:50. 113
Figure 93. Xps Depth Profile with Ratio of Silane to Ammonia=1:75. 114
Figure 94. Xps Depth Profile with Ratio of Silane/Argon to Ammonia=1:100 114

ABSTRACT

AN ATMOSPHERIC PRESSURE PLASMA CVD PROCESS FOR DEPOSITION OF SILICON NITRIDE FILMS

BY

SHUNFU HU

University of New Hampshire, September 2008

Amorphous silicon nitride with incorporated hydrogen has been widely used as the anti-reflection coating for solar cells. However, current solar industry processes for silicon nitride are mainly deposited under expensive vacuum environments which are also batch type processes. Silicon nitride deposited in atmospheric pressure plasma is needed to reduce the cost of solar cells.

A dielectric barrier discharge (DBD) can be used to deposit thin films under atmospheric pressure. In this thesis, a new atmospheric pressure plasma deposition system was built and silicon nitride films were deposited on 4 by 4 inches polycrystalline silicon wafers, 3 inches single crystalline silicon wafers and 1 inch KBr windows.

Various series of experiments were conducted to determine the silicon nitride films properties as a function of process parameters. Finally, the silicon nitride films were analyzed by XPS, FTIR, and SEM.

CHAPTER I

Introduction

Solar Cell Industry

People are aware that we are experiencing an energy crisis. Oil prices have increased nearly 8 times from 1999 to 2006 as shown in Figure 1. The price of crude oil was only $10 per barrel in 1999 while it reached $75 per barrel in 2006 [1]. The cost of electricity is going up, and more and more people are considering using solar energy as an alternative. It was reported that the solar industry was around 20 billion dollars in 2006 and it was estimated it might expand to 60 billion dollars by 2010 [2].

However, the challenge for solar energy is to produce lower cost solar electricity. Currently, solar photovoltaic energy is still more expensive than the general electricity people buy from hydropower, nuclear power and so on. The solar electricity price was $3.741 per watt in June 2007 while the general electricity in New Hampshire in June 2007 was only $ 1.395per watt [3, 4]. There are two chief obstacles that prevent the cost of solar energy from decreasing. One is the high cost of the silicon in solar cell. The other one is the need for efficient techniques to make solar panels.

In the current solar cell industry, the silicon nitride films used as the anti-reflection layer for solar panels are primarily produced in vacuum environments which are very expensive and time consuming.

This project was mainly focused on the design of a novel atmospheric pressure plasma CVD process to produce the silicon nitride films.

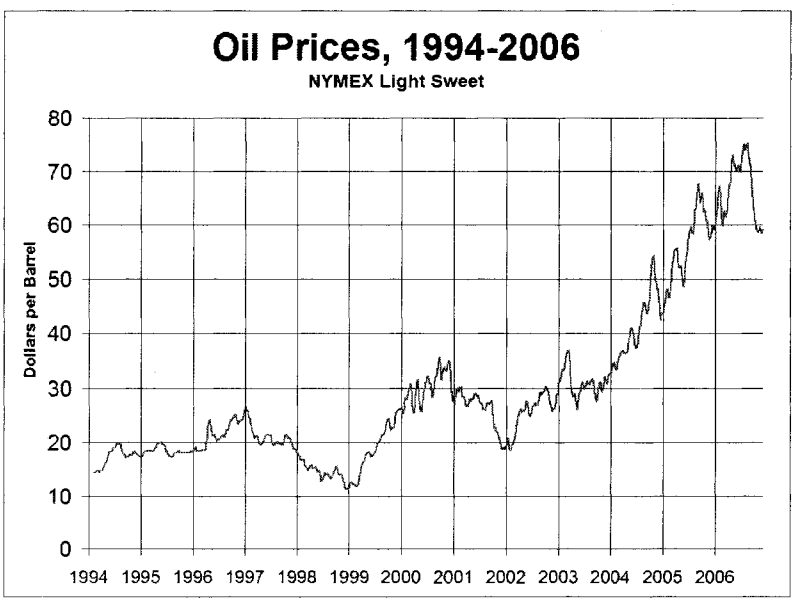

Figure 1. Oil prices, 1994-2006 (from NYMEX) http://jaduncan.net/peak-oil-uk-energy-security-in-the-21st-century.

Literature Review

Solar Cell

A solar cell, also known as photovoltaic cell (PV cell), is a device designed to convert solar sunlight into electricity. Modern solar cells are fundamentally P-N junctions. As shown in Figure 2, holes and electrons are

produced when the sunlight hits the P-N junction, generating electric current.

P-N junction

Pure single crystal silicon is considered to be a poor conductor. Dopants can be added to silicon with very low concentration and they greatly improve the electrical conductivity.

When boron is added to silicon, the boron atoms which have three valance electrons will combine with silicon atoms which have 4 valance electrons. This creates "holes" in the valance band. The holes can be treated as positive charge and randomly move around. The silicon with such dopants as boron is called P-type silicon.

On the other hand, when silicon is doped with atoms which have five valance electrons such as phosphorous, there are "extra" electrons in the valance band. This type of silicon material is called N-type silicon.

At the junction of these two materials, electrons from N-type material will diffuse across the junction and they will combine with the holes in the P-type material. After the diffusion, the area of P-type material close to the junction becomes negatively charged since the electrons are pulled towards it, and the region near the N-type material is positively charged. This region is called depletion region.

Electrons and holes are spontaneously produced when the sun lights hit the surface of the cell. When a potential is applied to the P-N junction, the movement of these holes and electrons leads to electrical current.

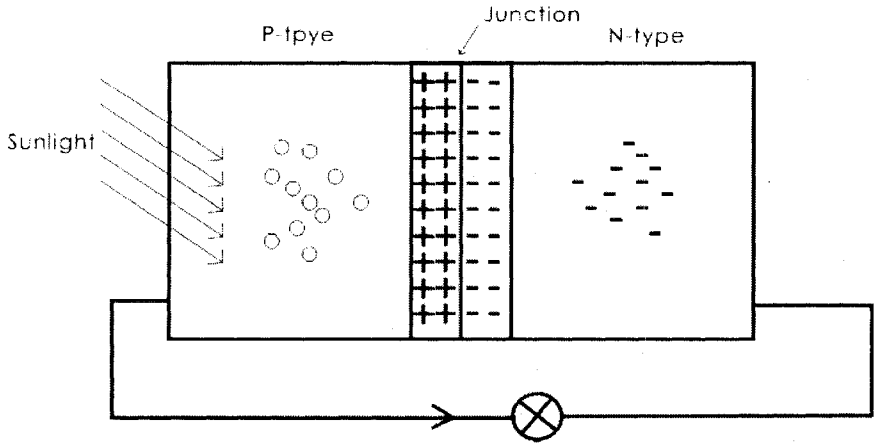

Figure 2. Typical P-N Junction Solar Cell.

Single Crystal Silicon

In the solar industry, silicon is the basic material used for photovoltaic devices. The reason that people use silicon is that it has band gap energy of 1.08 ev [5], corresponding to a wavelength of 1.15×10^3 Å. When photons have an energy greater than 1.08 electron Volts, they will be absorbed and release electrons. Note that, 1 eV is equivalent to a wavelength of 1.15×10^3 Å. So generally speaking, most of the solar spectrum can be converted into electricity.

Mechanism of Solar Cell

As mentioned above, a photovoltaic cell is built by building a thin layer of boron doped silicon together with another layer of phosphorous doped silicon. Electrons are released when sunlight hits the surface of the cell.

Figure 3 shows a schematic silicon solar cell.

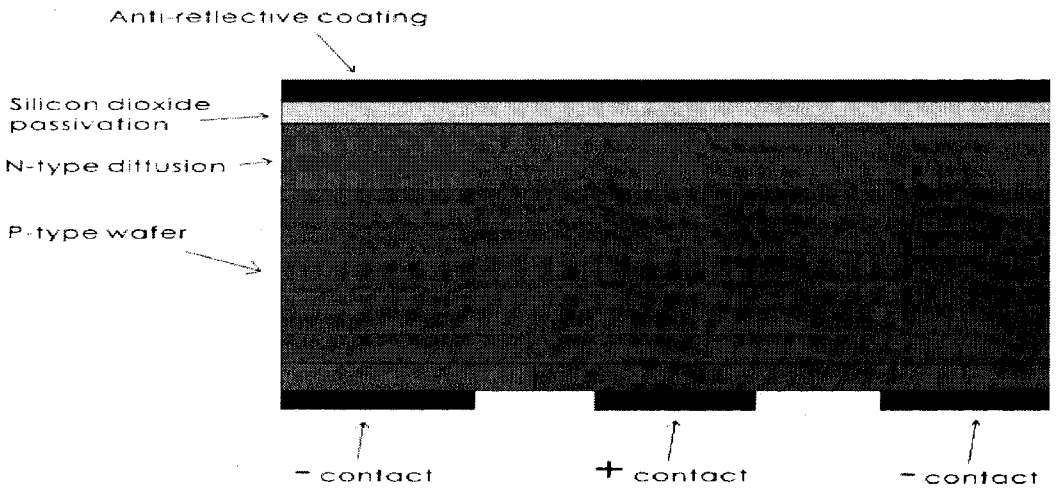

Figure 3. High Efficiency Commercial Single Crystal Silicon Solar Cell.

Anti-Reflection Layer

When the sunlight strikes on the surface of the solar cell, some light is partially reflected back to the atmospheric. The reduction of reflected light could be as high as 10% if the proper anti-reflection layer was chosen [6].

The refractive index of silicon is about 3.5 [7] at wavelengths of 700-800 [7] nm. In equation 1, reflectance R measures the intensity of the

reflected light with respect to the incident light. A simple calculation of the reflectance in air show what percentage of the light is reflected back. The refractive index of air n_{air} is 1, and the refractive index of silicon n_{si} is 3.5.

$$R \text{ (reflectance)} = \left(\frac{n_{air} - n_{si}}{n_{air} + n_{si}}\right)^2 = \left(\frac{1-3.5}{1+3.5}\right)^2 = 0.309 \qquad \textbf{Equation 1}$$

From the result, over 30% of the sun light is reflected back and not available for conversion to solar electricity [7].

Thin film anti-reflection coatings on the top of the solar cell could significantly reduce the loss of sunlight and greatly improve the efficiency of solar energy conversion.

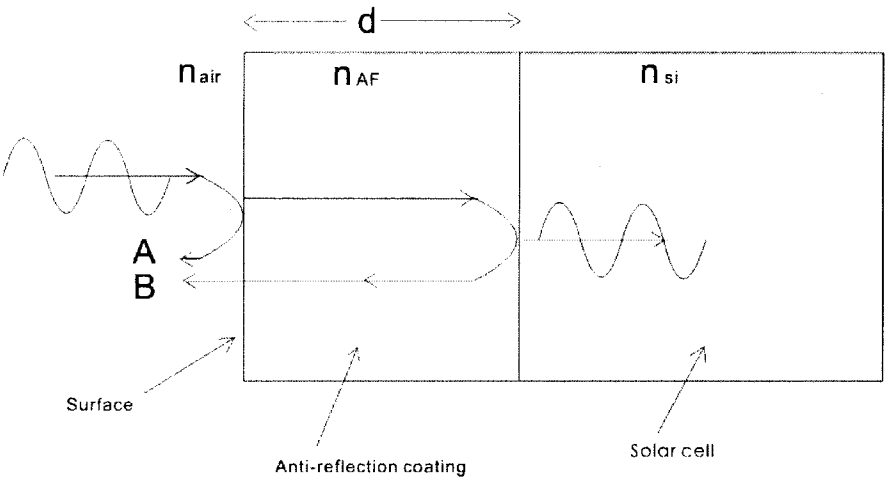

Figure 4. Antireflection Coatings for Reducing the Intensity of reflected light.

In Figure 4, the index of refraction of air is 1, the index of reflection of silicon is 3.5 and index of reflection of anti-reflection layer is 1.9 [7]. When light hits the surface between air and the anti-reflection coating, some of it becomes reflected. In Figure 4, this is reflected wave A. This wave A performs a phase change with 180° due to the reflection. Meanwhile, the wave A also enters the anti-reflection coating and reaches the surface between anti-reflection coating and silicon. Since the refractive index of silicon is greater than that of anti-reflection coating, the wave also becomes partially reflected by this surface. In Figure 4, this is marked as wave B and it also faces a 180° phase change due to the surface reflection. When wave B catches up with wave A, it passes a distance two times the thickness of the anti-reflection coating marked in the diagram as d. So, the phase difference is equivalent to $k_c(2d)$, where k_c is the wave vector in the anti-reflection coating and defined as $\frac{2\pi}{\lambda_c}$, λ_c is the wavelength of light within the anti-reflection coating, and the wavelength of light in the air is λ. According to equation 2, λ_c can be calculated:

$$\lambda_c = \lambda / n_{anti-reflection} \qquad \textbf{Equation 2}$$

The phase difference $\Delta\Phi$ between wave A and wave B can be obtained by equation 3:

$$\Delta\Phi\ (k_C\ (2d)) = (2\pi n_{anti-reflection} / \lambda)(2d). \qquad \textbf{Equation 3}$$

In order to generate destructive interference of waves A and B, the phase difference $\Delta\Phi$ must be π or its odd multiple of $m\pi$.

By the equation 4 below, the thickness (d) can be calculated.

$$d = m(\lambda / 4n_{anti-reflection}) \qquad \textbf{Equation 4}$$

Moreover, the amplitude of the wave A and wave B should be equivalent in order to obtain exact destructive interference. When the reflection coefficient between air and anti-reflection coating is equivalent to the reflection coefficient between anti-reflection coating and silicon, the amplitude of wave A is comparable with wave B.

$$n_{air} / n_{anti-reflection} = n_{anti-reflection} / n_{silicon} \quad \text{Or} \quad n_{anti-reflection} = \sqrt{n_{air} n_{silicon}} \qquad \textbf{Equation 5}$$

So, according to equation 5, when the refractive index of the anti-reflection coating is around $\sqrt{3.5}$ or 1.871, it creates destructive interference.

In solar cells, a thin film coating of dielectric material such as silicon nitride, Si_3N_4, can be used as the anti-reflection layer, since the amorphous silicon nitride has a refractive index about 2.02 [7].

Anti-reflection layer also can be used as to passivate dangling silicon bonds at the surface as well as in the silicon wafers. Hydrogen is incorporated in the anti-reflection layer coatings for this purpose. It was reported that it could increase the efficiency of solar cell panels by passivation of these dangling bonds [6, 8, 9, 10].

CHAPTER II

LITERATURE REVIEW

Properties of Silicon Nitride

Bulk silicon nitride, Si_3N_4, is a hard, dense and refractory material. As shown in Figures 5 and 6, the nitrogen atoms are tetrahedrally placed around the silicon atoms and the nitrogen atoms are surrounded by the silicon atoms at the vertices of a planar triangle.

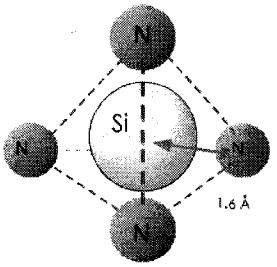

Figure 5. Silicon nitride structure.[7]

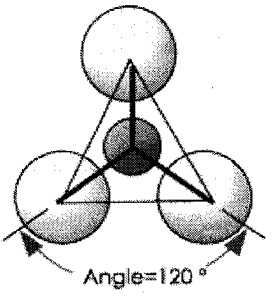

Figure 6. Silicon nitride structure.[7]

Amorphous silicon nitride films are widely used as a barrier material in the semiconductor industry to protect and insulate microelectronic devices [10]. Comparing silicon nitride to other dielectric materials, its advantages include: less susceptibility to diffusion of molecular and ionic impurities such as slow diffusion of hydrogen and other positive Na+, K+ ions, lower permeability to moisture, high electrical resistivity, excellent stability and strong hardness as hard coating [11].

Density	3 - 3.3 gm/cm^3,solid
Molar mass	140.28 g/mol
breakdown field	typically a few 10^6 V/cm
thermal conductivity	0.15 W/cm K (bulk)
Refractive index	around 1.9
dielectric constant	6-8 [depends on stoichiometry]

Table 1. Properties of bulk silicon nitride.

As shown in Table 1, bulk silicon nitride has a density about 3-3.3 gm/cm^3 with molar mass 140.28 g/mol. It has poor thermal conductivity with 0.15 W/cm K (bulk) which is similar to that of ceramic. The dielectric constant is almost 6-8 depending on the stoichiometry of silicon nitride.

Generally, amorphous silicon nitride is produced by CVD. In the CVD process, the precursors used are usually silane and ammonia. So, hydrogen is inevitably part of the silicon nitride. In the amorphous silicon nitride, not all the silicon and nitrogen are positioned in the exact same structure. Many un-attached bonds are present. So, hydrogen atoms will gradually attach to these broken bonds. The coating can contain up to about 20 atomic percentage hydrogen from the conventional plasma process [12].

The stoichiometry of the plasma produced silicon nitride can vary dramatically. This is a very important characteristic of the silicon nitride since it is closely related to the refractive index which is a key issue for solar cell anti-reflection coatings [13]. The refractive index can vary from 1.93-2.08 on the deposition conditions [14].

Chemical Vapor Deposition of Silicon Nitride Films

Chemical vapor deposition (CVD) is the chemical reaction of gas phase precursors to yield a solid deposit. This process involves the growth of a solid material from the gas phase employing a reactive mixture to deliver the active species onto a substrate.

This type of crystal growth process is widely used in the different semiconductor devices and for deposition of various protective coatings. There are various chemical vapor deposition processes such as: atmospheric pressure chemical vapor deposition (APCVD), low pressure chemical vapor deposition (LPCVD), plasma enhanced chemical vapor deposition (PECVD), photochemical vapor deposition (PCVD), and metal organic chemical vapor deposition (MOCVD) .

Chemical vapor deposition has the following advantages for film deposition: It can bring good thickness uniformity across the substrate with easily controlled stoichiometry as well as composition. It can produce films with good purity and density and superior structure perfection. Also, films deposited using CVD have good electronic properties and outstanding adhesion with the substrate.

Chemical vapor deposition includes the following steps as shown in Figure 7:

1, vaporization and transportation of the gaseous precursors into the reactor

2, chemical reactions in the gas phase

3, diffusion of the precursor molecules onto the substrate

4, adsorption of precursor molecules onto the substrate

5, decomposition of precursor onto the substrate and incorporation to the solid phase film and,

6, recombination of molecular byproducts and adsorptions into gas

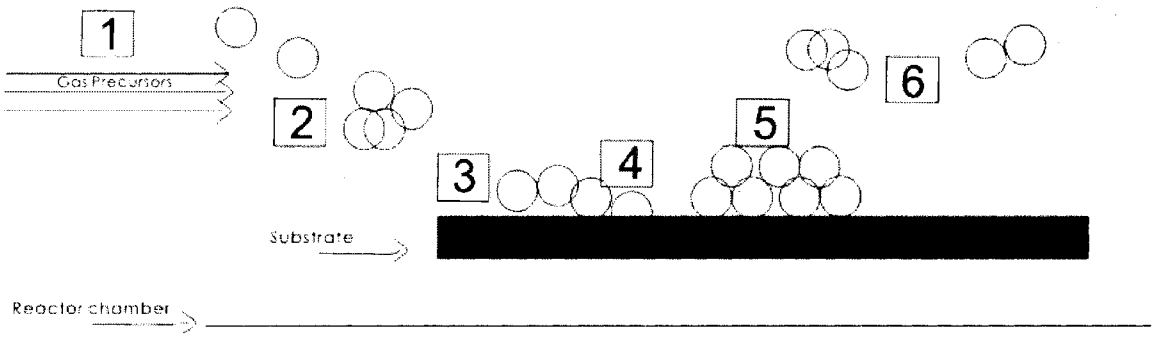

Figure 7. Basic chemical vapor deposition steps.

Thermal Chemical Vapor Deposition of Silicon Nitride

Chemical vapor deposition can be categorized as thermal CVD, laser assisted CVD (LCVD), plasma enhanced CVD (PECVD) and

atmospheric pressure CVD (APCVD) etc. Among these, thermal chemical vapor process is the most common technique broadly utilized [16].

Thermal CVD silicon nitride films are widely used in semiconductor fabrication. It can be employed as the mask for (local oxidation silicon) LOCOS in the MOS/CMOS silicon technology. Deposited silicon nitride can be also used as the barrier to sodium diffusion to protect gate oxides [15].

Thermal chemical vapor silicon nitride can be produced by using a tube reactor under very low pressure, usually below 1 Torr and with high temperatures around 800 Celsius Degree. Precursors include silane SiH_4 or dichlorosilane, $SiCl_2H_2$, and ammonia, NH_3, as the oxidant.

The deposition rates of this process may reach 1.66 Å/s. This throughput is decent and is very practical for the application where batch processing is needed.

Plasma Enhanced CVD Deposition for Silicon Nitride

Plasma enhanced chemical vapor deposition involves the presence of plasma during the film deposition. Thin films are deposited onto the substrate after the gaseous precursors are excited by the plasma and cause the chemical reaction.

The plasma consists of electrically positive and negative particles. During the plasma process, numerous electrons with energy ranges from 1ev to 10ev are generated in the plasma. Gaseous precursors are therefore ionized and decomposed by these energetic electrons into electrons, ions, atoms and molecules in ground and excited states, as well as free radicals. Compared with thermal CVD, plasma CVD can occur at lower temperature. PECVD is an excellent alternative process to deposit thin films at a comparable lower temperature than that of thermal chemical vapor deposition with equivalent film quality.

This approach is primarily used to deposit dielectric films such as silicon nitride, silicon dioxide and amorphous silicon.

Chemistry of PECVD Silicon Nitride

The silicon nitride film deposited under PECVD is usually nonstoichiometric and amorphous. Generally, the film holds a certain amount of hydrogen and has the formula Si_xN_y:H.

There are different precursors for the deposition of silicon nitride films. Silane with ammonia, or silane with nitrogen, and silane balanced with inert gas such as argon or hydrogen can be used.

The silane and ammonia are dissociated by the electrons in the plasma and generate the products shown below:

$$SiH_4 \longrightarrow SiH_2 + H_2$$

$$SiH_4 \longrightarrow SiH + H_2 + H$$

$$SiH_4 \longrightarrow SiH_3 + H$$

$$SiH_4 \longrightarrow Si + 2H_2$$

$$NH_3 \longrightarrow NH_2 + H$$

$$NH_3 \longrightarrow NH + H_2$$

These radical molecules also recombine into Si_2H_6 and N_2H_4:

$$NH + NH_2 \longrightarrow N_2H_4$$

$$SiH_2 + SiH_4 \longrightarrow Si_2H_6$$

The overall reaction can be summarized as below:

$$NH_3 + SiH_4 \longrightarrow Si_xN_y{:}H_z \ _{16}$$

D.Smith has reported in 1993 that radical molecules SiH_2, SiH_3 [19] are dominating the whole gas phase at low power and with small ammonia concentration. Also, the film deposited under this condition is rich with Si-H. With increased plasma power and ratio of NH_3/SiH_4, the triaminosilane ($Si(NH_2)_3$) is produced in the gas phase and the amount of hydrogenated species in the film is greatly reduced. The film mechanism is summarized below.

First, ammonia and silane react in the gas phase and produce tetra-aminosilane and hydrogen in the plasma:

$$4NH_3 + SiH_4 \longrightarrow Si(NH_2)_4 + 4H_2 \ _{16}$$

Second, the $Si(NH_2)_3$ molecules are deposited on the substrate after one amino group is lost.

Finally, these molecules diffuse and condense, generating silicon nitride film plus volatile NH_3.

The amount of hydrogen in this amorphous silicon nitride film and the bonding are essential to quality of the film. The etching rate in the aqueous HF solutions is related with the concentration of the hydrogen concentration. Also, the excess amount of hydrogen in the silicon nitride film where the film is employed as the passivation layer can bring on the electrical instability in MOS (Metal oxide semiconductor) devices [17, 18].

Plasma Theory

Plasma Physics

There are four states of matter: solids, liquids, gases and plasmas. Plasma is known as the fourth state of matter and actually nearly 99% of the visible universe consists of plasmas. Plasmas are primarily ionized gas with charged species, neutrals and fields that cause collective effects. One important characteristic of the plasma is that it carries electrical discharges and creates magnetic fields.

Plasmas can be divided into two categories, equilibrium and non-equilibrium plasmas. In the equilibrium plasmas, the charged species have the same kinetic energy as the neutral species and the kinetic energy is equally distributed in these species. This type of plasma is mainly a high

temperature plasma and the temperature of this plasma is usually beyond 4000K. Equilibrium plasma is also referred as a hot plasma.

Where charged species have much higher kinetic energy than neutral species, a non-equilibrium plasma is created. There is a large difference in energy between charged species and neutral species, and the reason for this is that under the effect of the applied field, the charged species disappear faster by transferring their energy to the neutral species through collisions. This type of plasma usually happens at low pressure and under temperature ranging from 300-2000K. Since non-equilibrium plasma happens at lower temperatures, it is also called a cold plasma.

Glow Discharge

Glow discharge is a basic type of plasma generated by applying a potential between two electrodes. Space between the electrodes is generally filled with inert gas and reactive gas with a pressure from a few mTorr to atmospheric pressure [20]. When a large potential is applied to the electrodes, electrons will be emitted through the cathode and afterward accelerated by the electric field to the anode. These electrons will strike gas atoms or molecules and cause excitation, ionization and dissociation. The excited species will emit light by returning to their ground state and that is why a plasma is always luminous. When the atoms are ionized, they

will release more secondary electrons which can also be accelerated by the electric field and give rise to more collisions [20].

A schematic of a glow discharge is shown below:

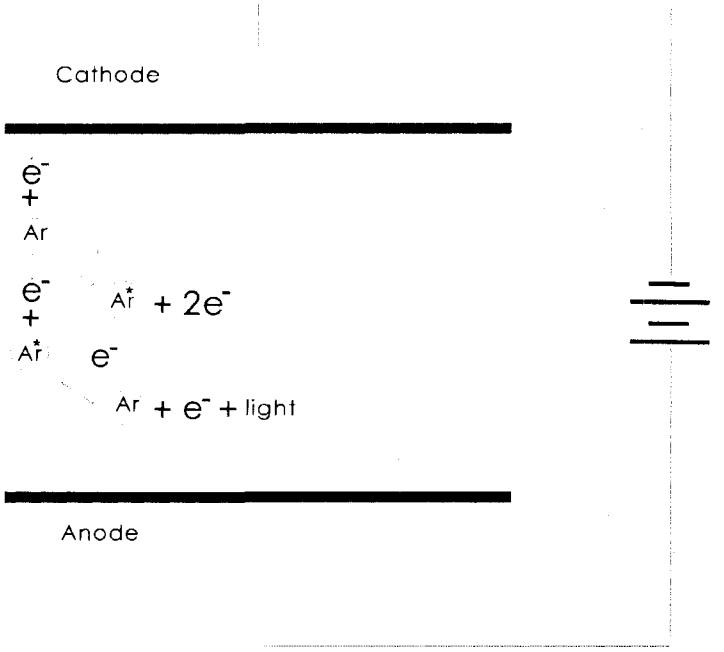

Figure 8. Schematic of glow discharge.

Glow discharge is a very complicated gas mixture with numerous electrons, atoms or molecules, radicals, ions and excited species. Generally speaking, this type of plasma has a large quantity of neutral species. Glow discharge can be further divided into different groups according to the power applied.

Dielectric Barrier Discharge

Dielectric barrier discharge is a type of non-equilibrium plasma which can operate at atmospheric pressure. This type of plasma can be generated by applying an alternating voltage to the electrodes which are covered by a dielectric material (glass, quartz, ceramic or polymers) or both. The gap distance of the two electrodes can vary from 0.1 mm to about several centimeters. This type of silent discharge can be run with an alternating voltage of 1-100kv, and the frequency may range from several Hz to M Hz. After the applied potential reaches the breakdown voltage, the discharge will occur. The dielectric material is very important to this configuration. The reason is that due to the dielectric materials, the current flow between the electrodes is restricted and will not develop into an arc discharge. Consequently, the discharge of filaments with nanosecond duration is homogeneously distributed across the entire electrodes.

There are two typical configurations of dielectric barrier discharge. One configuration is called volume discharge (VD) and the other is surface discharge (SD) [21, 22]. In the design of a volume discharge, two parallel plates are used. The discharge occurs between electrodes and is distributed over the electrode surface. See Figure 9. While in the arrangement of surface discharge, one electrode is covered dielectric material and on the reverse side of the dielectric material is another electrode. See Figure 10.

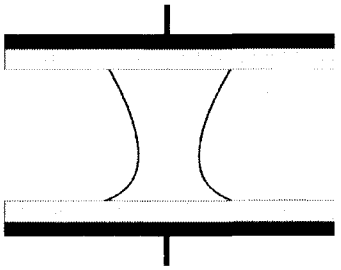

Figure 9. Principle configuration of VD.

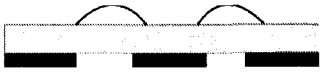

Figure 10. Principle configuration of SD.

In order to achieve a homogeneous plasma, the density of the electrons which remains in the gas before the next new discharge is very essential. And this density is significantly related to the amplitude of electric field. Experiment shows that at least of $10^6 - 10^7$ of electrons/cm^3 is necessary for the homogeneity [23].

Dielectric barrier discharge is widely used in various industries since it can be operated under high pressure and no vacuum system is needed.

Applications of Dielectric Barrier Discharge

Ozone Generation

Another application of dielectric barrier discharge is ozone (O_3) generation [24]. Since DBD has a very high efficiency and is very inexpensive, it is considered to be a process for large scale ozone generation. By introducing the oxygen, air or N_2/O_2 mixtures into the DBD plasma, O_2 molecules will be dissociated by electron collisions and then react with N atom or excited N_2 species. Ozone is produced in a three-body reaction including O and O_2 [25].

It is reported that ozone concentration can reach up to 5 wt. % from air and up to 18 wt. % from oxygen [26]. Industrial ozone generation facilities can generate hundreds kilograms ozone within an hour at very low energy consumption (several megawatts) [27,23].

Dielectric Barrier Discharge Excimer Lamps

Due to the simplicity, very high efficiency and low expense, dielectric barrier discharges could be used as lamps. These excimer lamps can generate high power, high efficiency and narrow band radiation near UV wavelength (wavelength=354nm) to the deep UV (wavelength=126). The basic lamp configuration includes two concentric quartz tubes, the outer and inner electrodes, and the high voltage generator.

Xe is typically used in this excimer lamp. The inner electrode covered with dielectric material is connected to the external discharge voltage. After breakdown occurs, the 172 nm photons can be emitted through the outer quartz tube which is transparent to the 172 nm radiation [29, 24].

Osram's Planon dielectric barrier discharge excimer lamp is the first DBD lamp introduced into the market. It is designed as a flat panel configuration, 8.5 mm thick. Two parallel glass sheets are arranged with a gap between them. Xenon gas is filled at very high pressure in the sealed space coated with phosphor. The radiation at 172 nm will stimulates the phosphor coating and it lasts about 100,000 hours [29].

Surface Treatment

Dielectric barrier discharge can also be employed as a treatment of textile and polymers [30, 31, 32]. A research group in France showed that polyester (PET) and polypropylene (PP) films can be modified using DBD plasma with air, helium and argon at 5.0 KPa [33]. The PET film was placed into the gap on the lower ceramic plate. The modification of the surface with plasma leads to increase the O/C ratio from 34.9% to 47.9% [33]. New

oxygen-containing groups are formed on the polymer films after the treatment. These oxygen-containing groups are found to be C-O and O-C=O group on the polymer surface by the XPS [33].

Thin Film Deposition

Gases mixture of silane (SiH_4) and N_2O balanced with N_2 can be used to deposit silicon oxide film which is widely used in microelectronic, optics and food packaging industries using dielectric barrier discharge at atmospheric pressure [34, 35, 36]. In this experimental set-up, two parallel electrodes are both covered with the dielectric material. The silicon wafer was inserted into the gap on the lower electrode. The experiment is run under low frequency from 1-10 KHz. The average thickness of the film was measured using a Tencor profilometer. Chemical composition was also analyzed by XPS and FTIR instruments. From the XPS measurement, no N is observed in the film and O/Si is around 2.4. The FTIR studying also confirms that there are only Si-O-Si rocking, bending and stretching, while no Si-H and Si-N are observed [36].

Hydrogenated amorphous carbon (a-C:H) films are also deposited using low-pressure dielectric barrier discharge with gap distance of 5 mm. The (a-C:H) film has properties, such as: superior hardness, chemical

inertness, and infrared transparency. These types of film are used as wear protective coating and scratch resistant coatings. In this study, hydrogenated amorphous carbon film is deposited on the silicon substrate using CH_4 and argon as precursors. Pre-treatment with argon DBD plasma is employed in order to get rid of the SiO_2 layer on the silicon substrate. The surface roughness of the film was analyzed the atomic force microscopy. It was shown that, the hardness increases from 12 to 19 GPa when the Ar/CH4 concentration increases from 0% to 67% [37].

CHAPTER III

Experimental Methods

This project is focused on the plasma deposition of silicon nitride thin films at near atmospheric pressure using dielectric barrier discharge process. The equipment used for the thin film coatings process includes: (1) the delivery system which brings the precursors into the chamber and controls the flow rate of these precursors, (2) the chamber where the plasma is ignited and the substrates are positioned in the plasma area, and (3) the exhaust system which drives the byproducts of waste gases away from the chamber.

Thin films were deposited after the design and assembly of the reactor. Afterward, these films were measured and analyzed to determine thickness, deposition rate, surface morphology, atomic composition, refractive index and bonding. Experiments were conducted to discover the effects to the film from varying the following parameters, such as: gas flow rates, temperature, and plasma power. In this chapter, the experimental system, deposition processes and film characterization techniques are discussed.

Apparatus

The apparatus for this project consists of four subsystems including: (1) gas delivery system, (2) the chamber for the DBD plasma, (3) the electric power supply and (4)the exhaust system.

Gas Delivery

The gas delivery system sends the precursors into the chamber where the plasma occurs and deposition happens. These precursors include 2% silane balanced with hydrogen, ammonia and argon or helium. In order to bring these precursors simultaneously into the chamber via an injector, separate tubing lines were employed and then merged into one line. The inlet manifold consists of 4 stainless steel lines and every line has a MKS Mass-flo ® controller, and two valves (one is for MKS Mass-flo ® controller and another is a gas bypass for pumping). They are connected by a 0.60 cm OD stainless steel tubing and VCR ® fittings. VCR ® fittings are chosen in order to obtain high purity metal-to-metal seal with leak tight service.

There were two types of injectors used in this project. As shown in Figure 11, the first type of injector was a welded stainless steel tube with

several holes. The second one shown in Figure 12 was made of two fiberglass sleeves and these were placed in between the lower electrodes. Gases come through tiny holes in the fiberglass sleeves providing more uniform gas distribution.

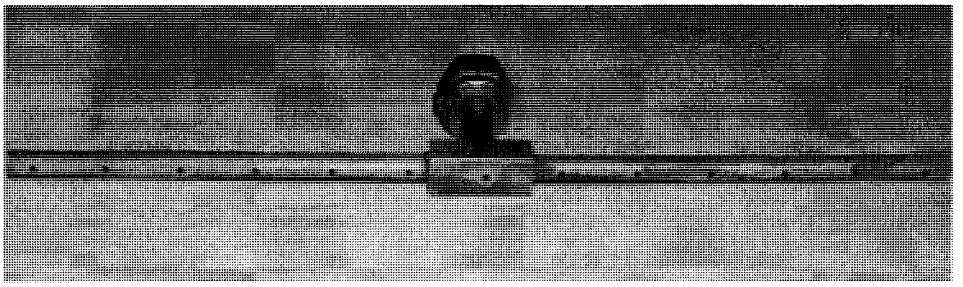

Figure 11. First Type of Injector.

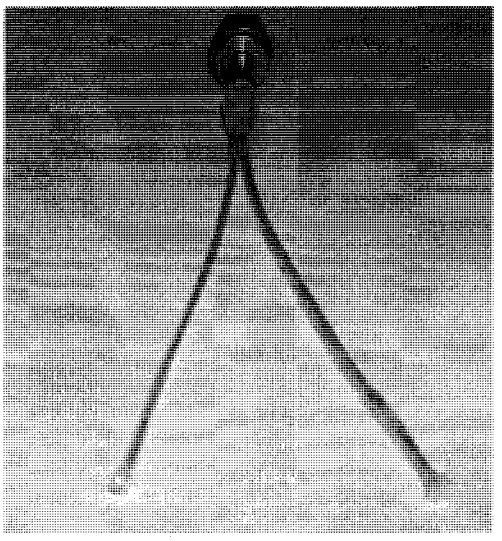

Figure 12. Second Type of Injector.

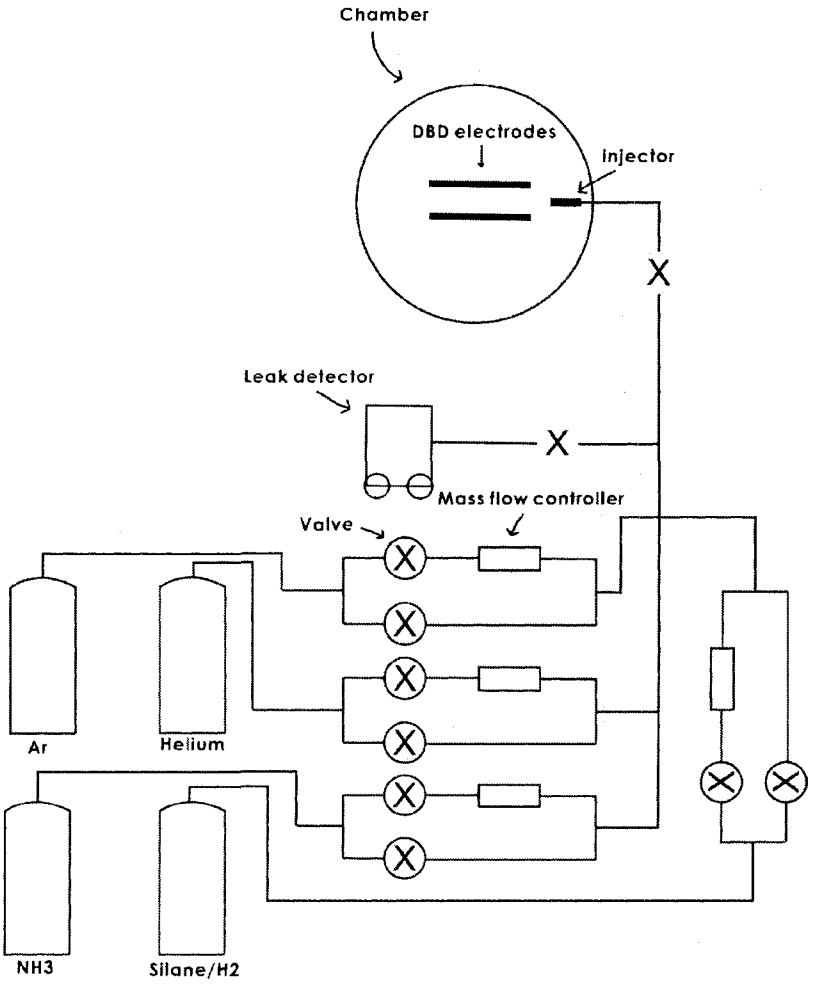

Figure 13. Schematic of Gas Delivery System.

Figure 13 shows the schematic of the delivery gas system. Precursors from cylinders went to the mass flow controller in the middle manifold. Two valves were used to control the gases. One was for the mass flow controller and the other one was used for the by-pass line. The gases were brought into the chamber through the injector which was positioned near the DBD electrodes.

Exhaust

The bottom of the chamber was connected to metal flexible hose. This hose was connected to an MKS capacitance Manometer and an MKS exhaust throttle valve. Exhaust gases were carried out to atmosphere using an Alcatel vacuum pump.

Electrical Power

The power supply consists of: (1) a Tektronix AFG3021 Function generator, (2)a Bey Electronics oil-cooled 1000 VA step up transformer, and (3) a Powertron model 500A RF amplifier. The output of the transformer was measured by a Tektronix digital Oscilloscope.

The function generator produces sine waves at frequencies from 1 μHz to 25 MHz with 5.6" display. The Bey Electronics transformer operates at a frequency range from 1KHz to 10KHz at one phase, with maximum 22 A and 22.5 V input and 0.2 A and 25,000 V output. Since it can generate significant heat, it was cooled in the Royal Purple Synthetic Transformer Oil. The Powertron 500A RF amplifier delivered an output from 0 to 22.5 V at various frequencies from 20 Hz up to 500K Hz.

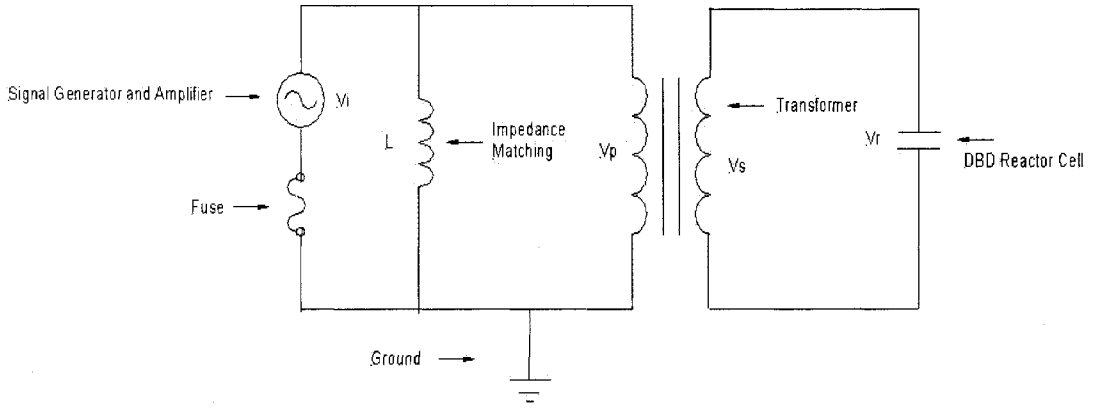

Figure 14. Schematics of Electrical Circuit.

As shown in Figure 14, the function generator and the power amplifier were connected to a transformer. An impedance matching network was used to match the transformer. The transformer was connected directly to the electrodes of the DBD.

This power supply unit was connected to the main chamber reactor through two ceramic feedthroughs, using 12 gage copper wire. These two feedthroughs are connected to the DBD electrodes with 18 AWG (America Wire Gauge) size high voltage, high temperature silicone appliance wire. The appliance wires inside the chamber were covered with a Teflon tube, 1/8 inch ID, ¼ inch OD and again wrapped with Teflon tape to provide further insulation from the electric field generated inside the chamber. The wires inside the feed throughes were also covered with

1/8 inch ID, ¼ inch OD Teflon Tubing to prevent arcing occurring between the wire and the stainless stain chamber surface.

One Magnetek Triad C-80 U Filter Reaction inductor is used to match the impedance of the power supply in order to make the output impedance equal to the input impedance of the load and maximize the power transfer, and minimize the reflections from the load. This impedance matching circuit was connected with the transformer in parallel. It could provide 0.024 H or 0.006 H of impedance to match the power supply.

Plasma power measurement

Due to the high voltage at both electrodes, the oscilloscope cannot be directly connected to the electrodes. Thus the actual power consumption of the plasma inside the chamber was still not fully known. Further measurement of plasma power as well as the limitation of the equipment was needed in order to obtain optimum plasma under various conditions.

In order to measure the high voltage as well as the current of the plasma, a new circuit was designed especially for the plasma power measurement shown in Figure 15.

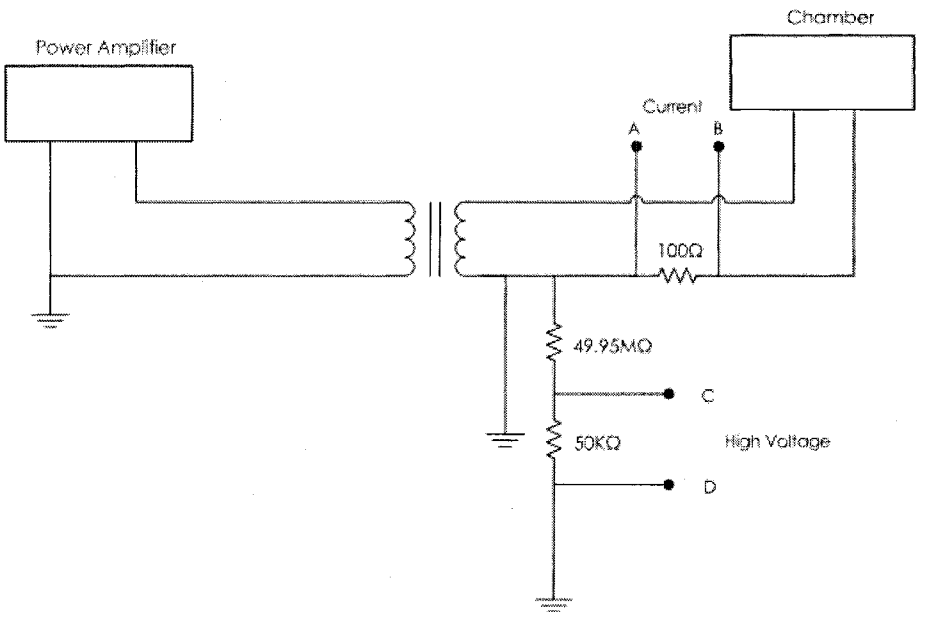

Figure 15. Diagram of the System Circuit for Plasma Measurement.

P2220 200M Hz 1x/10x passive probes from Tektronix were employed to measure the voltage and current of the plasma. Because of the high voltage of the input, several resistors were used in the circuit. As shown in Figure 15, one 49.95 MΩ resistor and a 50 KΩ were connected in series to the ground. If the voltage across the 50 KΩ was measured, the high voltage across the plasma is known. In the diagram, measuring the voltage between C and D will give the actual high voltage between the electrodes. The actual current could be measured between point A and B.

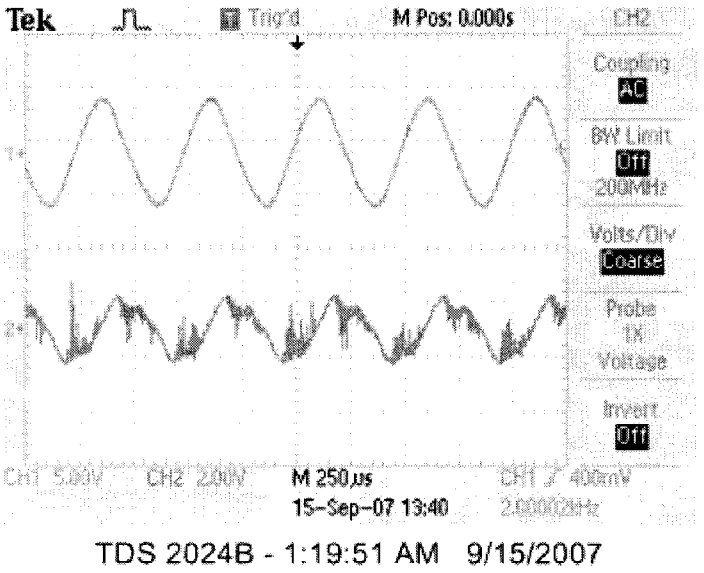

Figure 16. Typical Voltage and Current Waveforms of Plasma.

Figure 16 shows a snap of the oscilloscope for typical plasma voltage and current waveforms. Channel1 measures the voltage of plasma and is shown in the oscilloscope in the top waveform. Since the real voltage was reduced 1000 times by the additional circuit, every 1V unit in the oscilloscope stands for 1000 V. Channel2 measures the current of plasma and it is shown at the lower waveform. The fluctuation in the lower waveform is typical characteristic of DBD plasma since the plasma was comprised of many small filaments. For the ideal homogenous plasma, no fluctuation should be observed and it was obtained by using helium as the plasma precursor.

MATERIALS

Substrates

Three types of substrate materials were used in this project. The first one is a crystalline silicon wafer, 2" or 3 "diameter. The silicon wafers were test grade wafers which were doped with Phosphorous/Boron, 11 mm thick produced by Silicon sense Inc.

Polycrystalline silicon solar cell wafers, 4" by 4" diameter were also used. These wafers are widely utilized in the solar cell industry. GT solar Inc. provided these poly-crystalline silicon wafers.

Polished potassium bromide (KBr), 25mm x 2mm, windows were also used to determine the IR spectrum of silicon nitride film. KBr is transparent to infrared radiation from 4000 to 400 cm^{-1} [38]. These plates are produced by McCarthy Science Co.

Process Precursors

Process precursors include 2% silane (SiH_4) balanced with 98% Hydrogen (H_2) or ultra high purity argon, anhydrous ammonia (NH_3) and ultra high purity argon or helium. The silane balanced with hydrogen and anhydrous ammonia gases were produced by Scott Specialty Gases and ultra high purity argon and helium were produced by Northeast Airgas Company.

Silane Safety

Silane is a chemical compound with a pyrophoric nature. It is a colorless, toxic and spontaneously flammable gas with a repulsive odor. Since it is flammable, it may cause explosion with air; plus, silane can react violently with heavy metal halides as well as general halogen compounds[39].

Based on these properties of silane gas, $\frac{1}{4}$ inch or $\frac{3}{8}$ inch stainless steel with 0.035 inch thickness wall tubes should be used during the delivery to the main reactor chamber. The whole supply line should be leak checked to avoid any air leak. The exhaust duct should be made with steel or flame-retardant polymer vented by vacuum pumps using perfluoropolyether type oil. Generally speaking, brass valves with stainless steel delivery lines will provide leak-tight connection. The exhaust gas cannot be vented through a fan or hood; it should be diluted and then vented to the atmosphere [39].

In this thesis, 2% silane balanced with 98% hydrogen gas or inert argon gas is used. The diluted mixture of silane can decrease the flammability of the gas.

Dielectric Barrier Materials

In this project, quartz was employed for the dielectric barrier material. It is a traditional material for the dielectric layer. The dielectric barrier layer was a layer of quartz plate with dimensions 25.3 mm x 25.3

mm x 3 mm. Two types of quartz plates are used in the experiment. The only difference between the two types of quartz was that one of the surfaces was polished and the other one was rough without polishing. The quartz plate was positioned below the upper electrode with 4 metal claws. The dielectric constant of this type of quartz is 3.8 [41].

Reactor Chamber Configuration

The dialectic barrier material was made by quartz and this plate was put beneath the top electrode. The bottom electrode can hold up to 4 x 4 inch silicon wafers. Two heater bars were placed under the bottom electrode and it can heat up to 600°C. These two electrode plates were well insulated against stainless steel chamber. Injector located at the right side of chamber and different injectors can be connected to chamber.

Procedures

Sample Preparation

Silicon wafers were directly placed into the gap between the two electrodes. The conductive carbon paint was chosen to stick the silicon wafer to the lower electrode so that the gas flow will not blow away the wafer from the smooth electrode surface. For the 4"x4" poly crystalline silicon wafers, 4 small aluminum claws were used to hold the wafers in position. Because of the much heavier weight of KBr plates, no additional glue was used for adhesion.

Reactor Preparation

After the samples were positioned, the upper electrode and quartz plate were installed and the injector was connected. The chamber was pumped down to a few millitorr. Argon gas was introduced into the chamber. Upon reaching 600 Torr, argon gas flow was terminated and the chamber was pumped down. This procedure was repeated twice so that the residual gases such as oxygen could be eliminated from the chamber.

Film Deposition Runs

After the chamber was pumped down to a few militorr for the third time, the substrate heater was turned on. The temperature of the substrate was obtained by a type K thermocouple. The argon gas flow was turned on again and maintained at 400 sccm until the required substrate temperature was obtained. After the chamber pressure reached 600 Torr, the power amplifier and the function generator were turned on. The argon plasma was ignited at a selected frequency and maintained for 10 minutes to remove the surface oxide on silicon wafer as well as the water vapor remained in the lower and upper electrodes.

After 10 minute of this pre-treatment, the argon plasma was terminated. The whole system was pumped down again to remove the residual argon gas inside the chamber.

Ammonia then was introduced into the chamber together with the silane precursor balanced with hydrogen or argon. When the gas flow was stable and the pressure reached set point, the power amplifier and the function generator were turned on.

Then the amplitude was slowly increased. After the plasma was ignited the amplitude was increased until the current in the left current meter reached a set value. The maximum input current is 22.5A so that the transformer would not blow out.

The values in channel 1 and channel 2 of the oscilloscope were recorded. Channel 1 measured plasma voltage and channel 2 measured current. The frequency and the amplitude in the function generator were also recorded. The input current in the left current meter was documented, as well as run time and the substrate temperature, deposition pressure, and precursors flow rates.

Once the plasma was stable, the voltage and current of the plasma would remain constant for the entire run if no arcing or sparking occurred. When the deposition was finished, the function generator, then the power amplifier, and lastly the heater were turned off. Silane precursor was first shut down for safety. Ammonia and other gases were stopped after that.

The whole system then was pumped down and purged with argon three times so that no residual silane gases stayed in delivery lines. After

that, the valve to the chamber was closed; and the delivery lines would stay under vacuum until the next run. Samples were taken out after the chamber cooled down. These samples were saved in and labeled plastic bags. These samples were stored in the dry desiccators for further analysis.

Electrical Measurement

Due to the high voltage between the two DBD electrodes, the probe of the oscilloscope could not be directly hooked up to electrodes; A circuit was designed so that the measurement of electrode voltage and plasma current was possible.

THIN FILM ANALYSIS

Analysis of Deposited Thin Films

The deposited films were analyzed for film thickness, elemental composition, chemical bonding, morphology and refractive index. The analysis methods included: x-ray Photoelectron spectroscopy (XPS), x-ray diffraction (XRD), ellipsometry, fourier transform infrared spectroscopy (FTIR), scanning electron microscopy (SEM), and stylus film thickness profilometry.

X-ray Photoelectron Spectroscopy

XPS is a quantitative surface chemical analysis to measure the elemental composition of surfaces. When X-Ray irradiation reaches the surface being analyzed, emission of electrons will occur from the surface. The kinetic energy of electrons as well as the number of electrons excited from the surface will generate the XPS spectra.

XPS analysis in this thesis was performed by RBD enterprises located in Bend City, Oregon; In the XPS analysis, the binding energy of the electrons was detected. Every element will generate a series of specific XPS peaks at a specific binding energy characteristic of that element. The numbers of electrons at these specific peaks indicate the amount of elements within the area in which analysis was conducted.

Furthermore, depth profiles of the samples were also carried out. Depth profiles are used to determine the elemental composition as a function of depth. An argon ion gun was employed to sputter the surface of the samples and the sputter rate of samples was used to indicate the thickness of films.

Fourier Transform Infrared Spectroscopy

Fourier transform infrared spectroscopy is a widely used tool for identifying chemical bonding. Different vibrational modes of chemical bonds will be induced by the infrared light. These vibrational modes

include: symmetric stretch, asymmetric stretch, scissor bending, rocking and bending.

In the FTIR spectroscopy, a background spectrum must be taken in addition to the sample spectrum. A transmittance spectrum is obtained using equation 6,

$$\%T = \frac{I}{I_0}$$

Equation 6

where T = transmittance, I=intensity of transmitted and I_0 = intensity of incident.

The absorbance spectrum is obtained by the equation,

$$A = -\log_{10}{}^{T}$$

Equation 7

where A equals absorbance and T equals transmittance.

For silicon nitride film, the peak of amorphous Si_3N_4 is located at about 840 cm^{-1} [41, 42, 43]. There are several functional groups in the deposited silicon nitride films and they are listed below in Table 2.

PEAK	Silicon	N-H bending	Silicon Nitride	N-H stretching	Si-H stretching	Si-O
Wave number (cm^{-1})	610	1167	840	3320	2160	800-1000

Table 2. DBD Deposited Silicon Nitride Characteristic FTIR Peaks. [41, 42, 43].

The following chapter will present the analysis of the deposited silicon nitride film based on the dielectric barrier discharge.

CHAPTER IV

RESULTS AND DISCUSSION

Film Composition as a Function of Temperature

The substrate temperature was varied from 100 °C to 350 °C. All other deposition parameters remained constant; these parameters are listed in Table 3. These films were deposited on 3" single crystalline silicon wafers and KBr plates. Thicknesses of these films were measured by the TENCOR AS-100 profilometer. Atomic compositions and depth profiles were determined by XPS. Chemical bonds analysis was also conducted with FTIR. SEM was introduced to analyze the morphology of the film surface.

Parameter	Value
Frequency (Hz)	1000
Ar flow rate (sccm)	400
SiH_4/H_2 flow rate (sccm)	400
NH_3 flow rate (sccm)	200
Pressure (torr)	600
Input Current (A)	10
Gap Distance (mm)	5
Temperature (°C)	100,200,300,350

Table 3. Deposition Parameters in the Film Composition as a Function of Temperature Series.

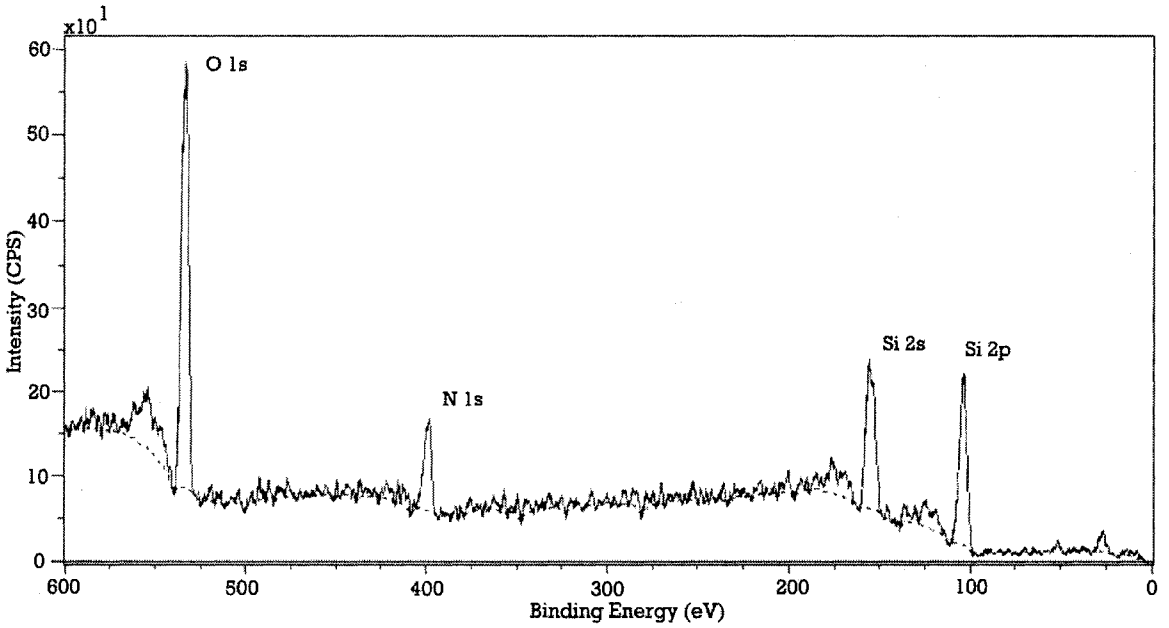

Figure 17. XPS Spectrum of Surface Survey of Silicon Nitride Film deposited at 300 °C.

Figure 17 shows the XPS spectrum of surface survey of silicon nitride film deposited at 300 °C. The oxygen atomic percentage is about 41%, the silicon atomic percentage is 43% and the nitrogen atomic percentage is 16%.

Because the silicon nitride surface absorbs air after deposition, the XPS surface survey is not representative of the bulk film. A depth profile that measures atomic percentage as a function of depth was obtained by XPS. The horizontal axis is the depth of the film while the vertical axis is the C, N, O or Si atomic percentage. The depth profiles of the silicon nitride films in this series of experiments are shown in Figures 18- 20.

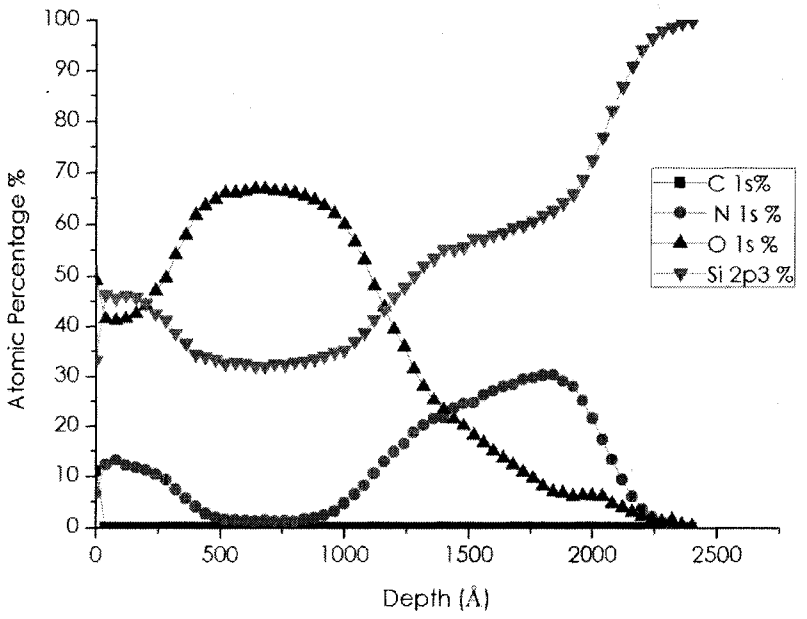

Figure 18. Depth Profile of 200 °C Film in Film Composition as a Function of Temperature Series.

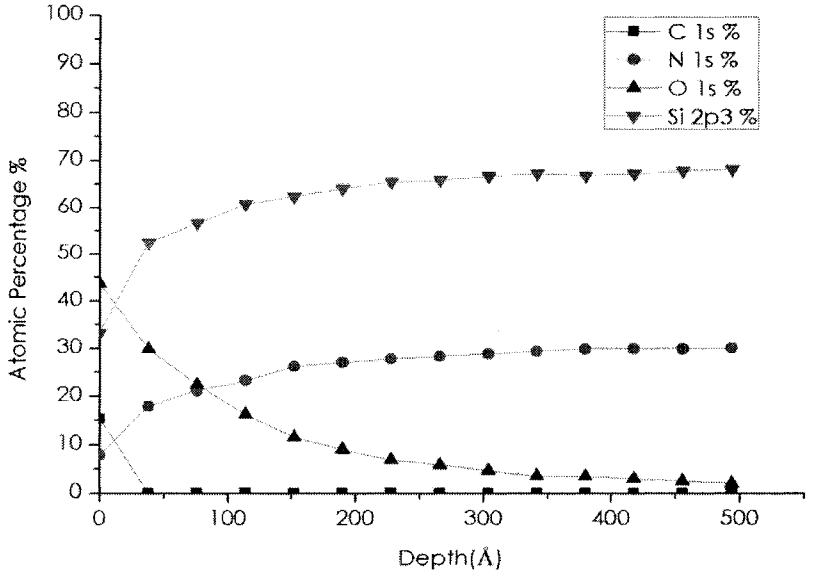

Figure 19. Depth Profile of 300 °C Film in Film Composition as a Function of Temperature Series.

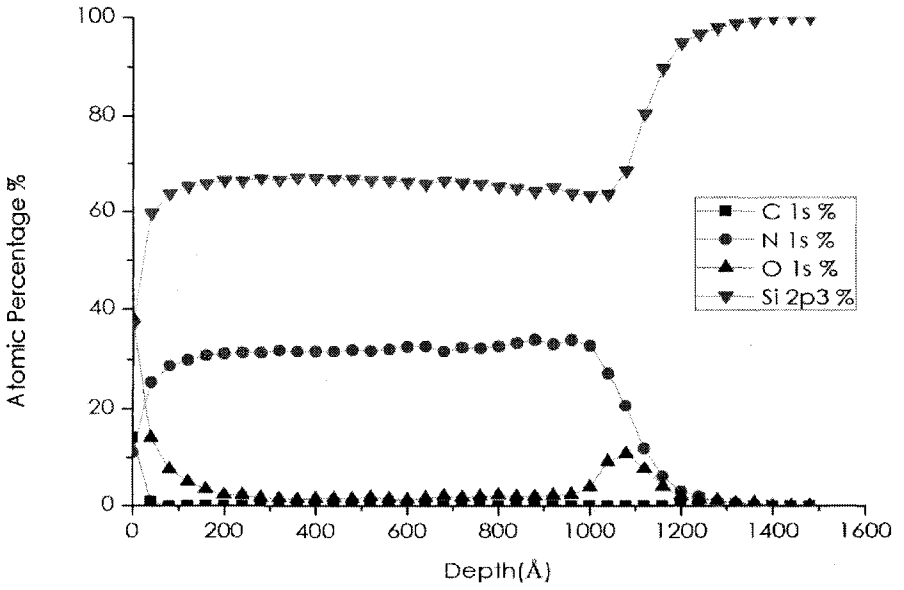

Figure 20. Depth Profile of 350 °C Film in Film Composition as a Function of Temperature Series.

When the substrate temperature was 100 °C, the plasma was very filamentary at the conditions of Table 3. The plasma disappeared after 20 minutes and only little film was observed after the silicon wafer was taken out of the chamber.

At 200 °C, the plasma is very homogeneous with very few filaments. The plasma became very homogeneous at 300 °C. There were no filaments in the plasma and the plasma was very stable during the entire deposition. At substrate temperature 350 °C, the plasma is even more homogeneous. Furthermore, the plasma was more luminous than at low temperature.

Based on the above XPS data, all films were silicon rich because the atomic percentage of silicon is higher than that of nitrogen. The silicon increased to 100% and nitrogen drop to 0% at about 1300 Å in the XPS data of 350 °C film. This is the silicon/film interface because the sputter gun was actually etching the pure silicon wafers.

Figure 18 shows that at 200 °C, the film composition became approximately constant after 1500Å at Si 60% N 23% O17%.The ratio of Si: N is 2.61. Before 1500 Å, oxygen is almost 66% and silicon is almost 33%. The ratio of Si: O is near 2. This is mainly silicon dioxide film in this range. Only some SiN in the interface.

Figure 19 shows that at 300 °C, the film composition became approximately constant after 300 Å at Si 67% N29% O4%. The ratio of Si: N is 2.31. Before 300 Å, oxygen decreases from 45% to 4%. Silicon increases from 33% to 67% and nitrogen increases from 7% to 29%.

Figure 20 shows that at 350 °C, the film composition became approximately constant after 200 Å at Si 66% N32% O2%. The ratio of Si: N is 2.06. Before 200Å, oxygen decreases from 39% to 2%. Silicon increased from 39% to 66% and nitrogen increases from 10% to 32%. This is the best film in this series.

Temperature	Ratio of Si: N	Constant Film Composition	Onset of Constant Composition

200 °C	2.61	Si 60% N 23% O17%	1500 Å
300 °C	2.31	Si 67% N29% O4%	300 Å
350 °C	2.06	Si 66% N32% O2%	200 Å

Table 4. Constant Film Composition and Onset of Constant Composition as a Function of Temperature.

Table 4 shows that ratio of Si: N decreases with increasing temperature. The oxygen atomic percentage decreases at higher temperature. The silicon and nitrogen atomic percentage increases at higher temperature. The onset of constant composition starts at less shallow in film at higher temperature.

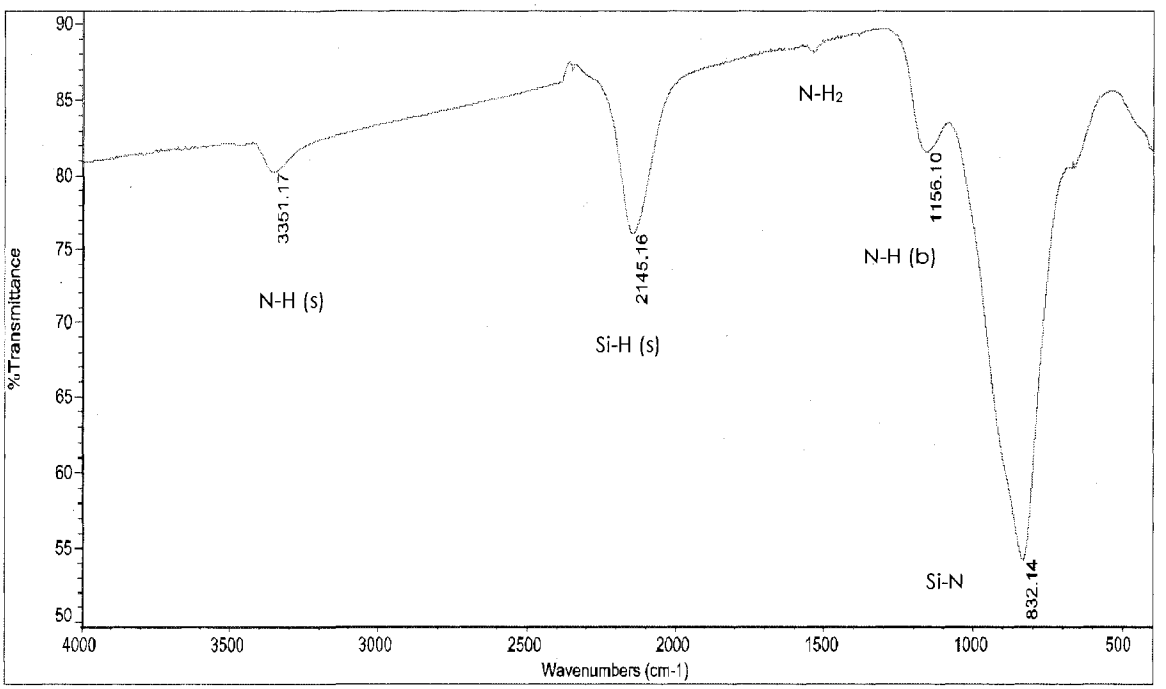

Figure 21. FTIR Spectrum of Film at 200°C in Film Composition as a Function of Temperature Series.

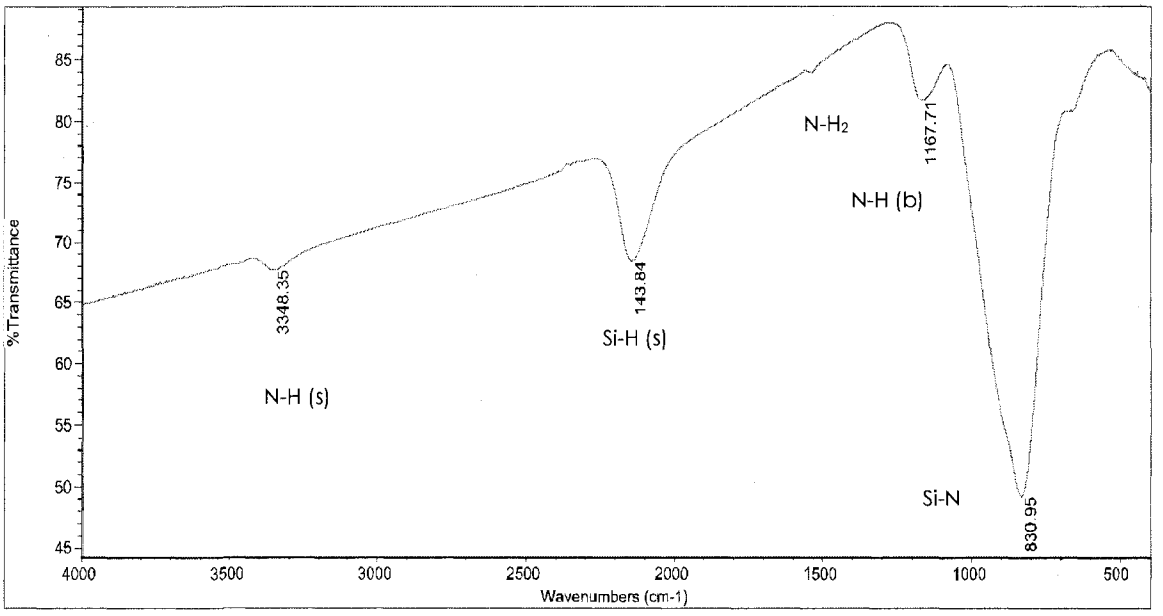

Figure 22. FTIR Spectrum of Film at 300°C in Film Composition as a Function of Temperature Series.

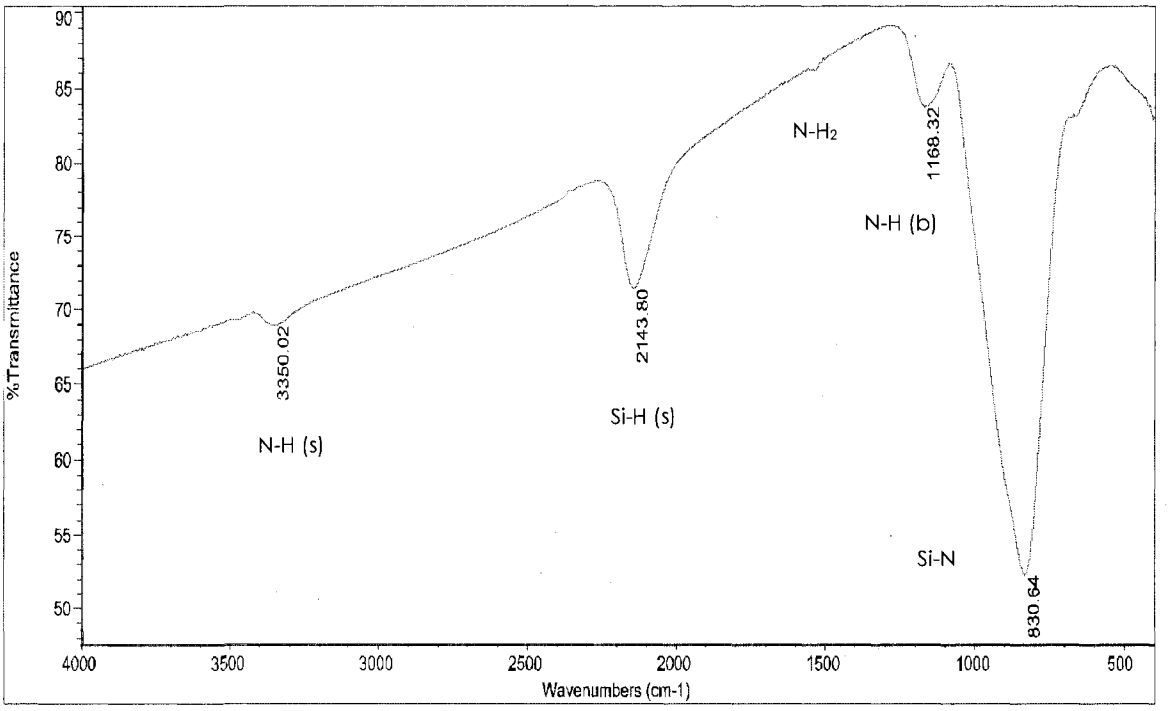

Figure 23. FTIR Spectrum of Film at 350°C in Film Composition as a Function of Temperature Series.

The silicon and nitrogen composition is almost the same in the films at 300 °C and 350 °C, and stayed constant after a few hundred Å depths for all films. The Si: N ratios of these films were nearly about 2:1 for both temperatures. However, the starting point of constant Si: N ratio varied for different temperatures. The film at 300 °C showed constant composition at 300 Å while the 350 °C began at near 200 Å; this depth for the 200 °C film was nearly 1400 Å. The silicon and nitrogen atomic percentage were much lower at 200 °C than both 300 and 350 °C, the every Si: N ratio was 2:1 at 200 °C. However, there was much oxygen in the film deposited at 200 °C. It was as high as 60% at maximum.

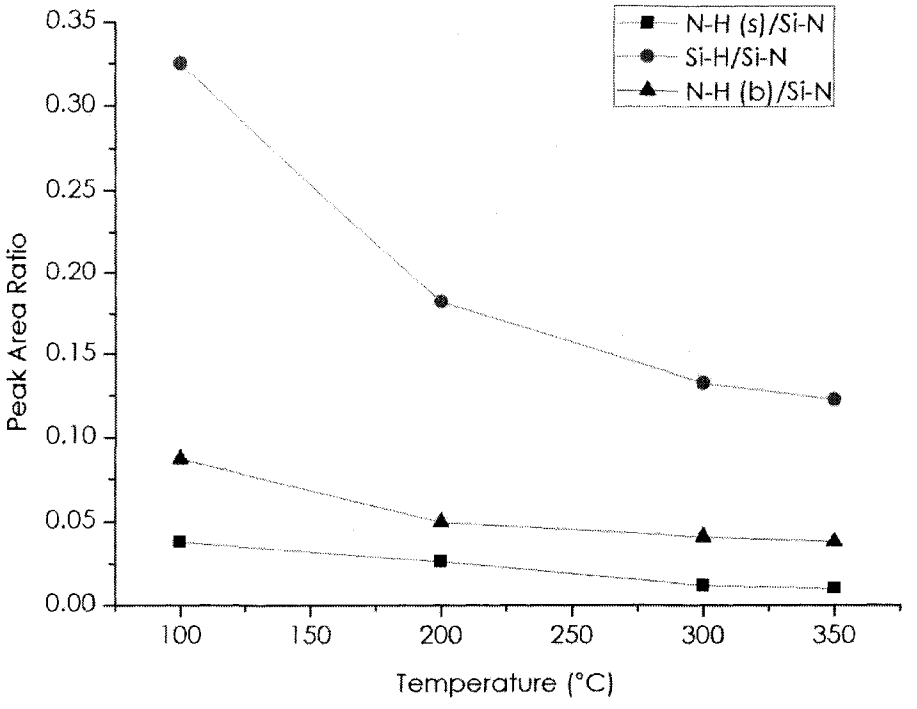

Figure 24. Ratio of N-H (s)/Si-N, Si-H/Si-N and N-H (b)/Si-N Peak Area versus Substrate Temperature.

The variation of atomic percentage as a function of film depth is related to the chemical bonding of the silicon nitride. After the films were taken out from the chamber for storage, they reacted with the air, causing the oxygen contamination. The denser the Si-N bonds in the film, the less likely is the reaction with oxygen. It was deduced from XPS data that the temperature played an important role in the oxygen content of the films. The oxygen content decreased when the temperature increased. It was also learned that the starting depth for constant silicon and nitrogen content without oxygen was an inverse function of temperature. These silicon nitride films deposited on the KBr windows were also analyzed by the FTIR.

Figure 24 shows the ratios of: (1) Si-H peak area to the SiN peak area, (2) N-H (s) peak area to SiN peak area, (3) N-H (b) peak area to the Si-N peak area as a function of substrate temperature. With increasing substrate temperature, all these ratios became lower. It shows the hydrogen content of the films decreased as substrate temperature increases.

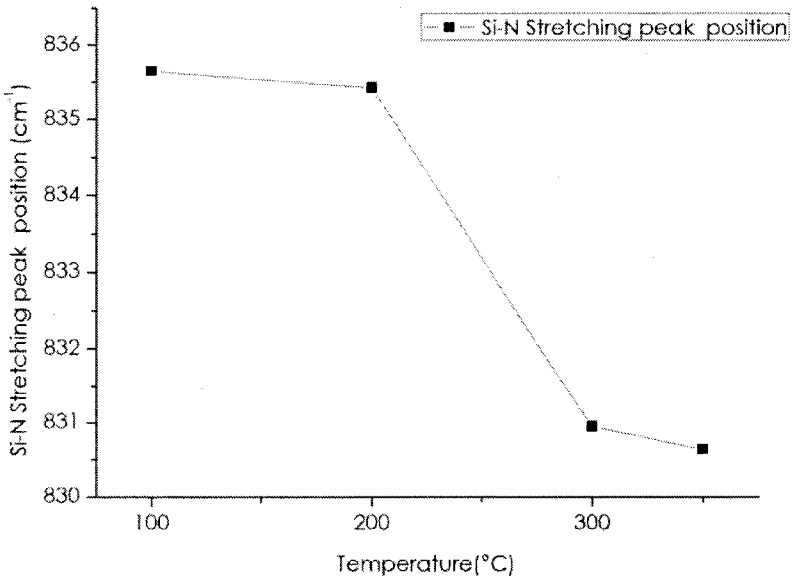

Figure 25. the Si-N Peak Frequency versus Substrate Temperature.

In Figure 25, illustrates the behavior of Si-N peak frequency versus the substrate temperature. The Si-N peak area shifted from high wave numbers to lower wavenumber as the substrate temperature increased [44]. It was well known that the incorporation of the Si-O groups as well as other Si-H groups in the silicon nitride film causes the shift of the Si-N peak [41, 42, 43]. This is consistent with the analysis of XPS data that showed the oxygen content decreased with increased substrate temperature.

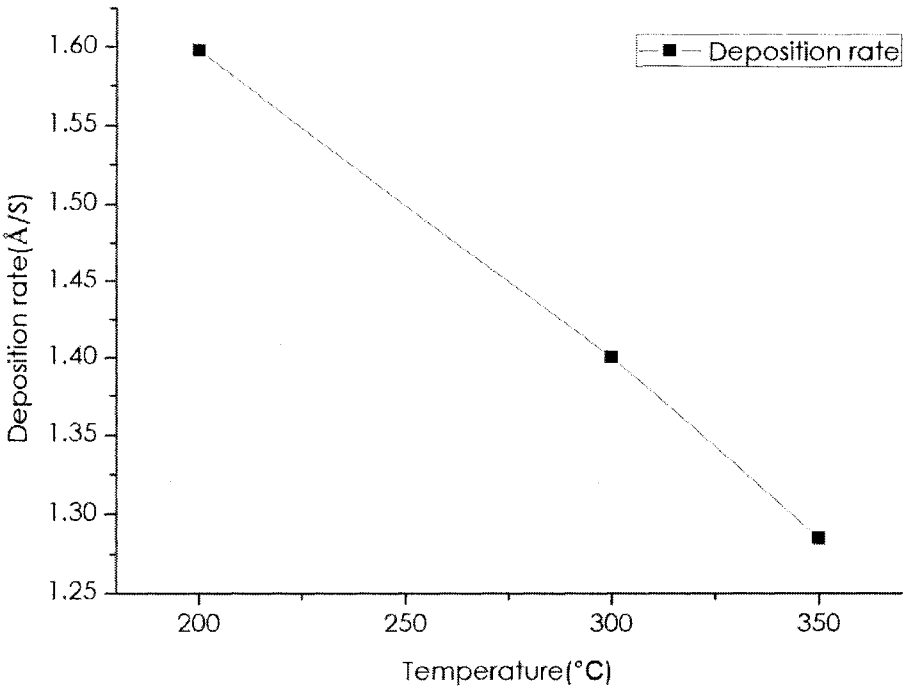

Figure 26. Film Deposition Rate (Å/s) Versus Substrate Temperature.

The film thicknesses were measured by a Tencor AS-1 profilometer using carbon conductive paint as the mask on the surface of the film. The deposition rates were calculated by dividing the thickness deposition by time. The Figure 26 shows that the deposition rate decreased from 1.6 Å/s to 1.3 Å/s with increasing substrate temperature. This is mainly due to denser film at higher temperature.

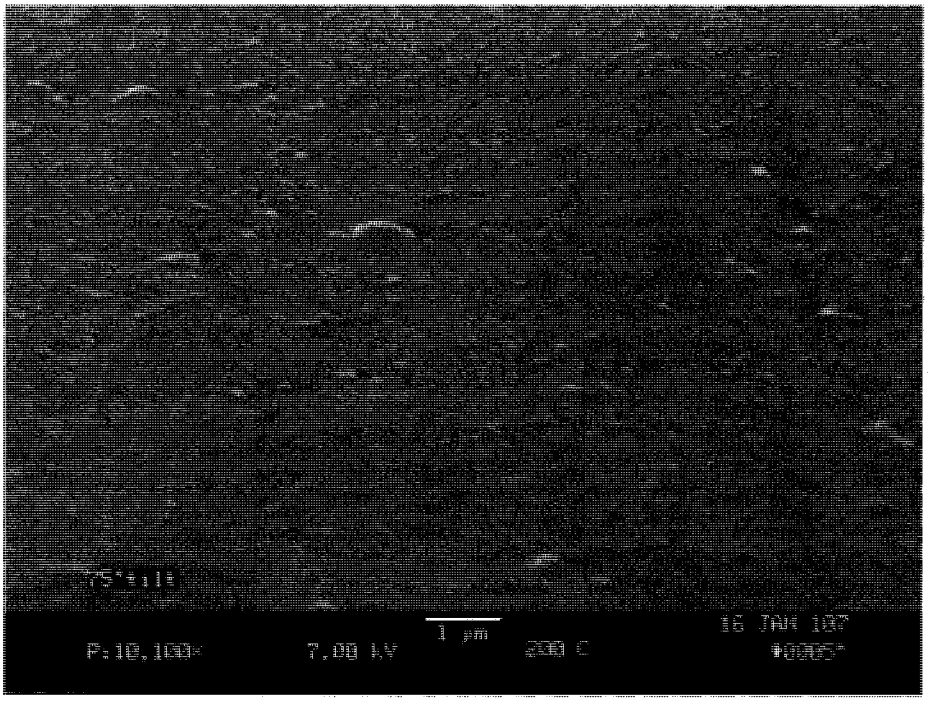

Figure 27. SEM Picture of Silicon Nitride Film Deposited at 200 °C with Control Condition.

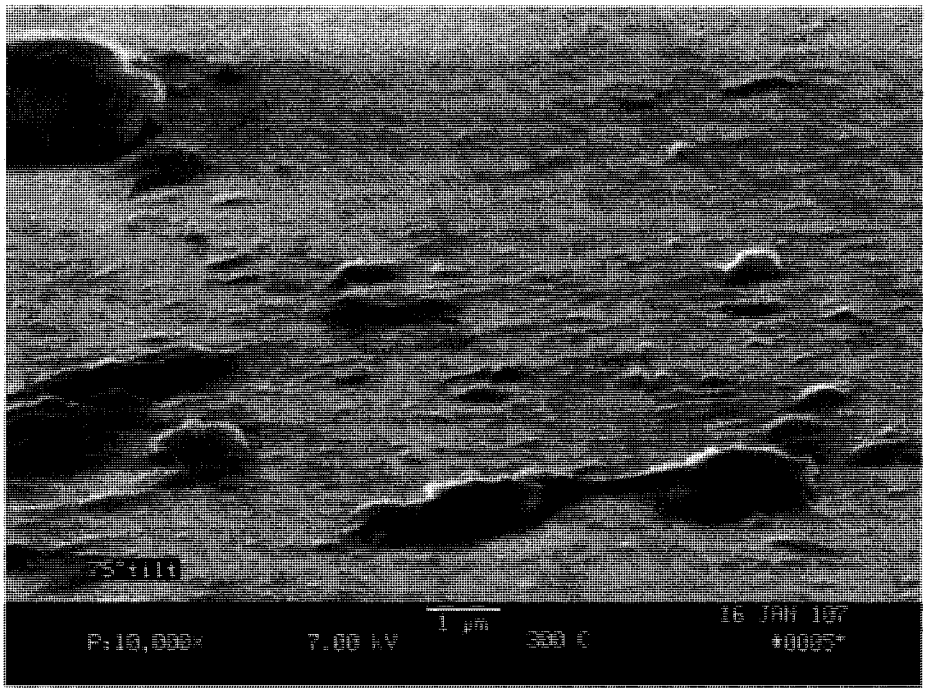

Figure 28. SEM Picture of Silicon Nitride Film Deposited at 300 °C with Control Condition

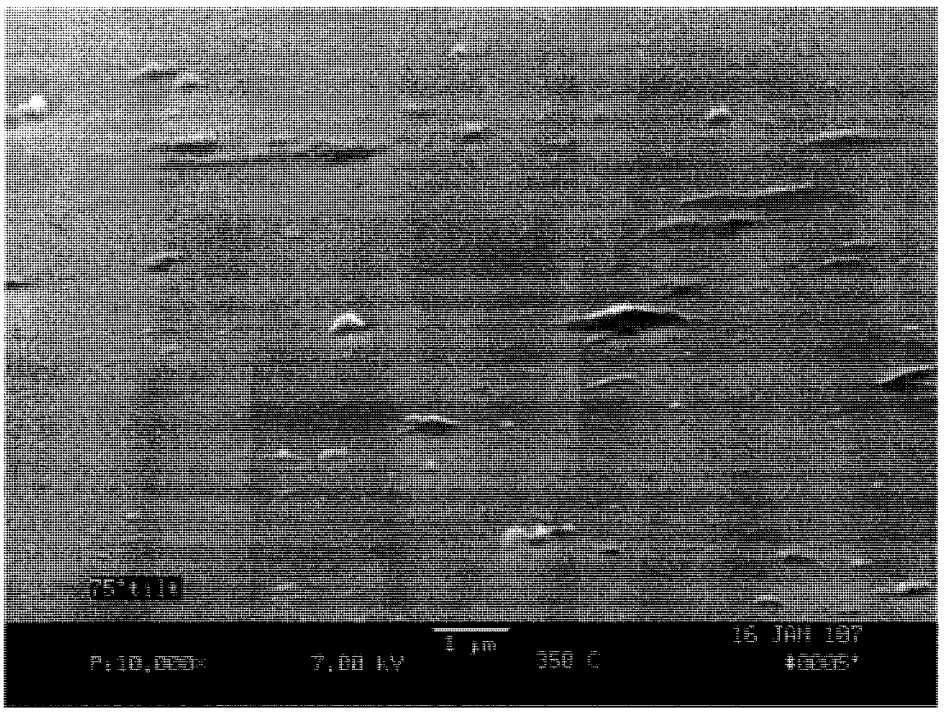

Figure 29. SEM Picture of Silicon Nitride Film Deposited at 350 °C with Control Condition.

The film shown in Figure 29 at 350 °C was much smoother than the film shown in Figure 27, 28 at 200 °C and 300 °C. From the above surface pictures, silicon nitride films became denser and smoother with increasing substrate temperature.

Film Composition as a Function of Residence Time

Gas residence time, τ, refers to the time the precursors remained in the plasma.

In this series, the total flow rate was varied. The other conditions were kept constant at 600 Torr. Residence time was inversely related to

the total gas flow.

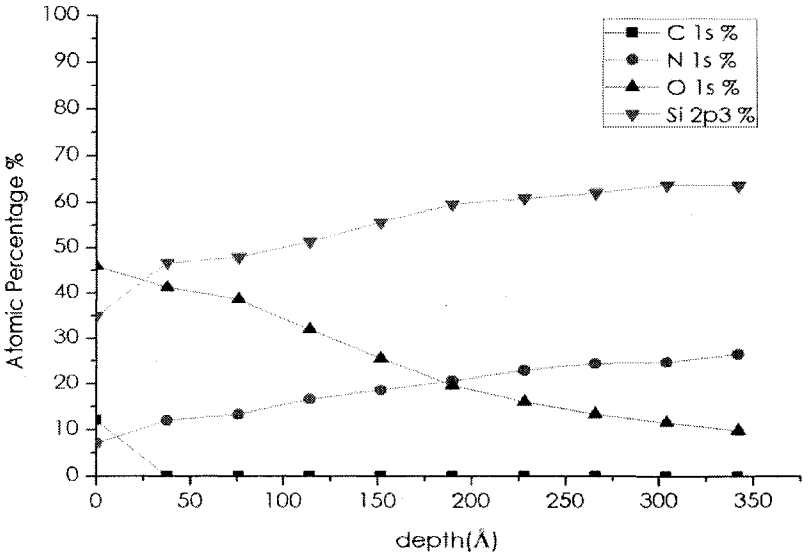

Figure 30. The XPS Depth Profile of Deposited Film at 500 sccm total flow rate.

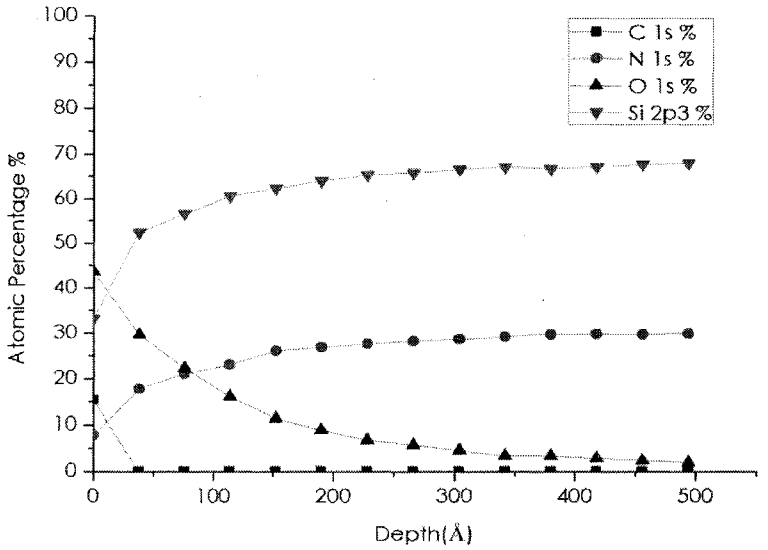

Figure 31. The XPS Depth Profile of Deposited Film at 1000 sccm total flow rate.

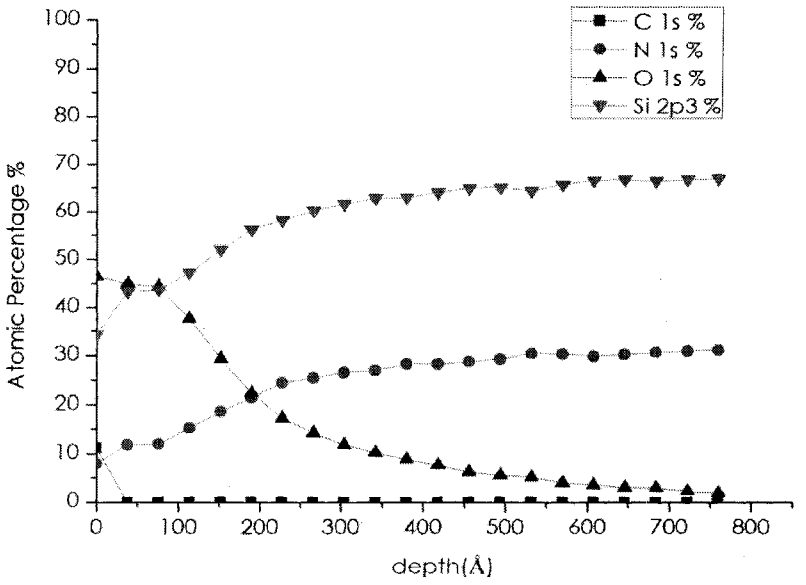

Figure 32. The XPS Depth Profile of Deposited Film at 1500 sccm total flow rate.

Figure 30 shows that with 500 sccm total flow rate, after 300Å, the film composition became approximately constant at Si 65% N 25% O 10%. The ratio of Si: N is 2.6. Before 300Å, oxygen decreases from 46% to 10%. Silicon increases from 34% to 65% and nitrogen increases from 7% to 25%.

Figure 31 shows that with 1000 sccm total flow rate, after 300Å, the film composition became approximately constant at Si 67% N 29% O 4%. The ratio of Si: N is 2.31. Before 300Å, oxygen decreases from 45% to 4%. Silicon increases from 34% to 67% and nitrogen increases from 7% to 29%.

Figure 32 shows that with 1500 sccm total flow rate, after 300Å, the film composition became approximately constant at Si 65% N 30% O 5%.

The ratio of Si: N is 2.17. Before 300Å, oxygen decreases from 46% to 5%. Silicon increases from 34% to 65% and nitrogen increases from 7% to 30%.

Total Flow Rate	Constant Film Composition	Onset of Constant Composition
500 sccm	Si 65% N 25% O 10%	300Å
1000 sccm	67% N 29% O 4%	300Å
1500 sccm	Si 65% N 30% O 5%	300Å

Table 5. Constant Film Composition and Onset of Constant Composition as a Function of Total Flow Rate.

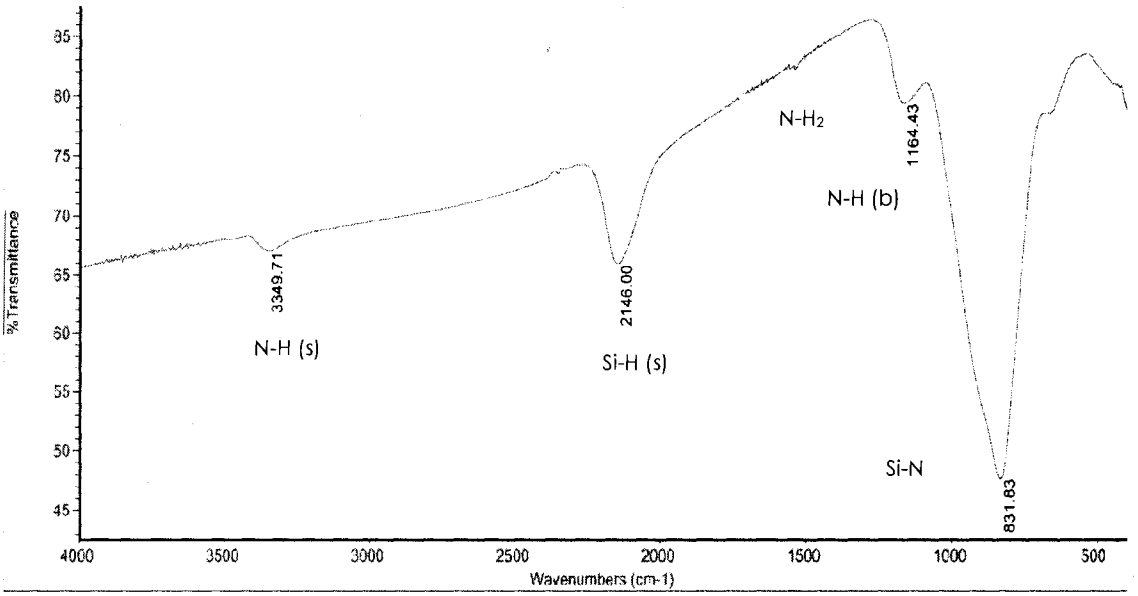

Figure 33. FTIR Spectrum of Film at 500 Sccm Total Flow Rate in Film Composition as a Function of Residence Time Series.

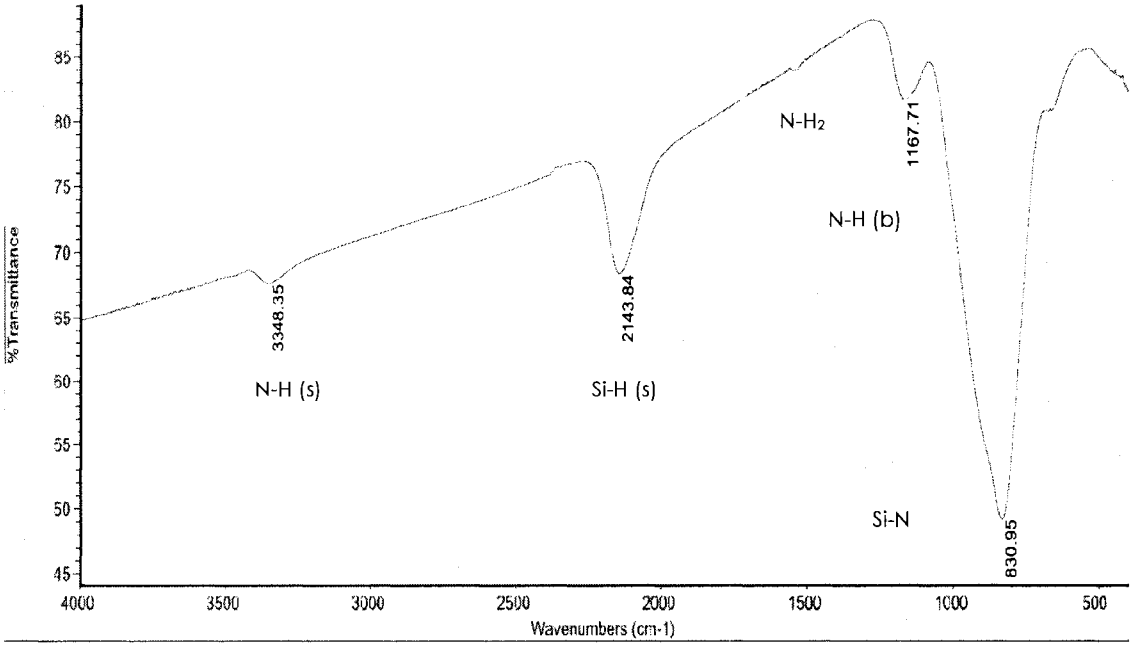

Figure 34. FTIR Spectrum of Film at 1000 Sccm Total Flow Rate in Film Composition as a Function of Residence Time Series.

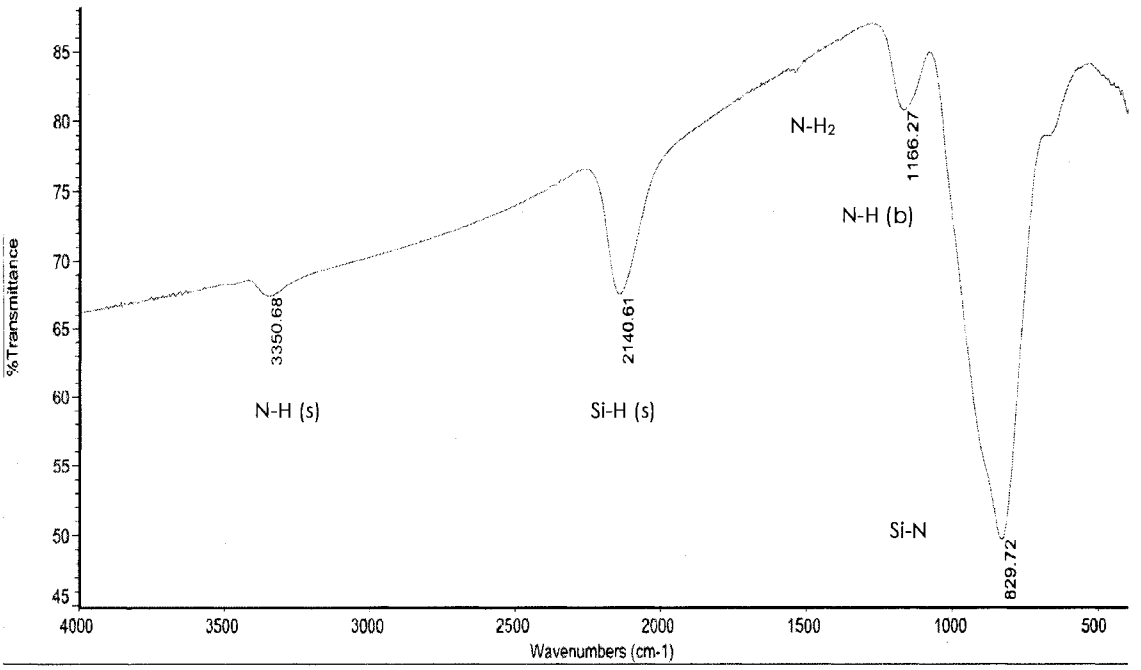

Figure 35. FTIR Spectrum of Film at 1500 Sccm Total Flow Rate in Film Composition as a Function of Residence Time Series.

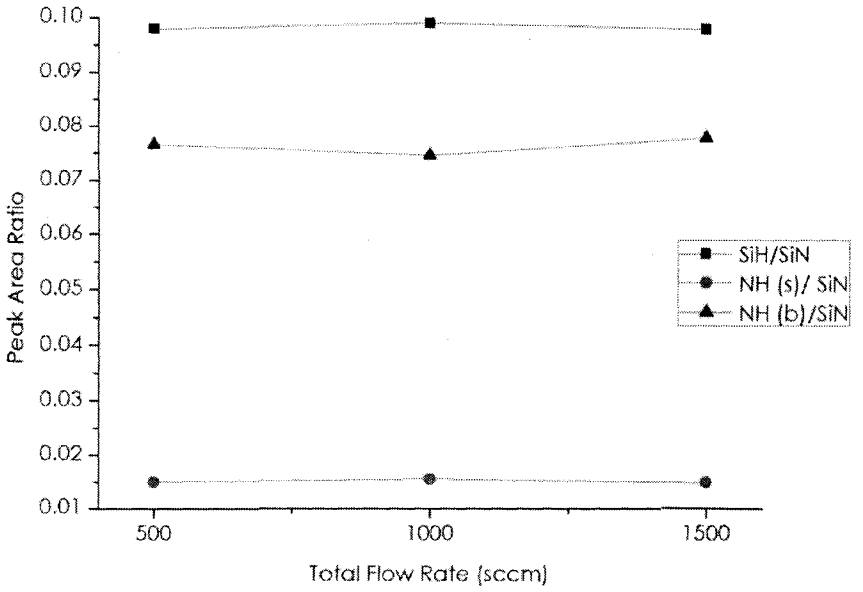

Figure 36. Peak Ratio versus Total Flow Rate.

The FTIR data of the residence time series in Figure 36 shows the ratio of N-H stretching, N-H bending, and Si-H peak area to Si-N peak areas. The ratio of NH (s)/SiN is the same at 0.015. The ratio of NH (s)/SiN is 0.076 and ratio of SiH/SiN is 0.097. These indicate hydrogen content in films is almost the same.

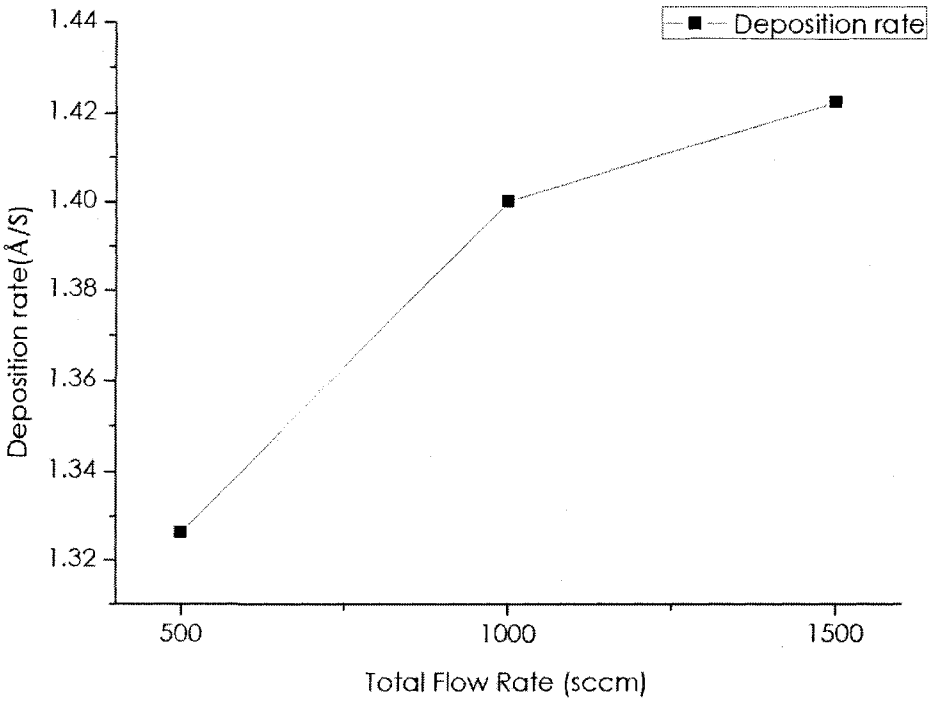

Figure 37. Deposition Rate (Å/s) Versus Times of Control Condition Residence Time.

Figure 37 shows the deposition rate versus the total flow rate. It indicates a slight increase in the deposition rate from 1.33 Å/s to 1.42 Å/s as the total flow increased.

Film Composition as a Function of Argon Dilution

The atoms of an inert gas such as argon or helium in metastable electronic states are considered to be significant in a plasma since they

are neutral particles that convey energy to the molecules of precursors. [45, 46]

In this series, all parameters were kept identical to the control condition in Table 3, except the argon flow rate. Table 6 shows the argon flows used in this set of experiments.

Run #	Argon (sccm)	NH_3 (sccm)	Silane (sccm)	H_2 (sccm)
1	0	200	8	392
2	200	200	8	392
3	400	200	8	392
4	800	200	8	392
5	1000	200	8	392

Table 6. Conditions of FILM COMPOSITION AS A FUNCTION OF ARGON DILUTION Series.

When no argon flow rate was introduced, the plasma was very filamentary and full of arcing. It was observed that the plasma homogeneity increases when the argon flow increases.

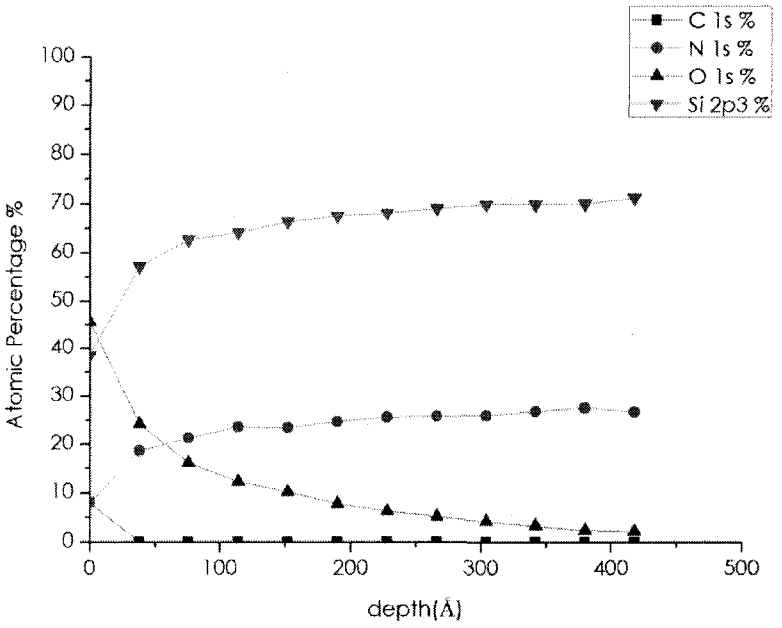

Figure 38. Depth Profile in Film Composition as a function of Argon Flow Series with Argon=0 Sccm.

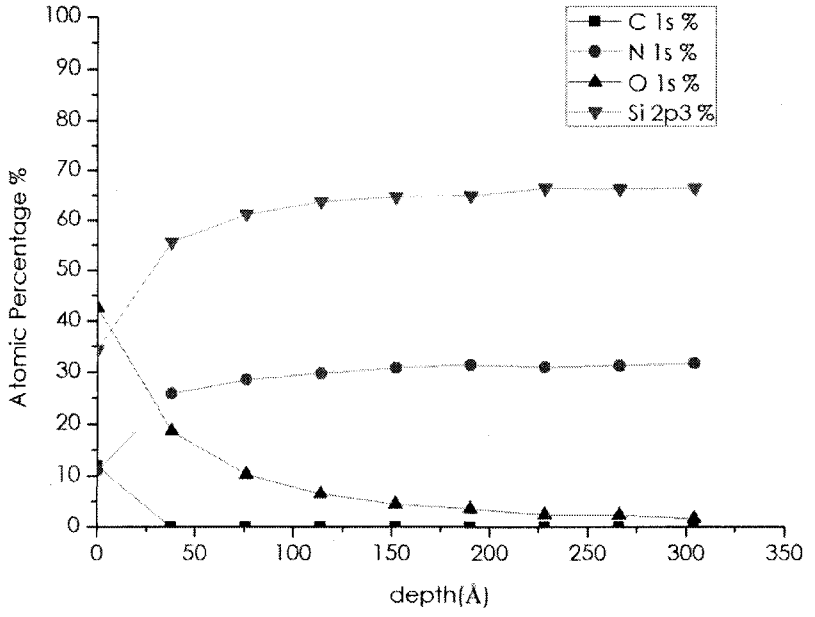

Figure 39. Depth Profile in Film Composition as a function of Argon Flow Series with Argon=200 Sccm.

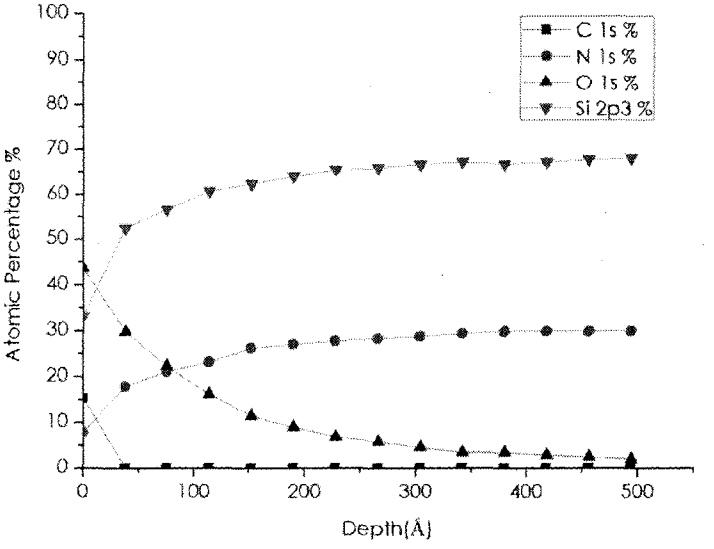

Figure 40. Depth Profile in Film Composition as a function of Argon Flow Series with Argon=400 Sccm.

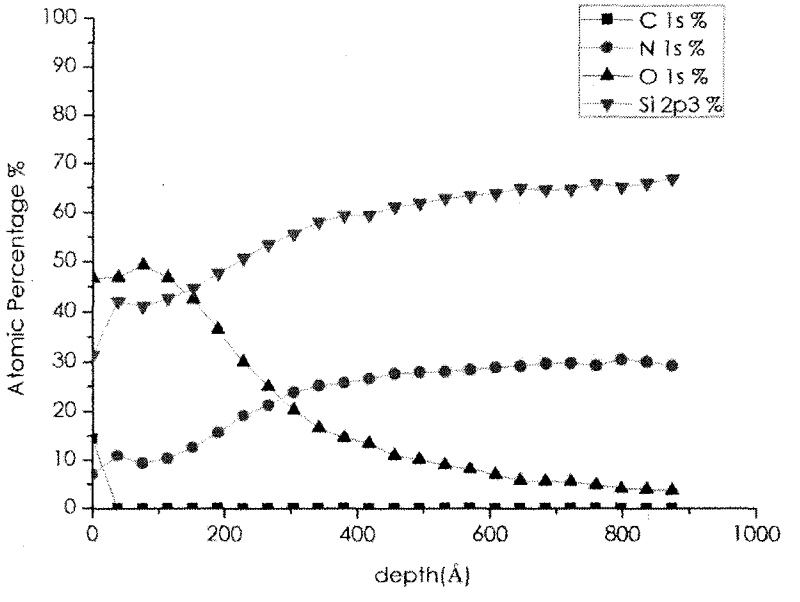

Figure 41. Depth Profile in Film Composition as a function of Argon Flow Series with Argon=800 Sccm.

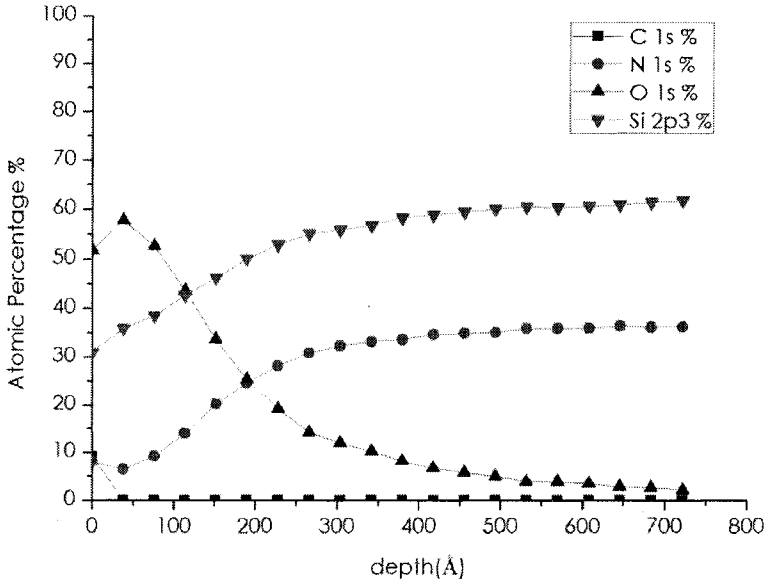

Figure 42. Depth Profile in Film Composition as a function of Argon Flow Series with Argon=1000 Sccm.

Figure 38 shows that at zero sccm argon flow rate, after 400Å, the film composition is: Si 70% N27% O 3%. The ratio of Si: N is 2.59. Before 400Å, the oxygen decreased from 46% to 3%. The silicon increased from 37% to 70% and the nitrogen increased from 7% to 27%.

Figure 39 shows that at 200 sccm argon flow rate, after 225Å, the film composition is: Si 69% N34% O 7%. The ratio of Si: N is 2.03. Before 225Å, the oxygen decreased from 43% to 7%. The silicon increased from 34% to 69% and the nitrogen increased from 7% to 34%.

Figure 40 shows that at 400 sccm argon flow rate, after 300Å, the film composition became approximately constant at Si 67% N 29% O 4%.

The ratio of Si: N is 2.31. Before 300Å, oxygen decreases from 45% to 4%. Silicon increases from 34% to 67% and nitrogen increases from 7% to 29%.

Figure 41 shows that at 800 sccm argon flow rate, after 625Å, the film composition is: Si 65% N30% O 5%. The ratio of Si: N is 2.17. Before 625Å, the oxygen decreased from 60% to 5%. The silicon increased from 30% to 65% and the nitrogen increased from 7% to 30%.

Figure 42 shows that at 1000 sccm argon flow rate, after 525Å, the film composition is: Si 63% N32% O 5%. The ratio of Si: N is 1.97. Before 525Å, the oxygen decreased from 57% to 5%. The silicon increased from 30% to 63% and the nitrogen increased from 9% to 32%.

Argon Flow (sccm)	Constant Film Composition	Onset of Constant Composition
0	Si 70% N27% O 3%	400Å
200	Si 69% N34% O 7%	225Å
400	Si 67% N 29% O 4%	300 Å
800	Si 65% N30% O 5%	625Å
1000	Si 63% N32% O 5%	525 Å

Table 7. Constant Film Composition and Onset of Constant Composition in Film Composition as a Function of Argon Dilution Series.

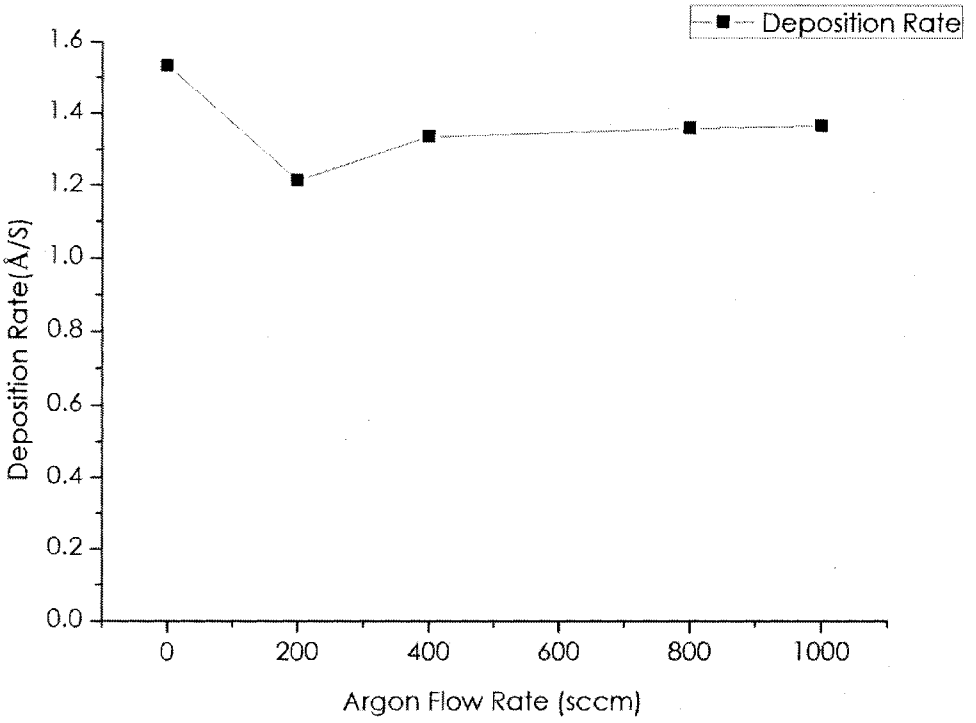

Figure 43. The Deposition Rate (Å) Versus Argon Flow Rate (Sccm).

In Figure 43, shows that the deposition rate is not significantly influenced by the argon flow rate. The deposition rate was highest when there was no argon flow.

However, it was noticed that when there was no argon flow introduced, the uniformity of the thin film was very poor. The argon flow does play an important role in the uniformity of the deposited films [48].

Film Composition as a Function of Stoichiometry

In these experiments, silicon nitride films were deposited using conditions of Table 3, except for the silane/H_2 and ammonia flows. Table 5 shows the flow rates of these gases.

Run #	NH_3 (sccm)	Argon (sccm)	SiH_4 (sccm)	H_2(sccm)	SiH_4:NH_3 ratio
1	50	400	8	392	4:25
2	100	400	8	392	2:25
3	200	400	8	392	1:25
4	400	400	8	392	1:50
5	600	400	8	392	1:75

Table 8. Conditions of Film Composition as a Function of Stoichiometry.

The plasma became weaker and less stable while the NH_3 flow rate was increased. The plasma is very stable with 50 sccm NH_3 gas flow rate, but with the 600 sccm NH_3 flow rate, the plasma was unstable and in fact, part of plasma disappeared. As the NH_3 flow rate increased, the color of the plasma turned greener. The homogeneity of the plasma remained almost the same in this series.

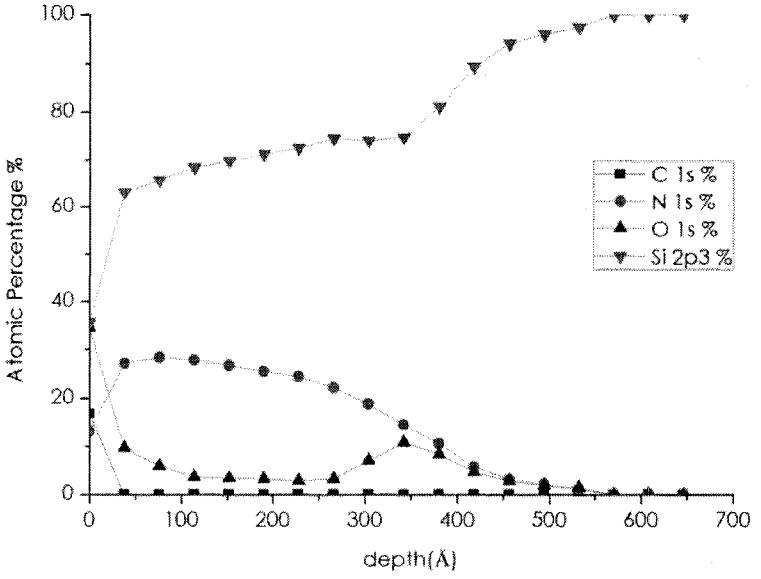

Figure 44. Depth Profile of Film Composition as a Function of Stoichiometry with NH_3 Flow Rate= 50 Sccm.

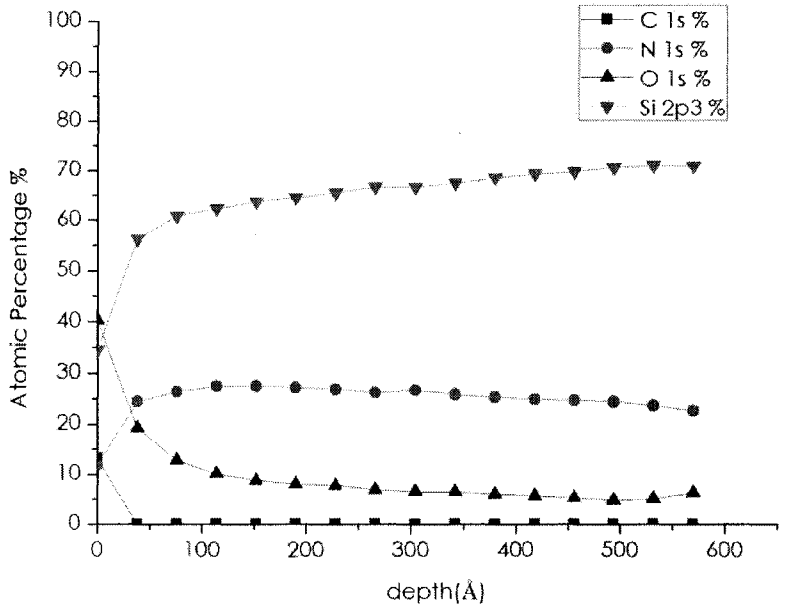

Figure 45. Depth Profile of Film Composition as a Function of Stoichiometry with NH_3 Flow Rate= 100 Sccm.

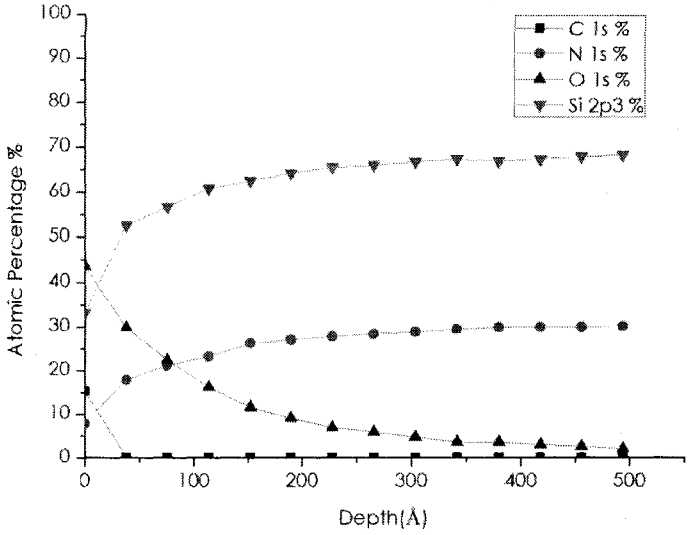

Figure 46. Depth Profile of Film Composition as a Function of Stoichiometry with NH_3 Flow Rate= 200 Sccm.

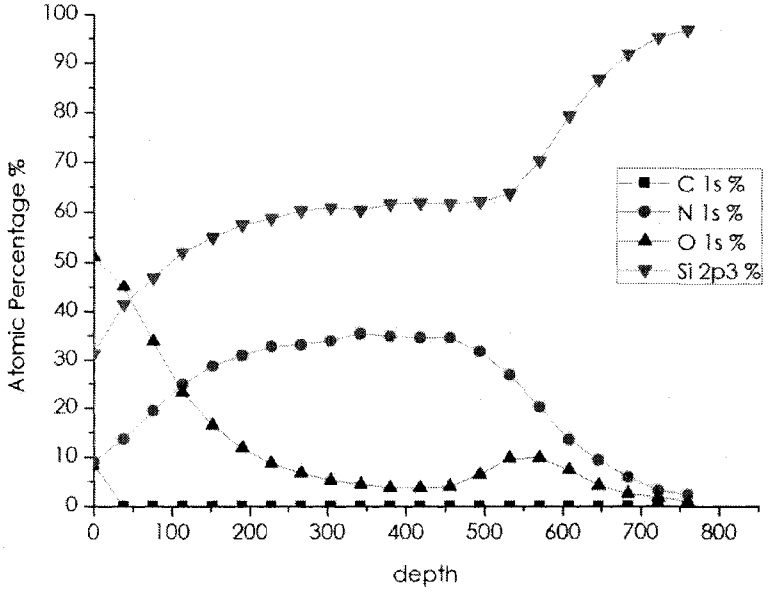

Figure 47. Depth Profile of Film Composition as a Function of Stoichiometry with NH_3 Flow Rate= 400 Sccm.

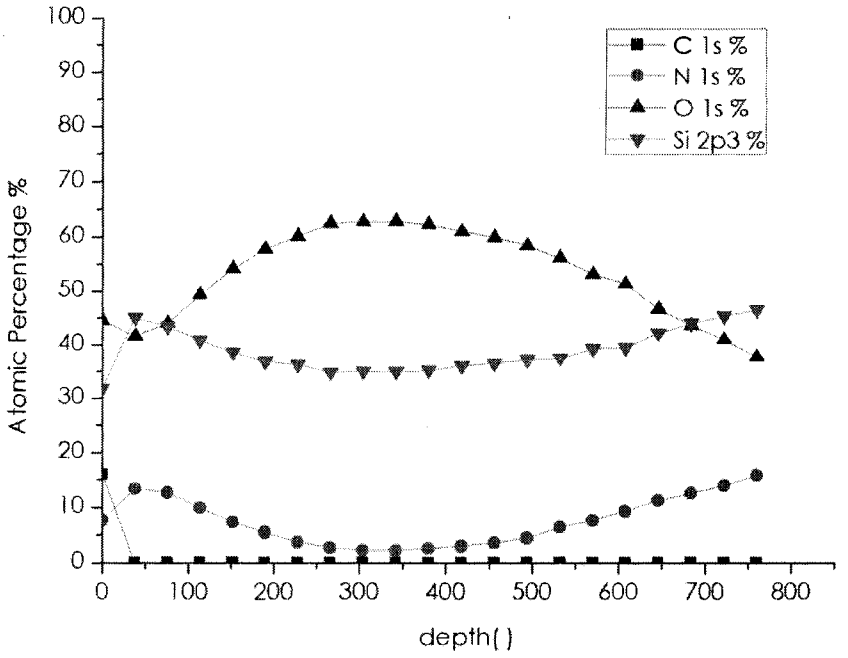

Figure 48. Depth Profile of Film Composition as a Function of Stoichiometry with NH_3 Flow Rate= 600 Sccm.

Figure 44 shows at 50 sccm of NH_3 flow rate, film composition became approximately after 45Å. The film composition is Si 65% N 30% O 10%. The ratio of Si: N is 2.17. Before 45 Å, The oxygen decreased from 35% to 10%. The silicon increased from 35% to 65% and nitrogen increased from 12% to 30%.

Figure 45 shows at 100 sccm of NH_3 flow rate, film composition became approximately after 100Å. The film composition is Si 65% N 25% O 10%. The ratio of Si: N is 2.6. Before 100 Å, The oxygen decreased from 42% to 10%. The silicon increased from 35% to 65% and nitrogen increased from 12% to 25%.

Figure 46 shows at 200 sccm of NH_3 flow rate, the film composition became approximately constant after 300Å at Si 67% N 29% O 4%. The ratio of Si: N is 2.31. Before 300Å, oxygen decreases from 45% to 4%. Silicon increases from 34% to 67% and nitrogen increases from 7% to 29%.

Figure 47 shows at 400 sccm of NH_3 flow rate, film composition became approximately after 350Å. The film composition is Si 60% N30% O 10%. The ratio of Si: N is 2.0. Before 350 Å, The oxygen decreased from 52% to 10%. The silicon increased from 30% to 65% and nitrogen increased from 10% to 30%.

Figure 48 shows at 800 sccm of NH_3 flow rate, film composition became approximately after 750Å. The film composition is Si 50% N20% O 30%. The ratio of Si: N is 2.5. Before 750 Å, The film composition is Si 35% N5% O 60%. This is mainly silicon dioxide before 750 Å

NH_3 Flow (sccm)	Constant Film Composition	Onset of Constant Composition
50	Si 65% N 30% O 10%	45 Å
100	Si 65% N 25% O 10%	100Å
200	Si 67% N 29% O 4%	300Å
400	Si 60% N30% O 10%	350Å
600	Si 50% N20% O 30%	750 Å

Table 9. Constant Film Composition and Onset of Constant Composition in Film Composition as a Function of Stoichiometry series.

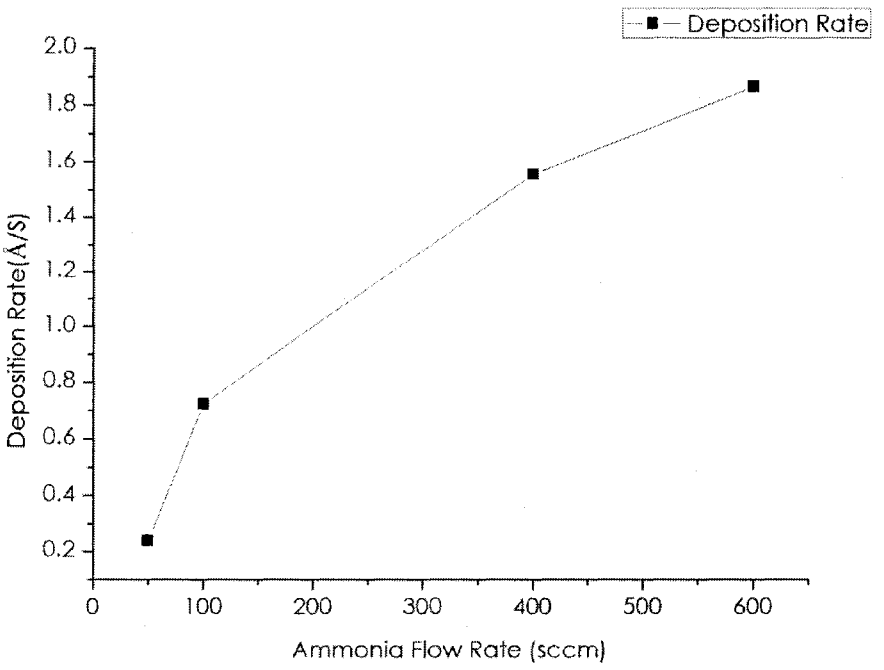

Figure 49. Deposition Rate of Films in Film Composition as a Function of Stoichiometry series.

Figure 49 shows that the deposition rate increases with the NH_3 flow rate. At 50 sccm NH_3 flow rate, the deposition rate is only 0.22 Å /s. The deposition rate increased to nearly 1.9 Å /s for the 500 sccm NH3 flow rate.

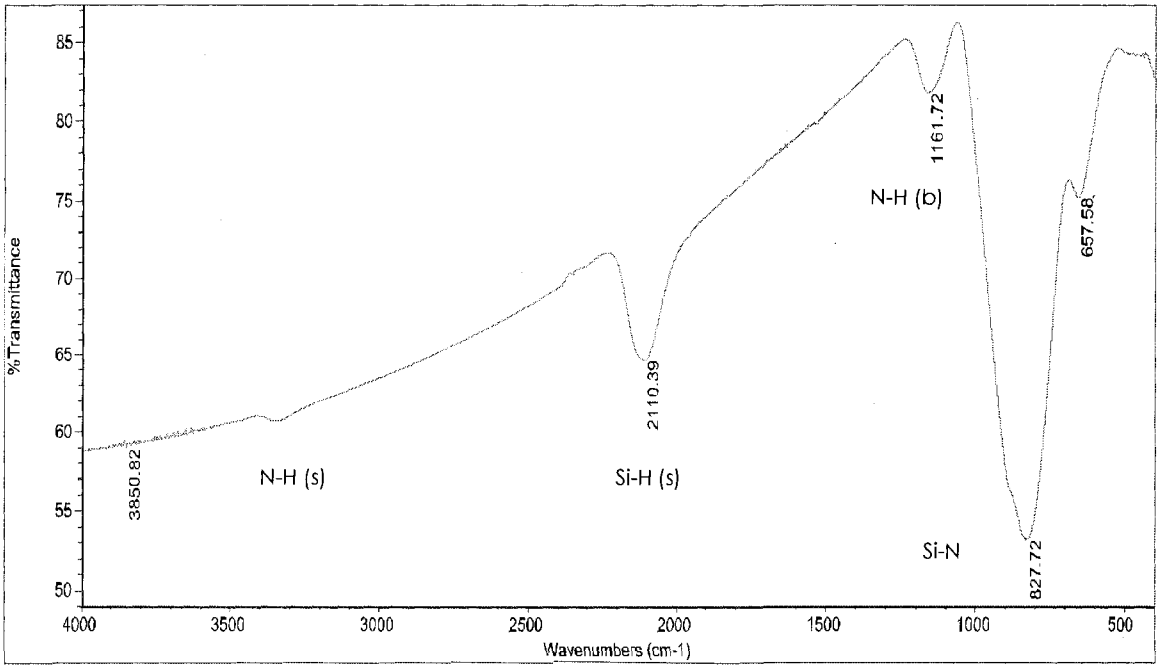

Figure 50. FTIR Spectrum of Film with 50 sccm of NH_3 Flow Rate in Film Composition as a Function of Stoichiometry Series.

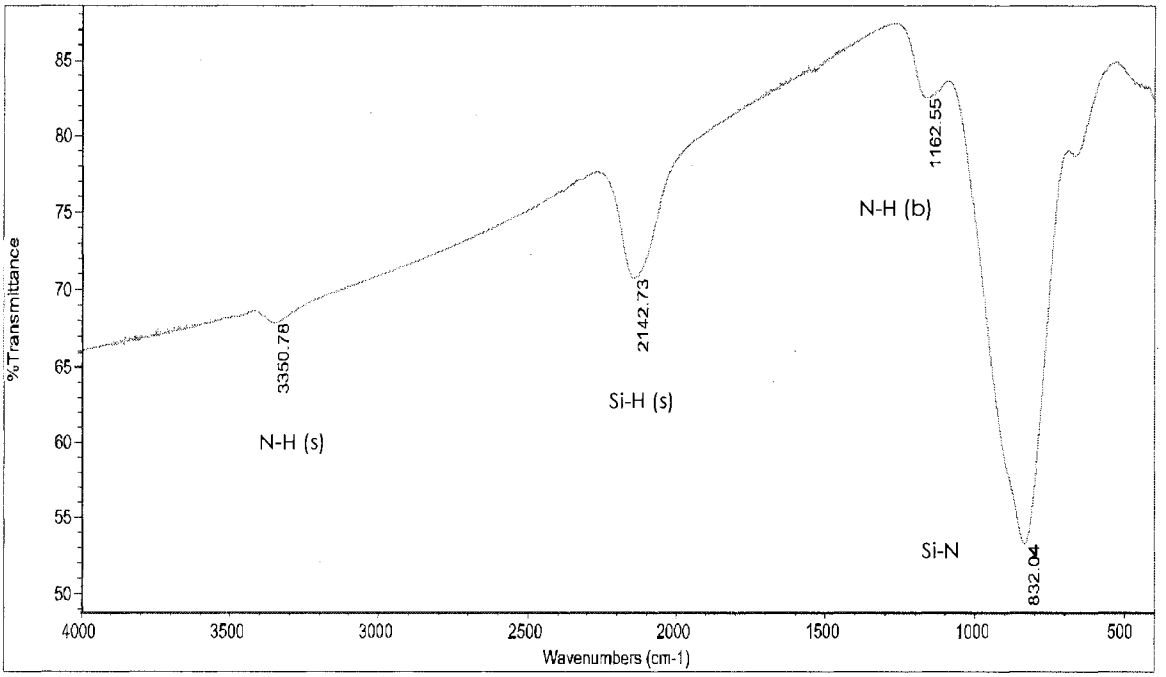

Figure 51. FTIR Spectrum of Film with 100 sccm of NH_3 Flow Rate in Film Composition as a Function of Stoichiometry Series.

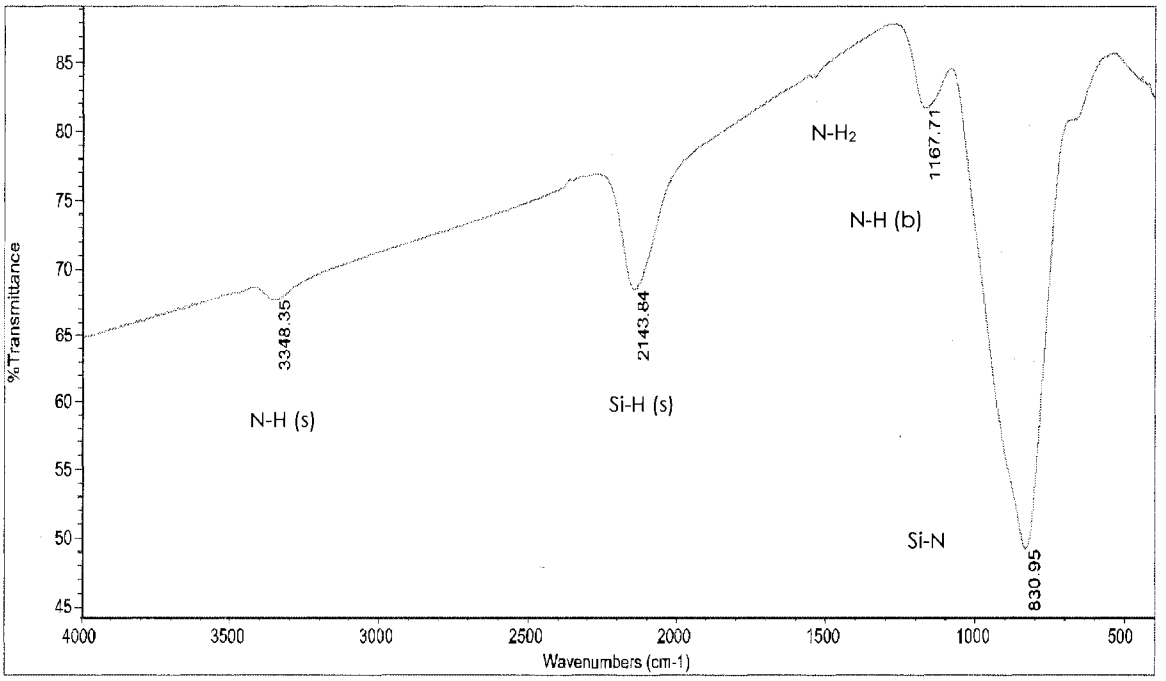

Figure 52. FTIR Spectrum of Film with 200 sccm of NH_3 Flow Rate in Film Composition as a Function of Stoichiometry Series.

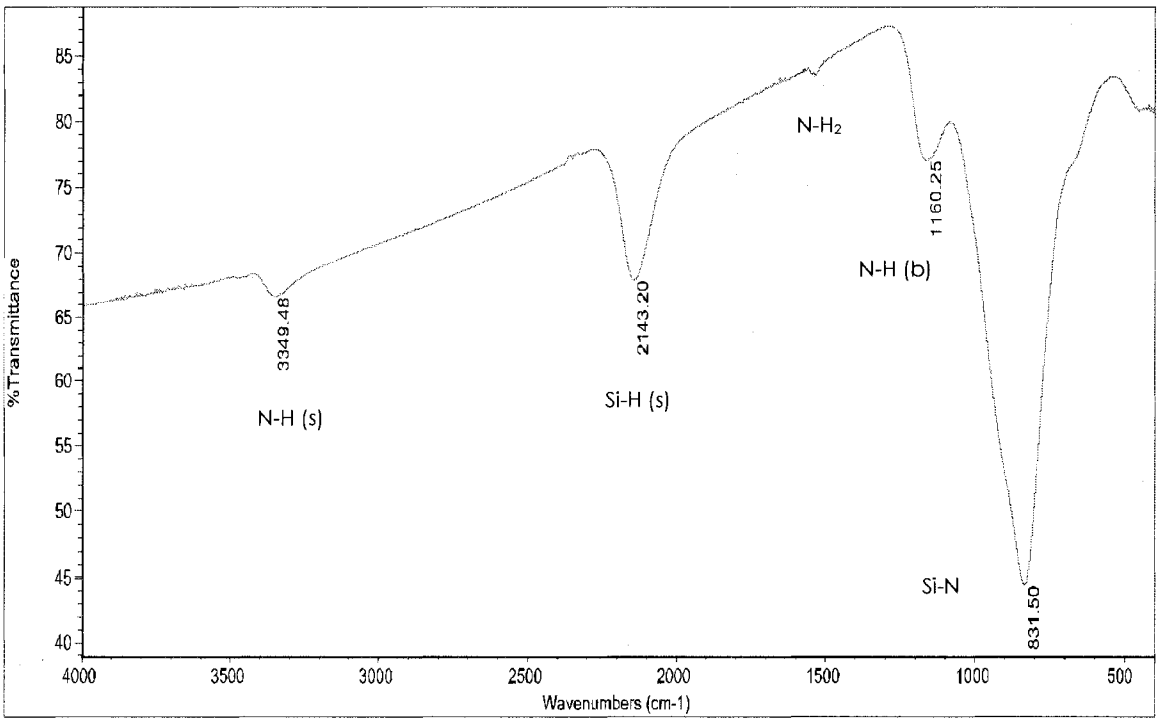

Figure 53. FTIR Spectrum of Film with 400 sccm of NH_3 Flow Rate in Film Composition as a Function of Stoichiometry Series.

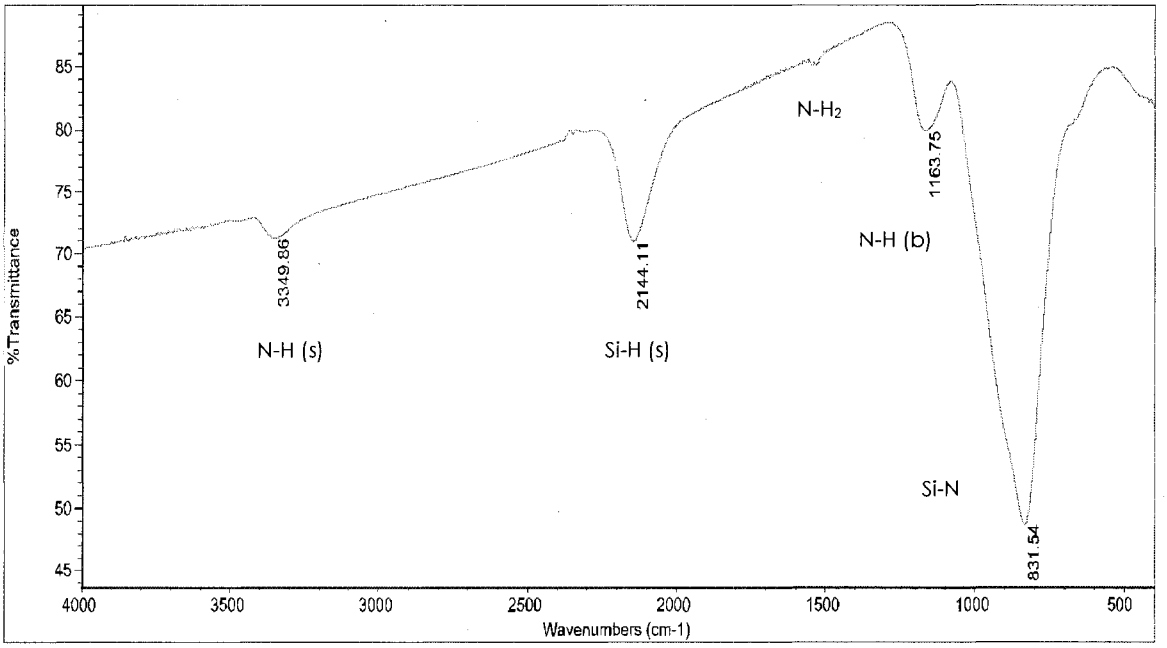

Figure 54. FTIR Spectrum of Film with 600 sccm of NH_3 Flow Rate in Film Composition as a Function of Stoichiometry Series.

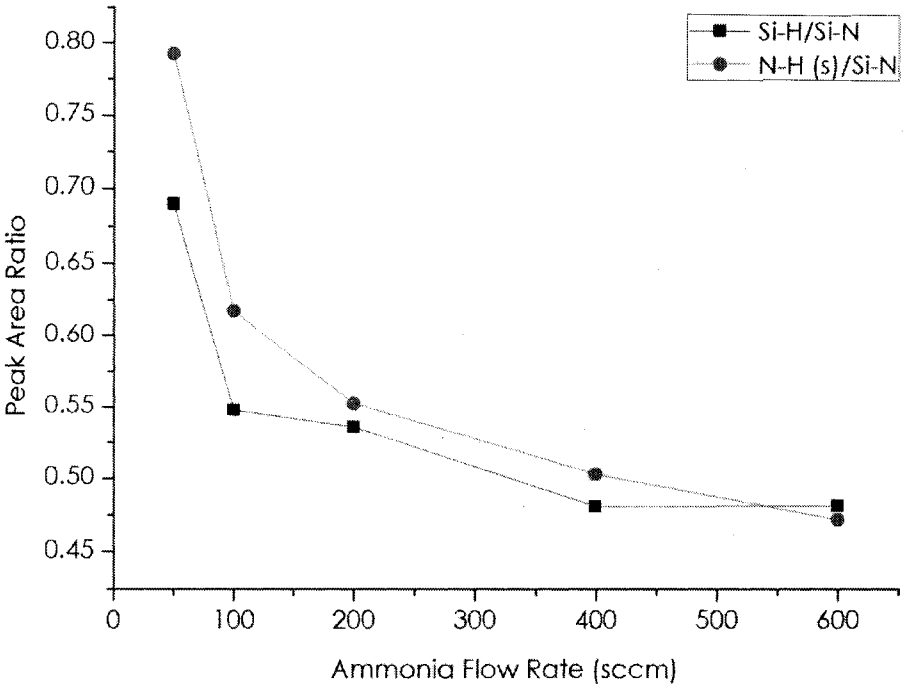

Figure 55. The Si-H and N-H (S) to Si-N Peak Area Ratio.

Figure 55 shows that the ratio of Si-H and N-H (s) to Si-N decreases with the increase of the NH_3 flow rate. This indicates that the hydrogen content of the film decreased at higher NH_3 flows.

Film Composition as a Function of Frequency

The applied frequency can affect the ion and atom density as well as the energy of the plasma particles [49]. In turn, these variances could have an effect on the deposited silicon nitride films. The kinetic energy of ions affected by the excitation frequency will have impact on the

deposition rate [50]. It was also reported that at lower frequency the ion bombardment was very intense and that could lead to more ions and free radicals density [51].

In this series of experiments, all other deposition conditions were kept the same as Table 3 except for the frequency. The frequency was adjusted by the function generator to be: 1.5 KHz, 3 KHz, and 4 KHz etc as shown in Table 6.

Run #	Frequency (K Hz)	SiH_4 (sccm)	H_2 (sccm)	NH_3 (sccm)	Ar (sccm)
1	1.5	8	392	200	400
2	2	8	392	200	400
3	3	8	392	200	400
4	3.5	8	392	200	400
5	4	8	392	200	400

Table 10. Parameters of Film Composition as a Function of Frequency.

The plasma became more homogeneous when the applied frequency increased. The plasma at 1.5 KHz was more homogeneous and less filamentary than it in the 1 KHz. However, due to the limitation of the transformer as well as the power amplifier, no plasma can be obtained above 4K Hz, and the plasma became very unstable at the frequency of

3.5 K Hz. For this series, the best range of frequency at the 5mm gap was between 0.8K to 3K Hz.

At lower frequencies, the initial input current to ignite the plasma was smaller than it was for the higher frequencies. For example, at 1.5K, it only required about 7 A current to ignite the plasma, while at 3.5K Hz, the input current reached about 13A.

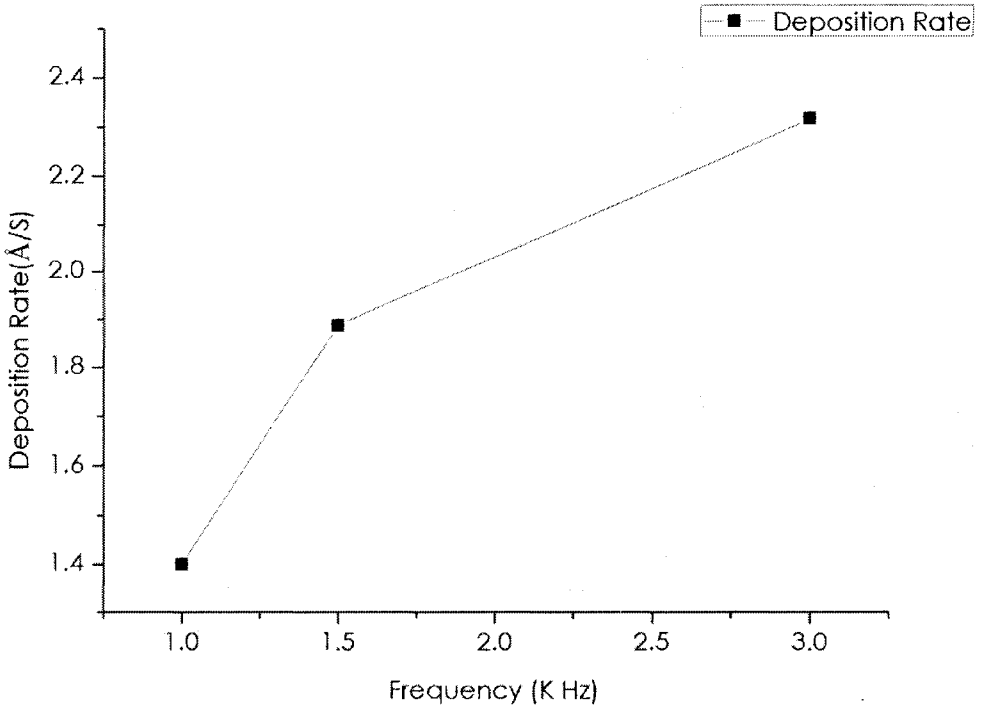

Figure 56. Deposition Rate versus the Frequency.

The applied frequency does have a significant effect on the deposition rate of the films. Figure 56 shows the deposition rate versus frequency. At 3K Hz frequency, the deposition rate reached about 2.3 Å/s while at 1K Hz frequency, the deposition rate was only 1.4 Å/s.

The uniformity of the film was greatly affected by the frequency. At higher frequencies, the uniformity of the whole film across the wafer was greatly reduced. Also, due to the higher frequency, the carbon conductive paint used to measure the thickness on the surface of the silicon wafer was spread across the wafers; no such phenomenon was detected at lower frequencies.

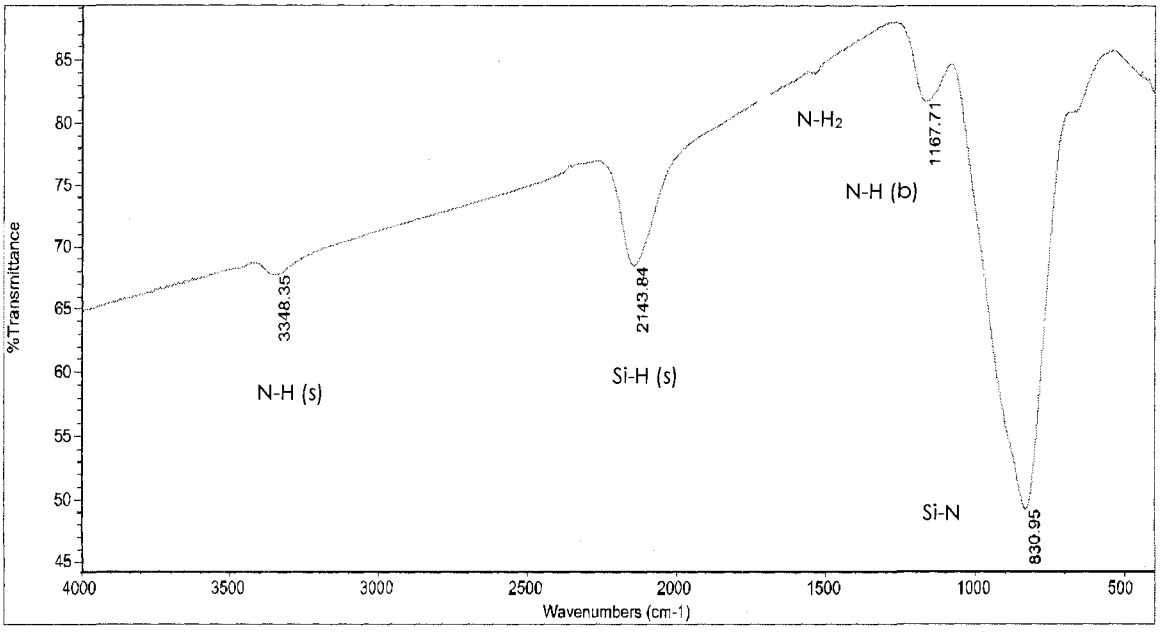

Figure 57. FTIR Spectrum of Film at 1K Hz Frequency in Film Composition as a Function of Frequency Series.

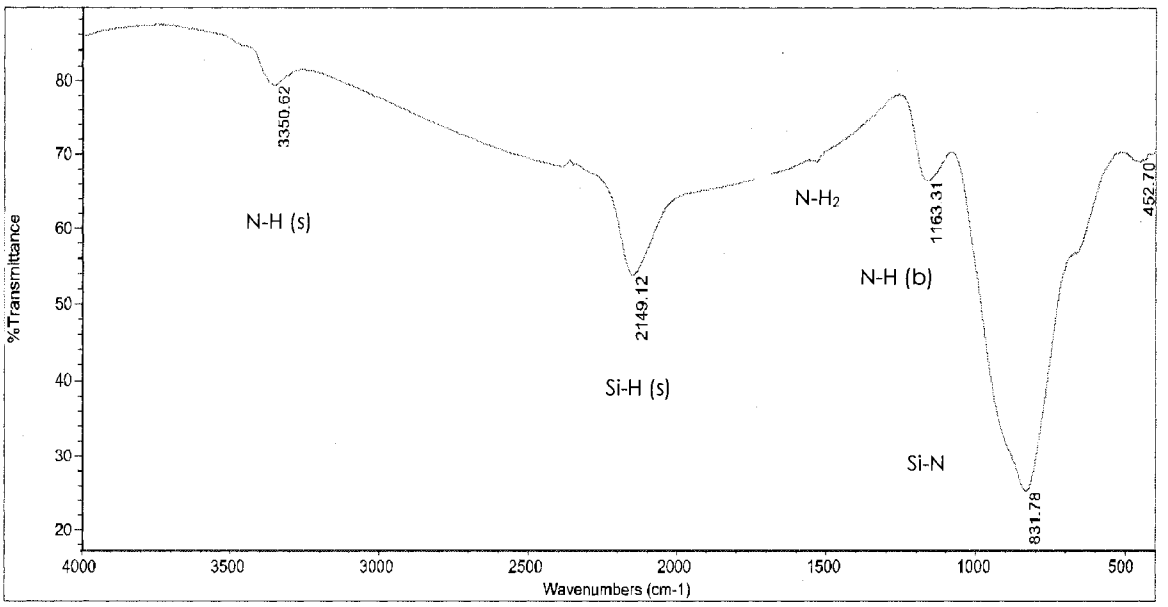

Figure 58. FTIR Spectrum of Film at 1.5K Hz Frequency in Film Composition as a Function of Frequency Series.

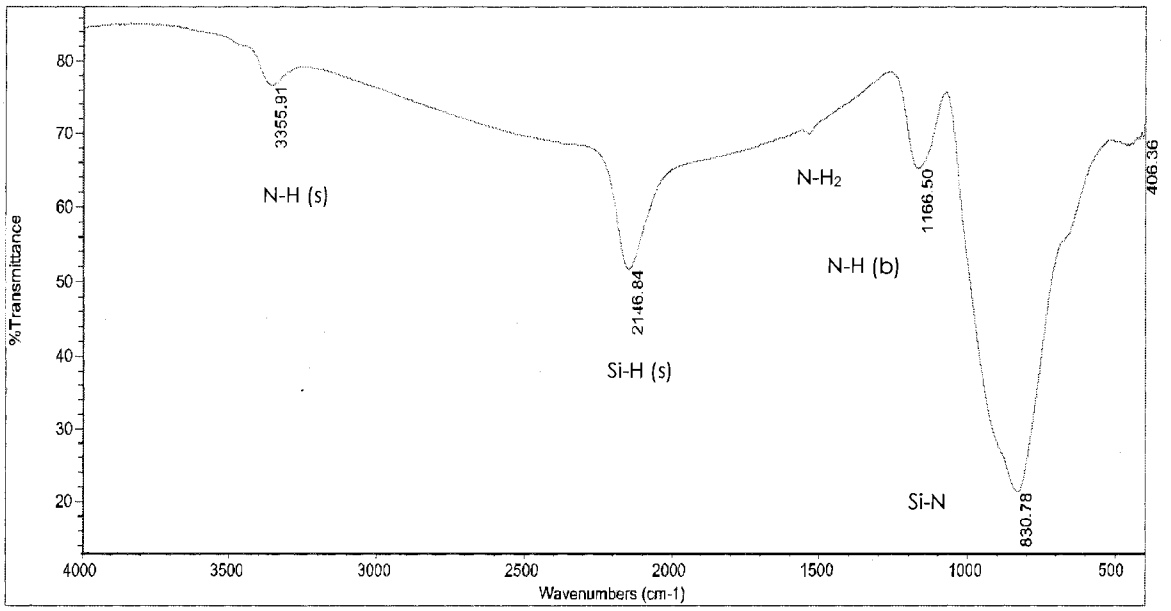

Figure 59. FTIR Spectrum of Film at 2K Hz Frequency in Film Composition as a Function of Frequency Series.

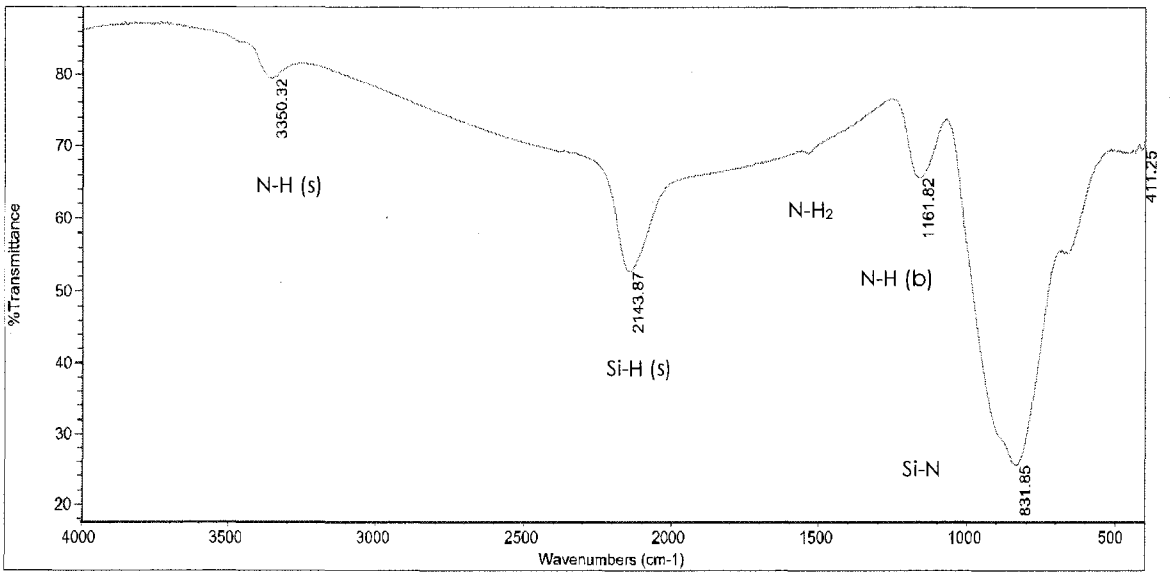

Figure 60. FTIR Spectrum of Film at 3K Hz Frequency in Film Composition as a Function of Frequency Series.

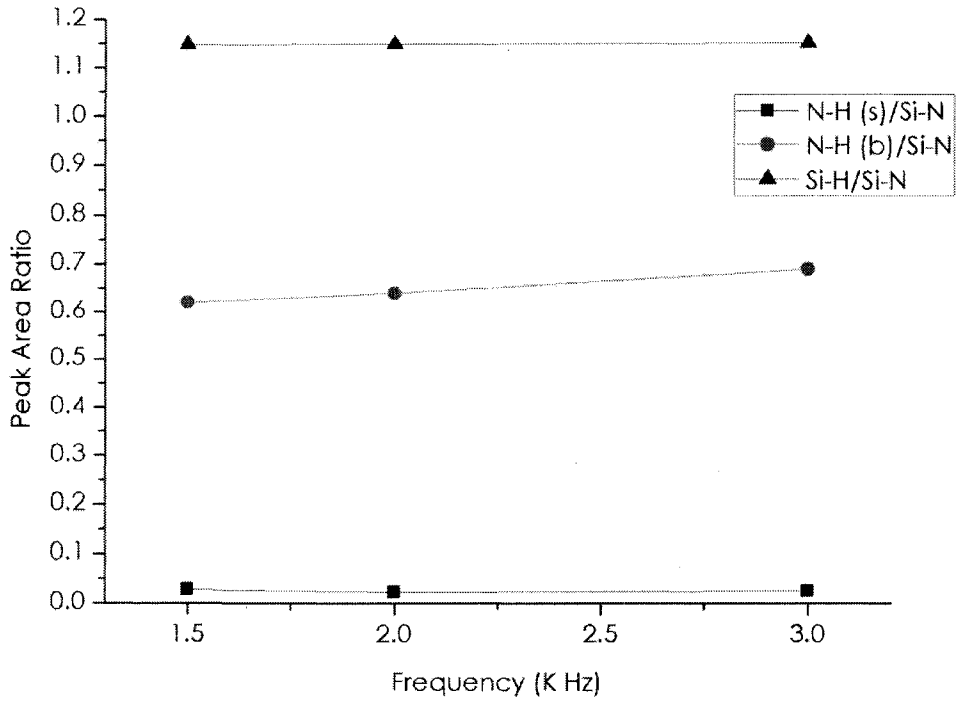

Figure 61. FTIR Peak Ratios of Film in Film Composition as a Function of Frequency series.

Figure 61 shows FTIR peak ratios of N-H peak area to Si-N peak area and Si-H peak area to Si-N peak area. It shows that there was no significant difference within this series. The hydrogen bonding within the deposited films appeared to be almost the same at various frequencies.

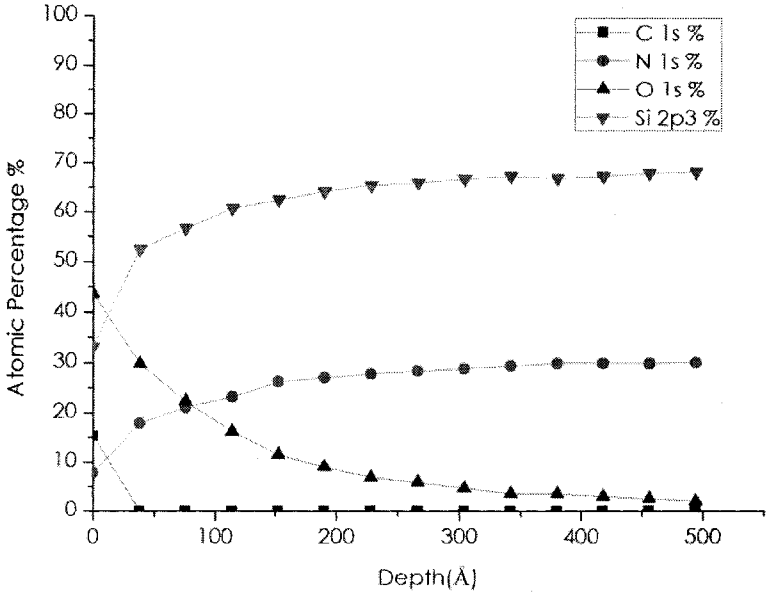

Figure 62. XPS Depth Profile of Film Composition as a Function of Frequency at Frequency 1 K Hz.

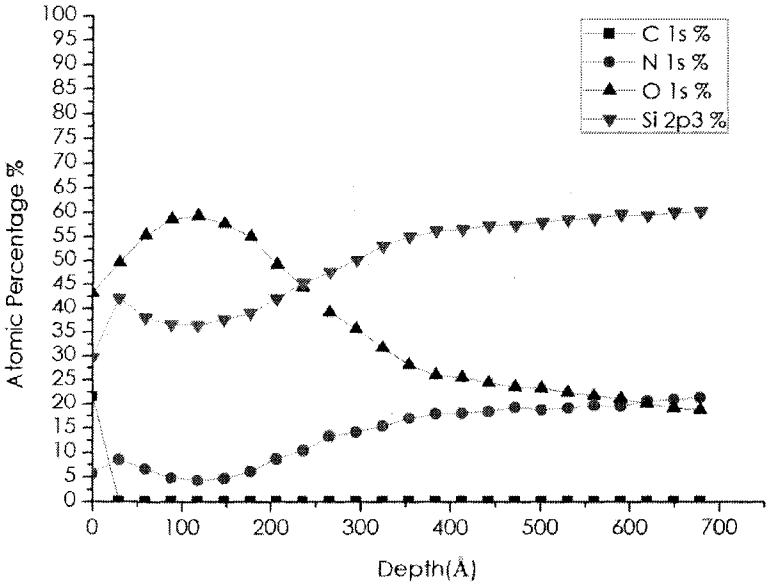

Figure 63. XPS Depth Profile of Film Composition as a Function of Frequency at Frequency 1.5K Hz.

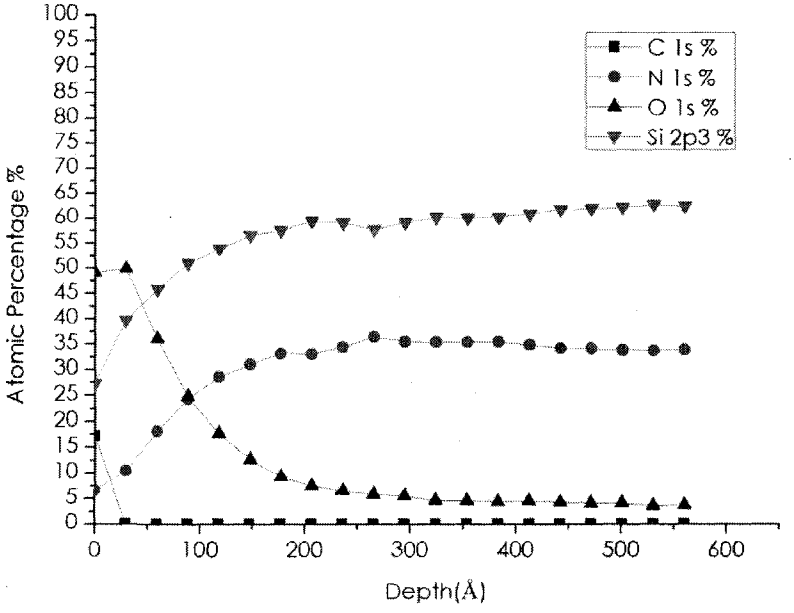

Figure 64. XPS Depth Profile of Film Composition as a Function of Frequency at Frequency 3K Hz.

Figure 62 shows at 1K Hz frequency, the film composition became approximately constant after 300Å at Si 67% N 29% O 4%. The ratio of Si: N is 2.31. Before 300Å, oxygen decreases from 45% to 4%. Silicon increases from 34% to 67% and nitrogen increases from 7% to 29%.

Figure 63 shows at 1.5K Hz frequency, the film composition became approximately constant after 350Å at Si 57% N 17% O 26%. The ratio of Si: N is 3.35. Before 350Å, the film composition is Si 35% N 5% O 60%. This is mostly silicon dioxide.

Figure 64 shows at 3K Hz frequency, the film composition became approximately constant after 200Å at Si 60% N 35% O 5%. The ratio of Si: N is 1.7. Before 200Å, oxygen decreases from 50% to 5%. Silicon increases from 27% to 60% and nitrogen increases from 7% to 35%.

Frequency	Constant Film Composition	Onset of Constant Composition
1K Hz	Si 67% N 29% O 4%	300Å
1.5K Hz	Si 57% N 17% O 26%	350Å
3K Hz	Si 60% N 35% O 5%	200Å

Table 11. Constant Film Composition and Onset of Constant Composition of Films in Film Composition as a Function of Frequency Series.

Film Composition Using Nitrogen as Precursor

In this series of experiments, the nitrogen was used instead of ammonia. Otherwise, the conditions were those of Table 3 except for temperature was 350°C. No argon flow was introduced in this series and the total flow rate was kept constant at 1000 sccm. The silane to nitrogen ratios are listed in Table 7.

Run #	Silane:N_2	Silane (sccm)	H_2 (sccm)	N_2 (sccm)
1	1:75	8	392	600
2	1:50	10	490	500
3	1:200	4	196	800

Table 12. Parameters of Precursors in Film Composition Using Nitrogen as Precursor.

The plasma was very homogeneous when nitrogen was introduced at a silane: N_2 ratio of 1:50; however, the plasma became unstable with an increase in the nitrogen gas flow rate. When the ratio of silane: N_2 was 1:200, the plasma is unstable and very weak.

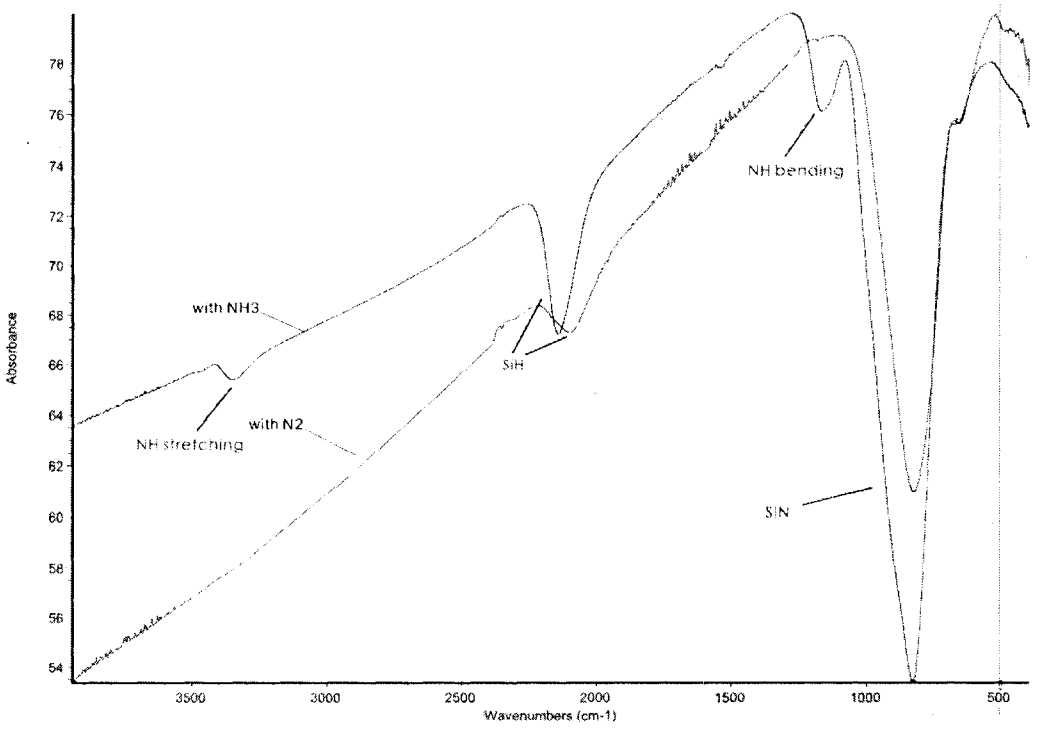

Figure 65. FTIR Absorbance Spectrums with Ammonia and Nitrogen.

Figure 65 shows that with nitrogen as the precursor instead of ammonia, no N-H stretching (near 3348 cm^{-1}) and N-H bending (near 1167 cm^{-1}) peaks are observed in the FTIR spectrum. The Si-H peak (near 2143 cm^{-1}) was very weak when nitrogen was used.

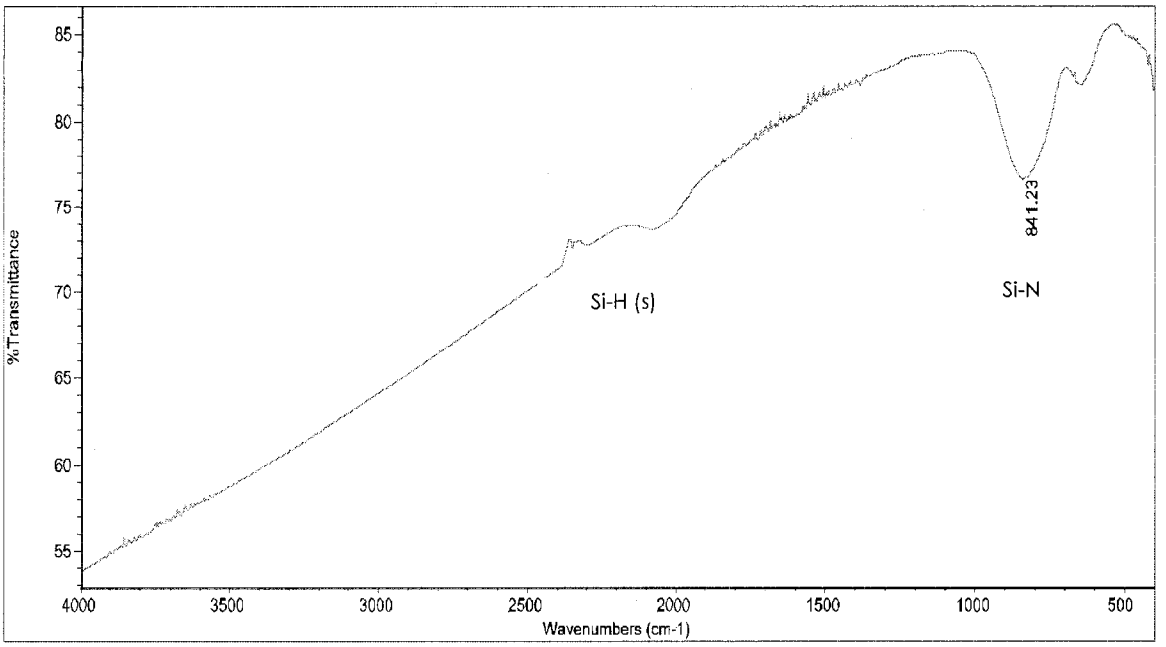

Figure 66. FTIR Spectrum of Film with N_2=500 sccm in Film Composition using Nitrogen as Precursor.

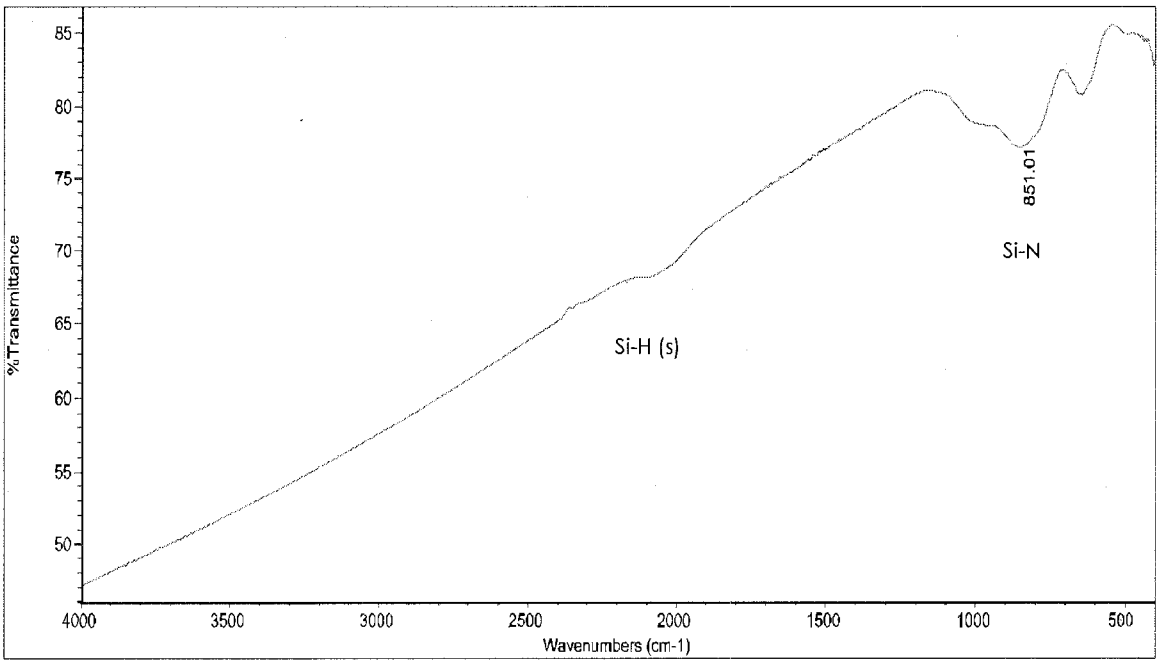

Figure 67. FTIR Spectrum of Film with N_2=600 sccm in Film Composition using Nitrogen as Precursor.

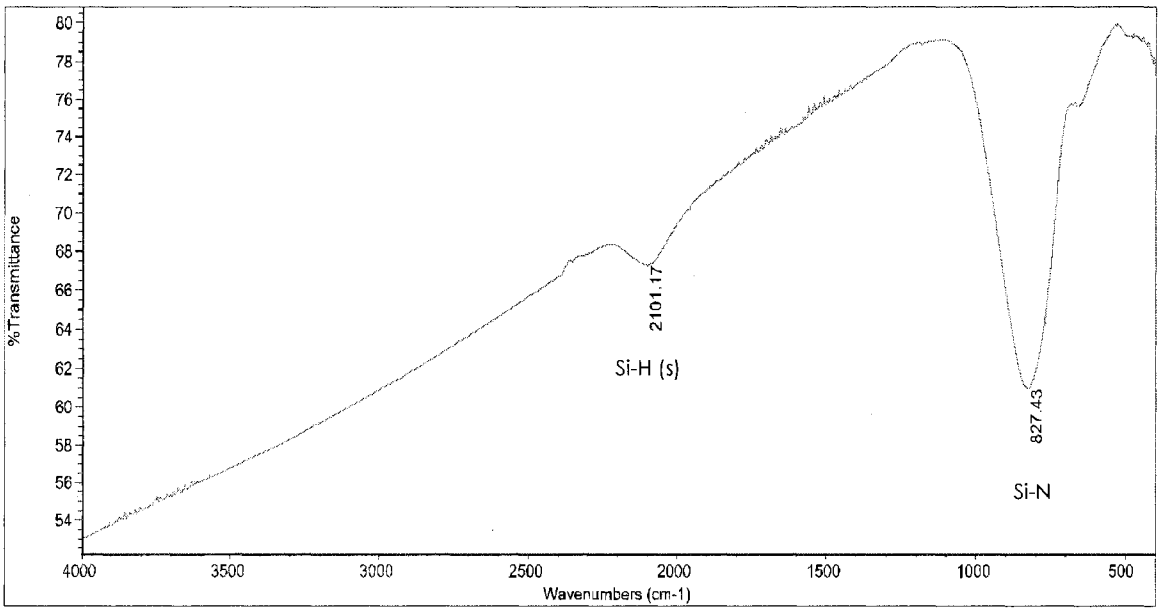

Figure 68. FTIR Spectrum of Film with N_2=800 sccm in Film Composition using Nitrogen as Precursor.

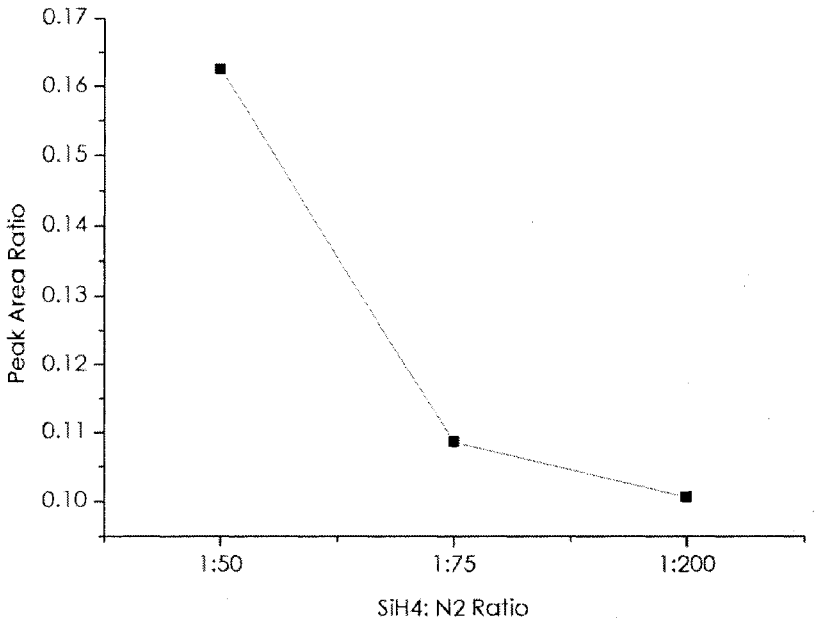

Figure 69. FTIR Si-H/Si-N Peak Ratio of Film Composition as a Function of Nitrogen Precursor.

Figure 69 shows that the Si-H/Si-N ratio decreased when the nitrogen gas flow increased. This illustrates that when the ratio of nitrogen to silane/H_2 increased, the hydrogen bonding as Si-H decreased.

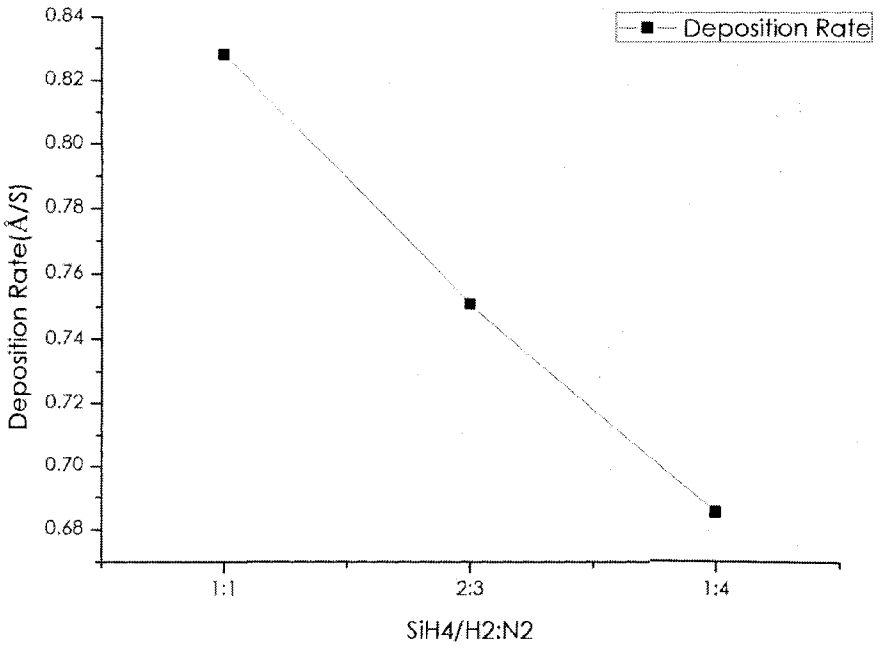

Figure 70. Film Deposition Rate of Films in Film Composition as a Function of Nitrogen Precursor.

The deposition rate declined from 0.84 Å/s to 0.69 Å/s when the ratio of nitrogen to silane increased. However, in this series, the deposition rate of the silicon nitride film was very low compared to films made with ammonia (1.6 Å/s). This is probably due to the chemical bond strength in N_2 is greater than the nitrogen-hydrogen bonding in the ammonia. It is much harder for the plasma to break the nitrogen-nitrogen bonding than nitrogen-hydrogen bonding.

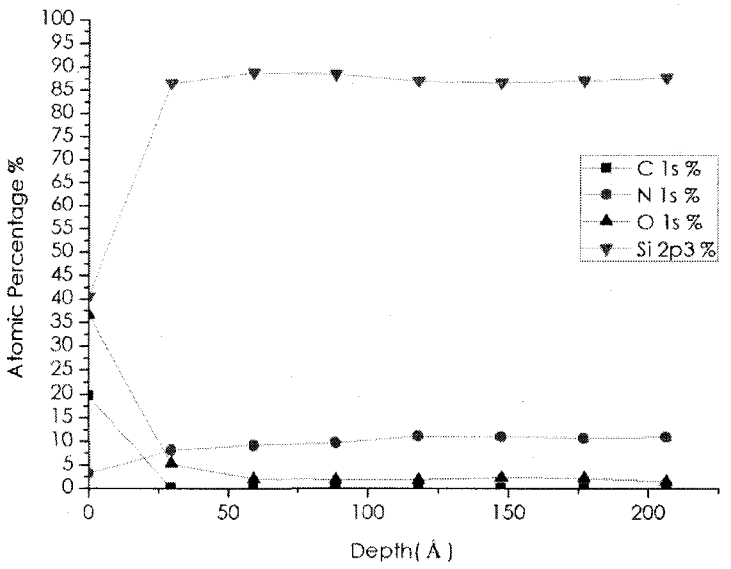

Figure 71. Depth Profile of Film in Film Composition as a Function of Nitrogen Precursor with N_2:SiH_4 =50:1.

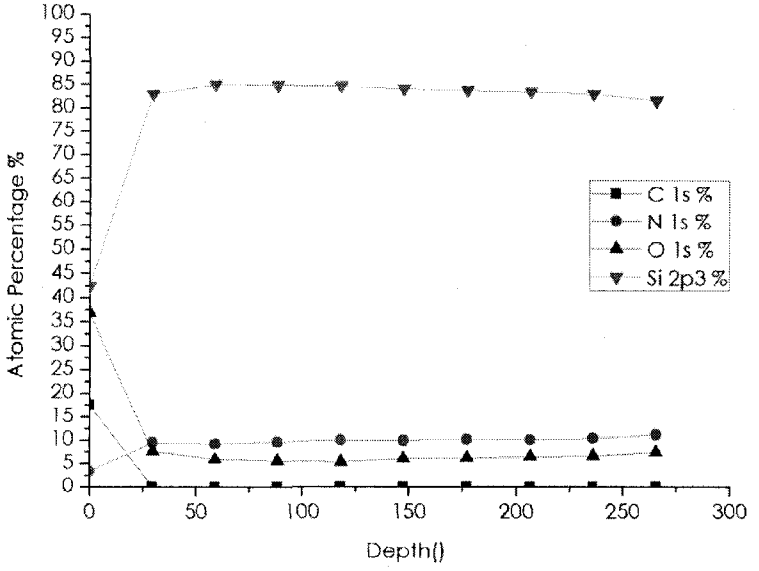

Figure 72. Depth Profile of Film Composition as A Function of Nitrogen Precursor with N_2:SiH_4=75:1.

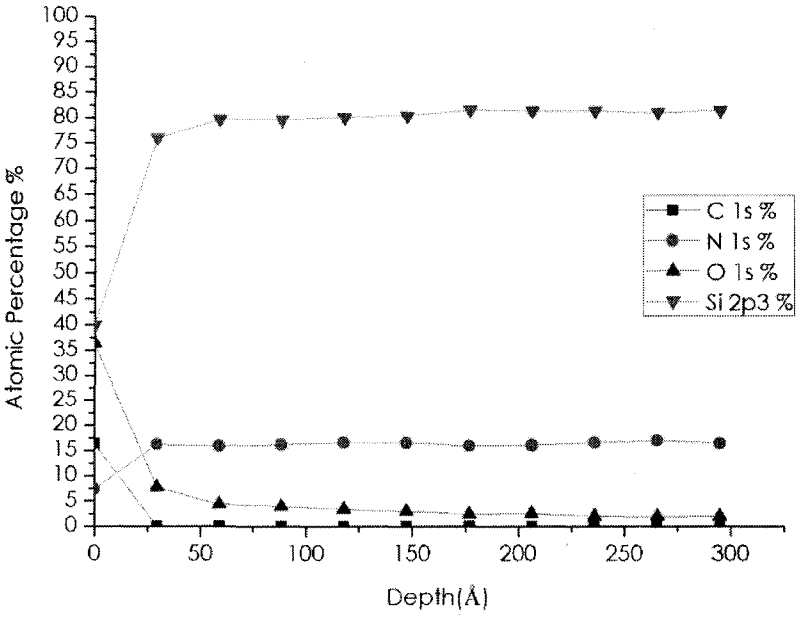

Figure 73. Depth Profile of Film Composition as a Function of Nitrogen Precursor with N_2:SiH_4 =200:1.

Figure 72 shows at SiH_4:N_2=1:75, film composition became approximately constant after 25Å at Si 86% N11% O 3%. The ratio of Si: N is 7.82. Before 25Å, the oxygen decreased from 37% to 3%. The silicon increased from 40% to 86% and nitrogen increased from 2% to 11%.

Figure 71 shows at SiH_4:N_2=1:50, film composition became approximately constant after 25Å at Si 83% N11% O 6%. The ratio of Si: N is 7.55. Before 25Å, the oxygen decreased from 37% to 6%. The silicon increased from 40% to 83% and nitrogen increased from 2% to 6%.

Figure 73 shows at SiH_4:N_2=1:200, film composition became approximately constant after 75Å at Si 78% N18% O 4%. The ratio of Si: N is

4.33. Before 75Å, the oxygen decreased from 37% to 4%. The silicon increased from 40% to 78% and nitrogen increased from 7% to 18%.

Ratio of N_2:SiH_4	Constant Film Composition	Onset of Constant Composition
50:1	Si 83% N11% O 6%	25Å
75:1	Si 86% N11% O 3%	25Å
200:1	Si 78% N18% O 4%	75Å

Table 13. Constant Film Composition and Onset of Constant Composition as a Function of Ratio of N_2:SiH_4.

From the above Figures of XPS depth profiles, the deposited silicon nitride films were silicon rich films. The silicon atomic percentage decreased from 86% to 78% as the ratio of nitrogen to silane increased from 75:1 to 200:1. The nitrogen atomic percentage increased 11% to 18% when the ratio of nitrogen to silane increased from 50:1 to 200:1. The ratio of silicon to nitrogen drops at higher ratio of nitrogen to silane.

Film Composition with Varied H_2 flow rate with silane/Argon and ammonia

We already knew that the argon gas in the plasma played a significant role in plasma behavior as well as the deposited silicon nitride films. However, the investigation of hydrogen flow rate effect to the

plasma as well as the films was been undertaken. What's more, hydrogen molecules are also believed to have an essential effect to the plasma recombination, which means that ions in the plasma form new neutral atoms by capturing the free energetic electrons [52].

In this series, the gas used was 2% silane while the amount of argon was 98%.

In this series, the ratio of silane to ammonia was constant at 25:1. The hydrogen gas flow rates were varied from 0 sccm to 700 sccm and the total gas flow rate was maintained at 1000 sccm. The other parameters were those of Table 3. Table 8 shows:

Run #	Silane (sccm)	argon (sccm)	Ammonia (sccm)	Hydrogen (sccm)
1	133.2	532.8	333	0
2	131.2	524.8	328	15
3	126.6	506.4	316	50
4	120	480	300	100
5	106.6	426.4	266	200
6	93.2	372.8	233	300
7	66.6	266.4	166	500
8	40	160	100	700

Table 14. Parameters of Gas Precursors in the Film Composition as a Function of Varied H_2 Flow Rate with Silane/Argon and Ammonia.

During this series of experiment, hydrogen content played an important role in the homogeneity of the plasma. The plasma became more and more homogeneous with the increased hydrogen flow rate. But the plasma was very filamentary when hydrogen flow rate was stopped.

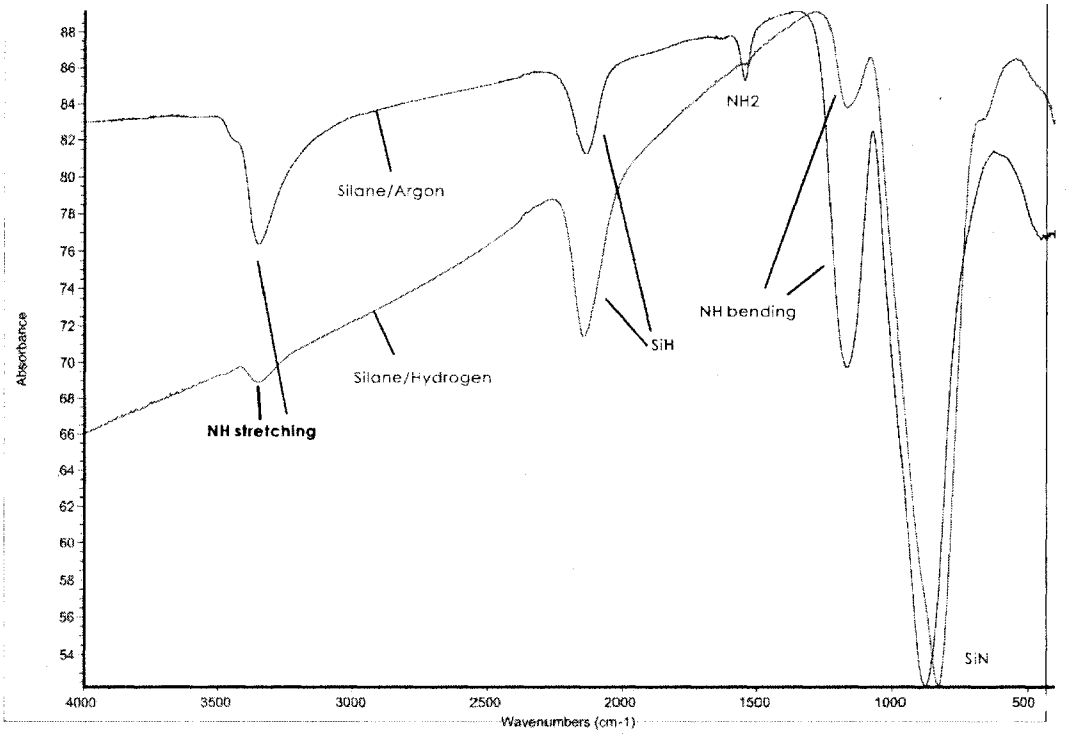

Figure 74. FTIR Spectrums with Utility of Silane/Argon and Silane/Hydrogen.

Figure 74 shows two FTIR spectrums of deposited silicon nitride films. The upper silicon nitride spectrum was deposited using silane/Argon flow of 666 sccm and an ammonia flow of 333 sccm without any hydrogen. The lower silicon nitride spectrum was deposited using a silane/hydrogen flow of 400 sccm, ammonia at 200 sccm and argon at 400 sccm. One noticeable difference is the NH_2 scissors bending peak located at

wavenumber around 1545 cm^{-1} [43]. Plus, the N-H bending (near 1167 cm^{-1}) and N-H stretching (near 3350 cm^{-1}) peaks are stronger in the silane/argon film compared to the film deposited with silane/hydrogen and ammonia. The NH2 scissors bending peak became weaker and weaker along with the increase of hydrogen flow rate and it almost disappeared when the hydrogen flow rate reached 700 sccm.

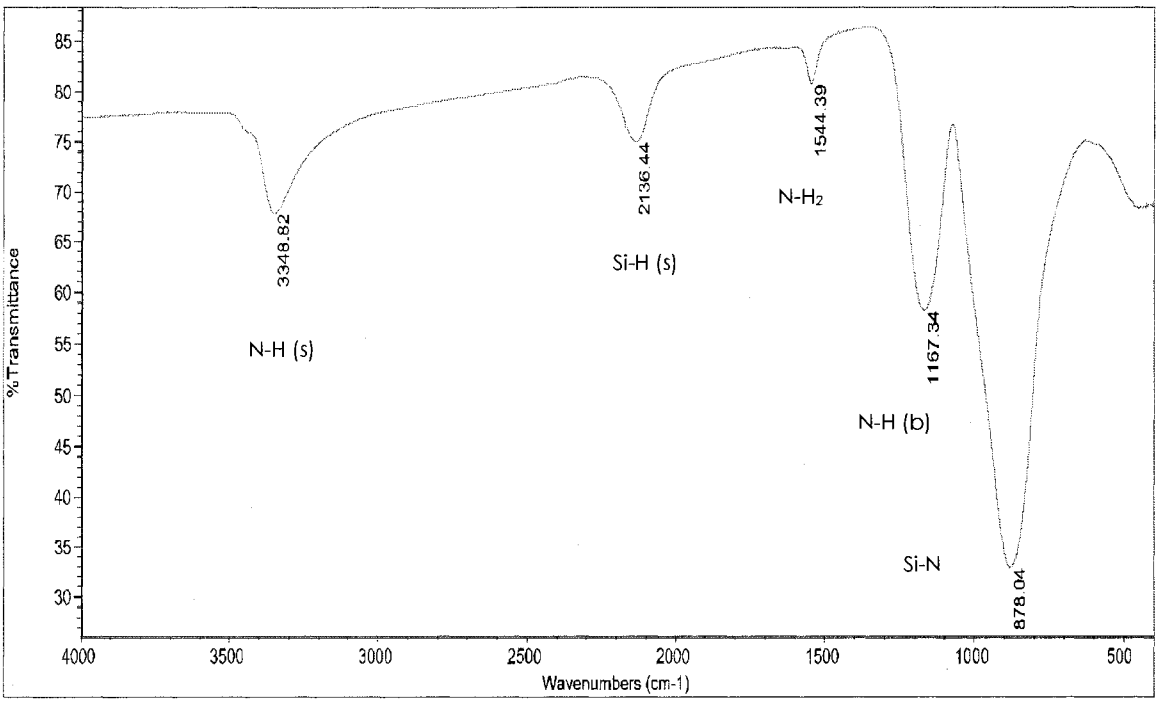

Figure 75. FTIR Spectrum of Film at H2=0 sccm in Film Composition with Varied H_2 Flow Rate with SiH_4/Ar and Ammonia.

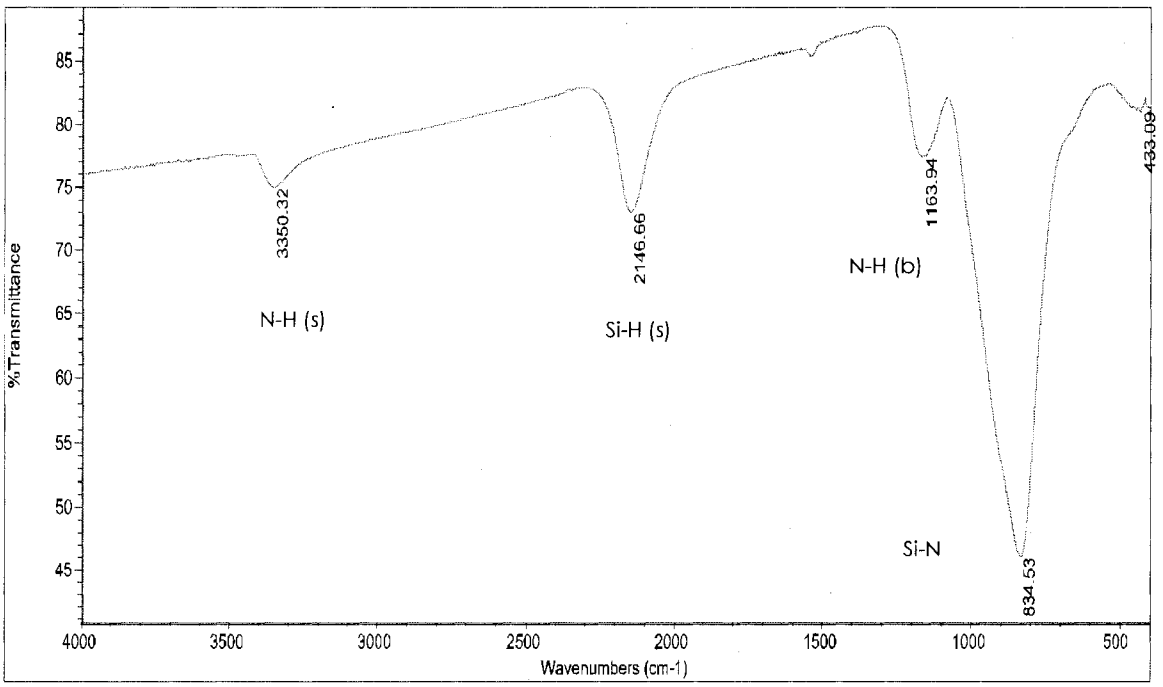

Figure 76. FTIR Spectrum of Film at H2=15 sccm in Film Composition with Varied H_2 Flow Rate with SiH_4/Ar and Ammonia.

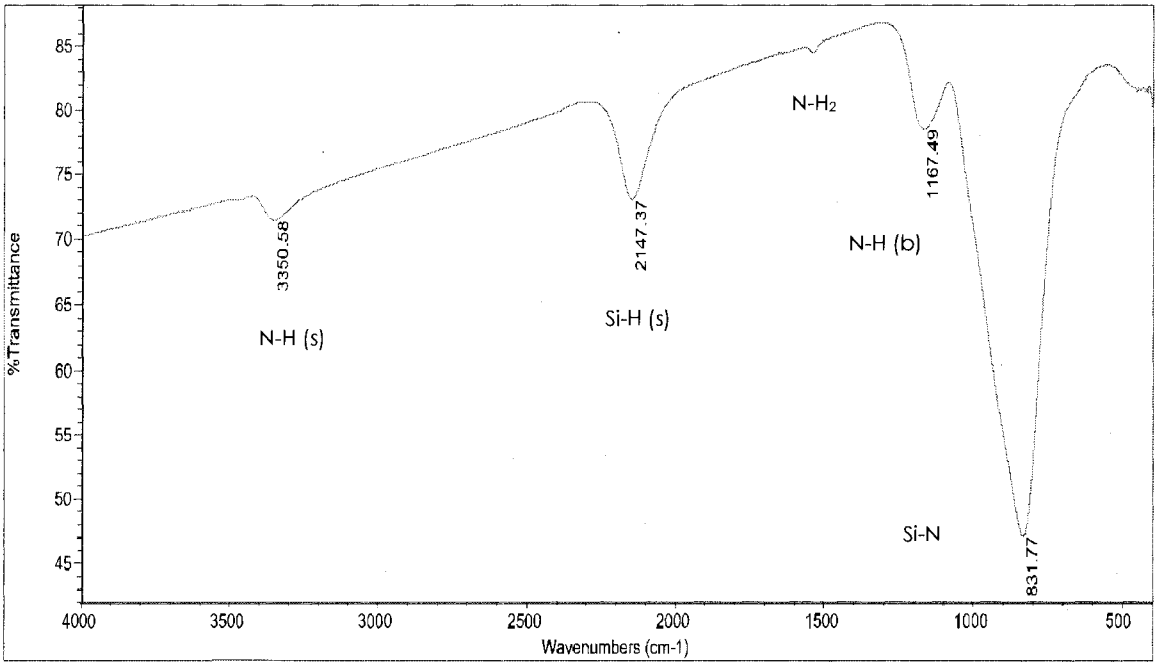

Figure 77. FTIR Spectrum of Film at H2=50 sccm in Film Composition with Varied H_2 Flow Rate with SiH_4/Ar and Ammonia.

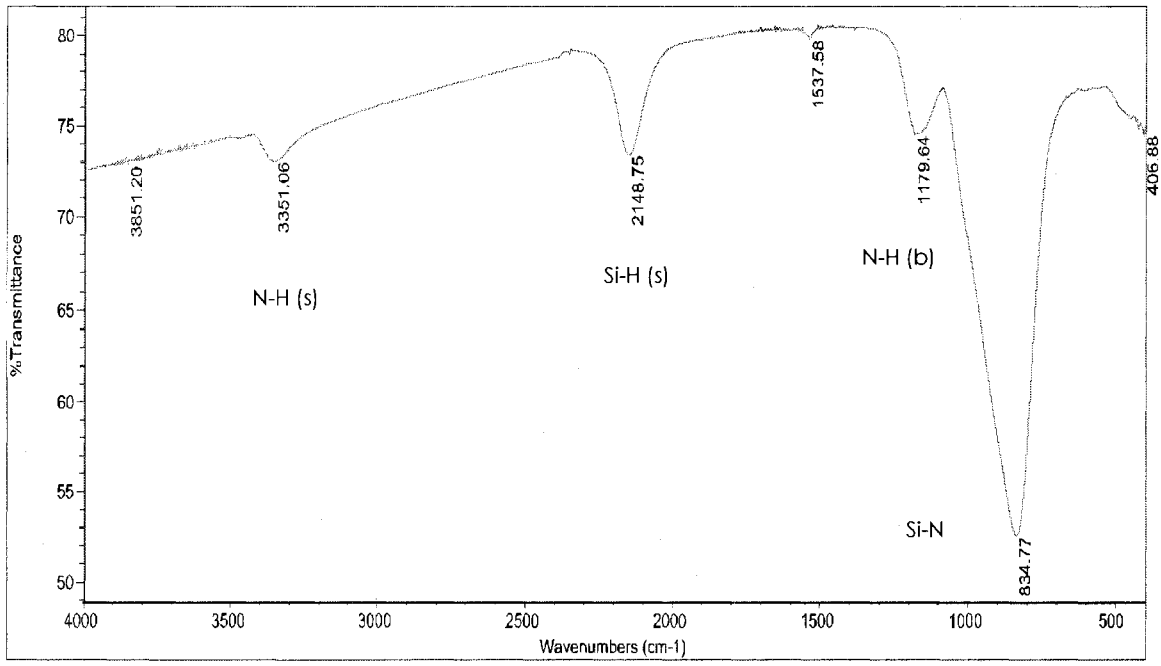

Figure 78. FTIR Spectrum of Film at H2=100 sccm in Film Composition with Varied H_2 Flow Rate with SiH_4/Ar and Ammonia.

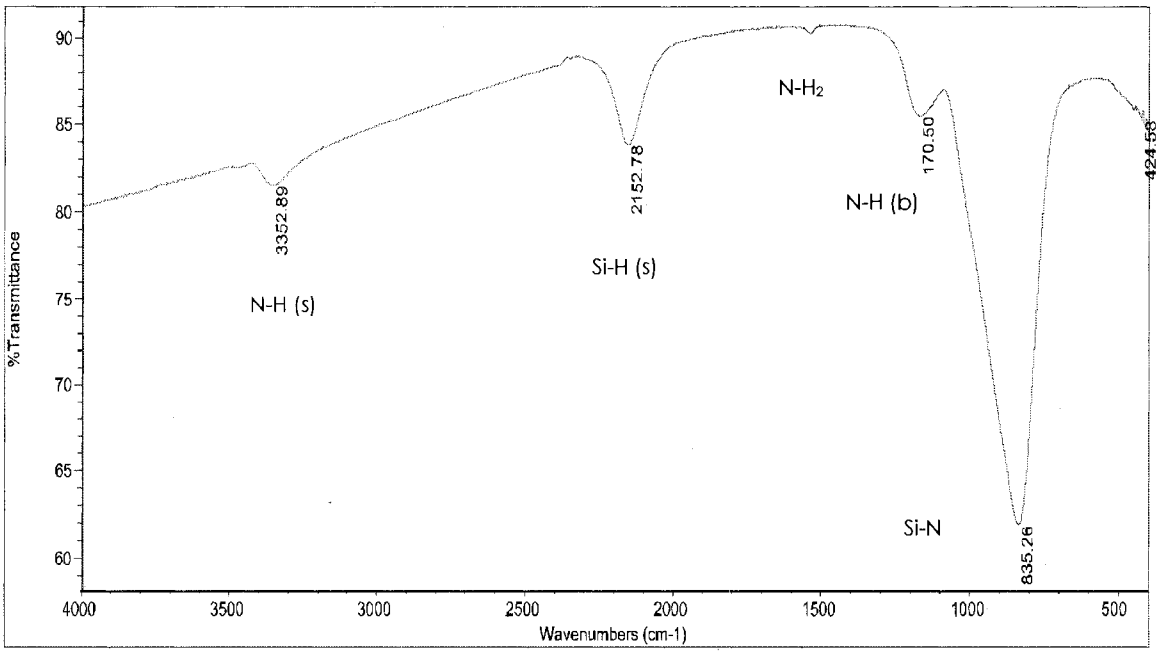

Figure 79. FTIR Spectrum of Film at H2=200 sccm in Film Composition with Varied H_2 Flow Rate with SiH_4/Ar and Ammonia.

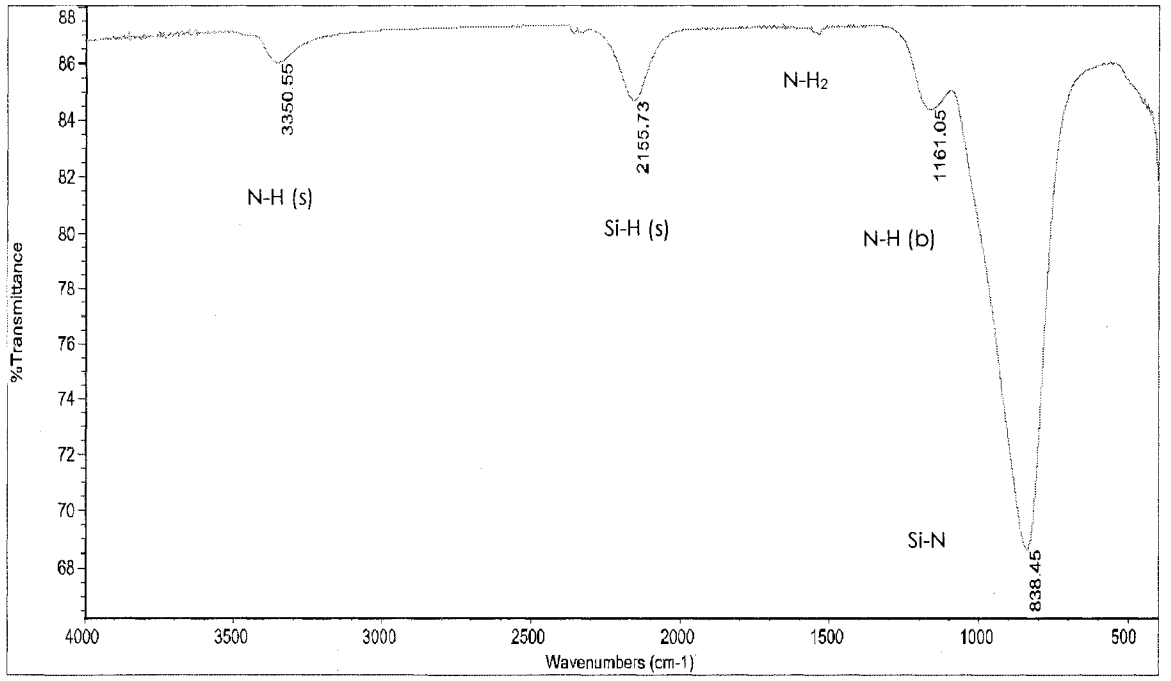

Figure 80. FTIR Spectrum of Film at H2=300 sccm in Film Composition with Varied H_2 Flow Rate with SiH_4/Ar and Ammonia.

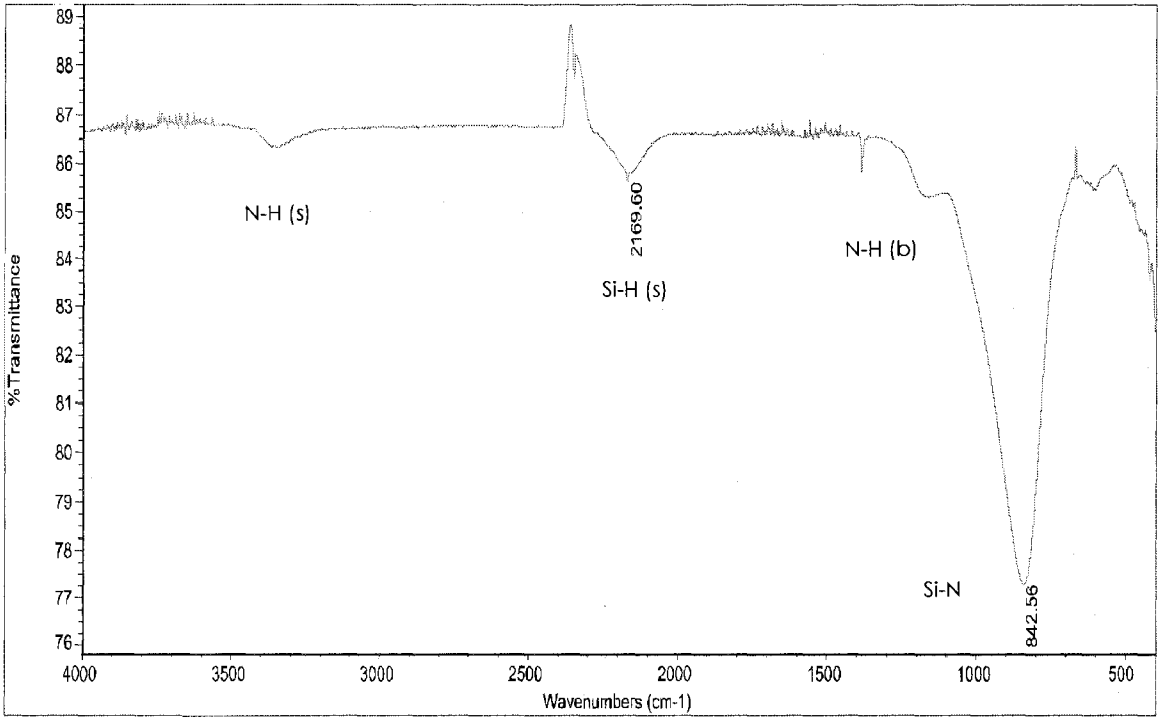

Figure 81. FTIR Spectrum of Film at H2=700 sccm in Film Composition with Varied H_2 Flow Rate with SiH_4/Ar and Ammonia.

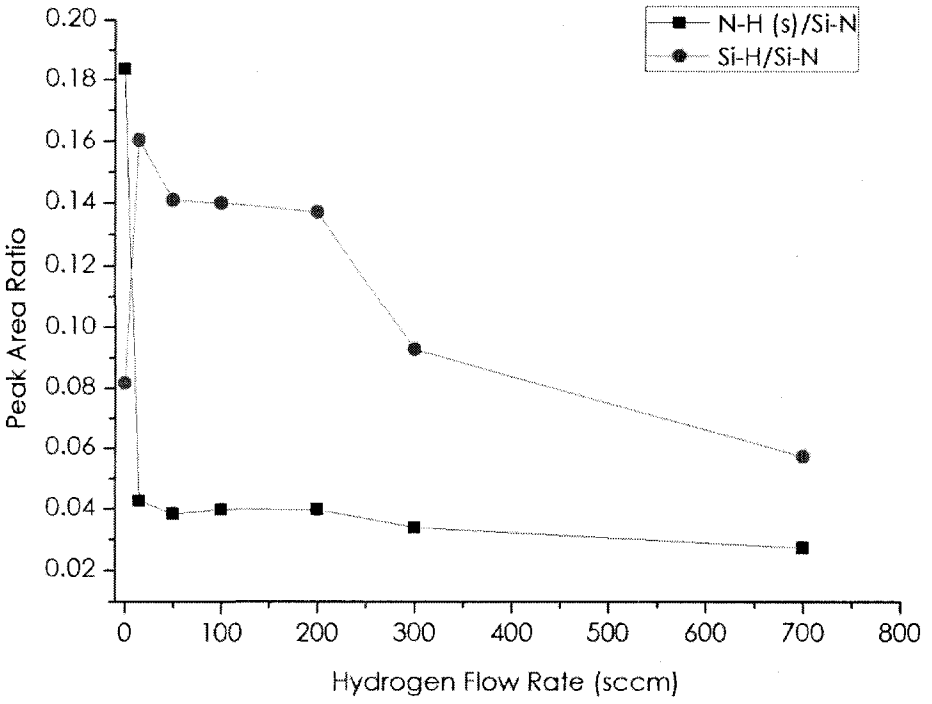

Figure 82. FTIR Spectrum Peak Ratio of Film Composition as a Function of Varied H_2 Flow Rate with SiH_4/Ar and Ammonia.

Figure 82 shows the peak ratios of N-H (s)/Si-N and Si-H/Si-N in this series. In this Figure, there was a very big change at 0 sccm hydrogen flow. That confirmed that the hydrogen flow rate was very essential to the properties of deposited silicon nitride. Besides this critical point, both N-H/Si-N and Si-H/Si-N ratios decreased when the hydrogen flow rate increased.

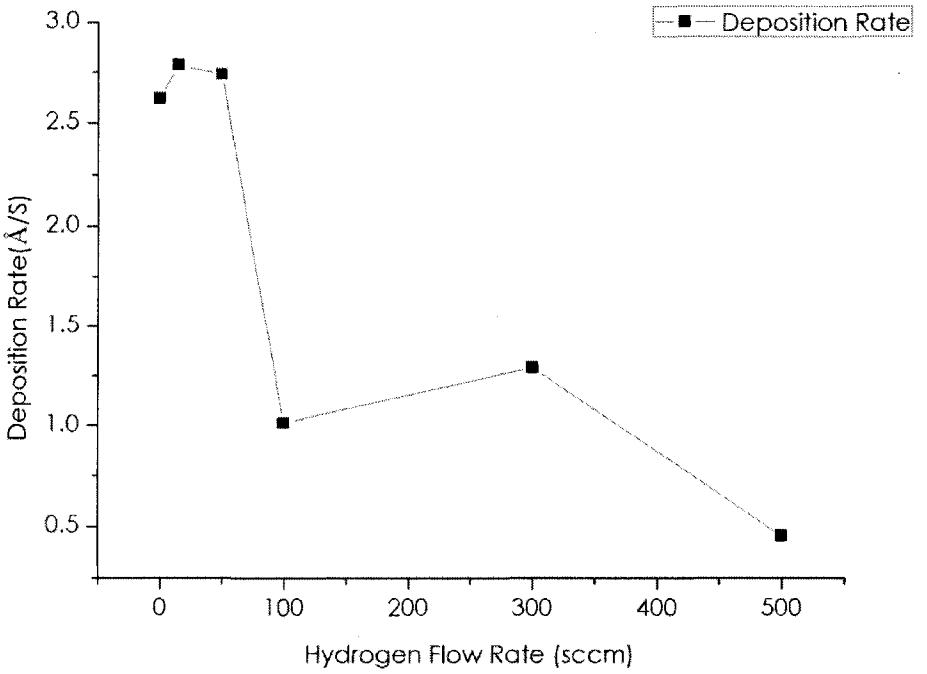

Figure 83. Deposition Rate of Film Composition as a Function of Varied H_2 Flow Rate with SiH_4/Ar And Ammonia.

The silicon nitride film deposition rate was remarkable in this series. When a few sccm of hydrogen was introduced into the plasma, the deposition rate reached nearly 2.7 Å/s. It is almost 2 times the deposition rate of conditions in Table 3. However, the deposition rates dropped very quickly after the amount of hydrogen was increased.

What's more, the uniformity of silicon nitride film was dramatically enhanced in this series compared to other series; especially when a few sccm hydrogen flow rate was introduced, the film was very uniform.

However, the uniformity of silicon nitride film deposited without introducing hydrogen was very poor. There were "worm like" spots all

cross the silicon wafers, and that was due to the very filamentary plasma when no hydrogen gas flow was established. These filaments stayed at the same positions for a long time and made these "worm like" films.

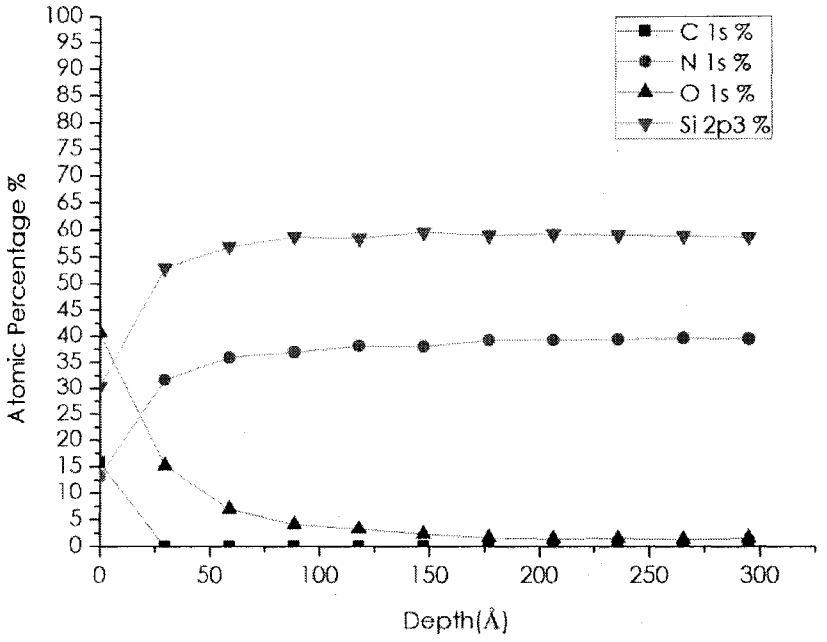

Figure 84. XPS Depth Profile of Film in Film Composition as a Function of Varied H_2 Flow Rate with SiH_4/Ar and Ammonia with H_2=0 Sccm.

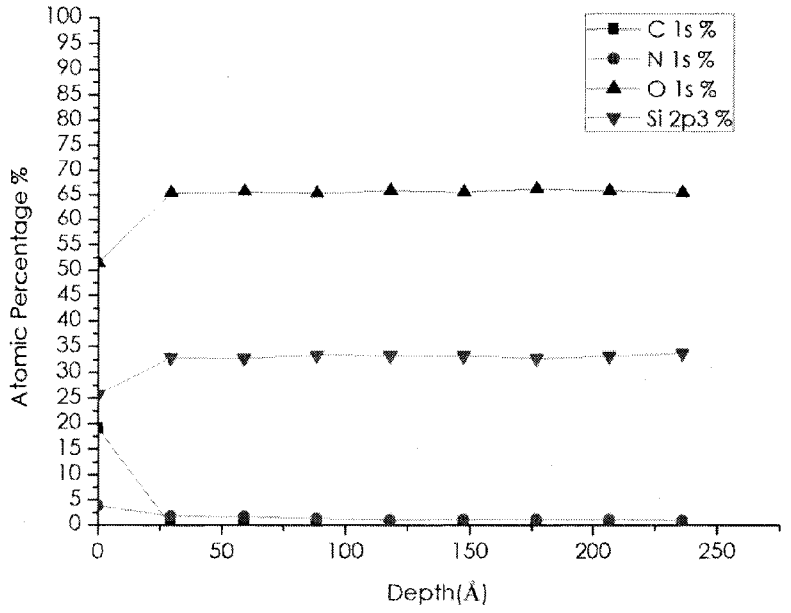

Figure 85. XPS Depth Profile of Film in Film Composition as a Function of Varied H_2 Flow Rate with SiH_4/Ar and Ammonia with H_2=15 Sccm.

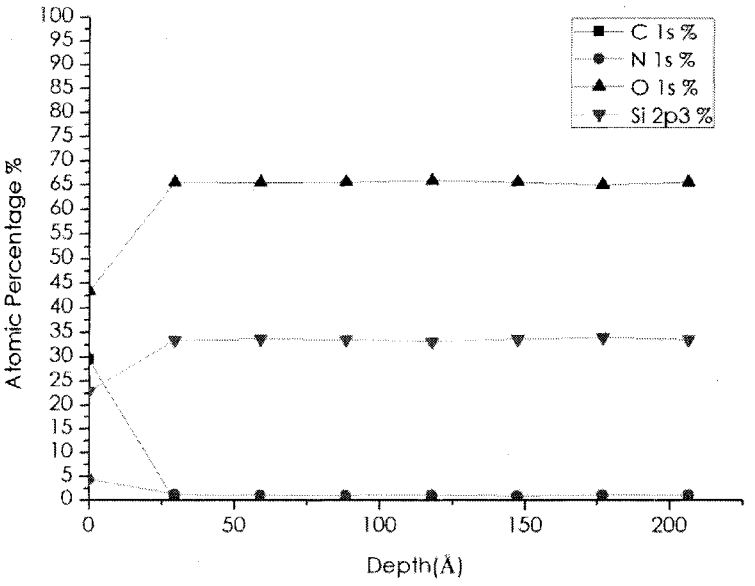

Figure 86. XPS Depth Profile of Film in Film Composition as a Function of Varied H_2 Flow Rate with SiH_4/Ar and Ammonia with H_2=50 Sccm.

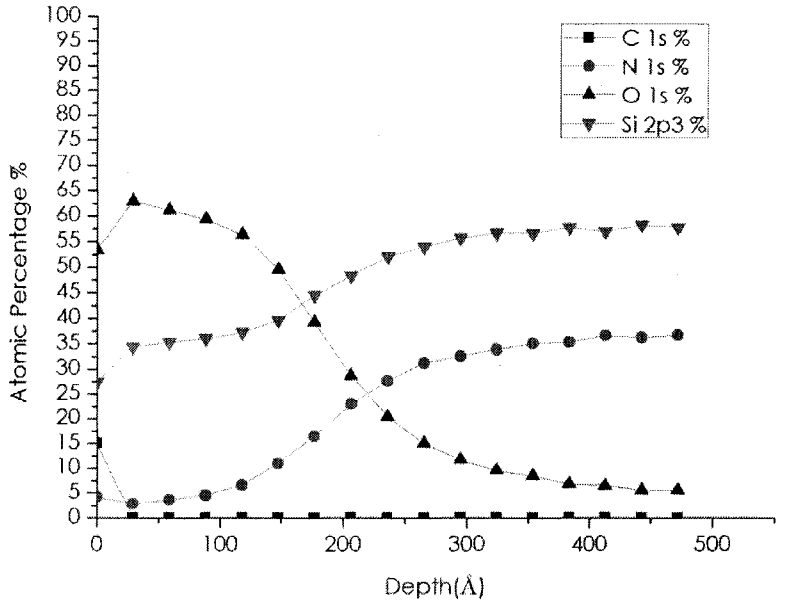

Figure 87. XPS Depth Profile of Film in Film Composition as a Function of Varied H_2 Flow Rate with SiH_4/Ar and Ammonia with H_2=100 Sccm.

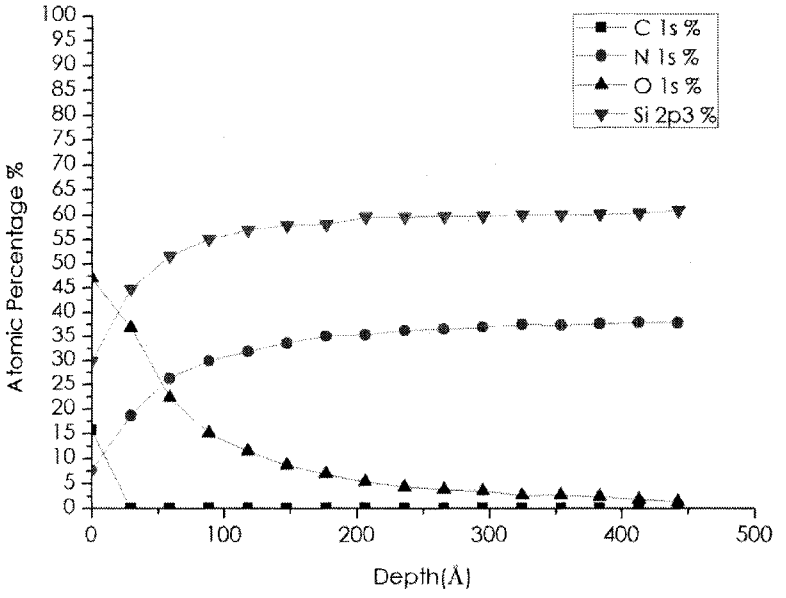

Figure 88. XPS Depth Profile of Film in Film Composition as a Function of Varied H_2 Flow Rate with SiH_4/Ar and Ammonia with H_2=200 Sccm.

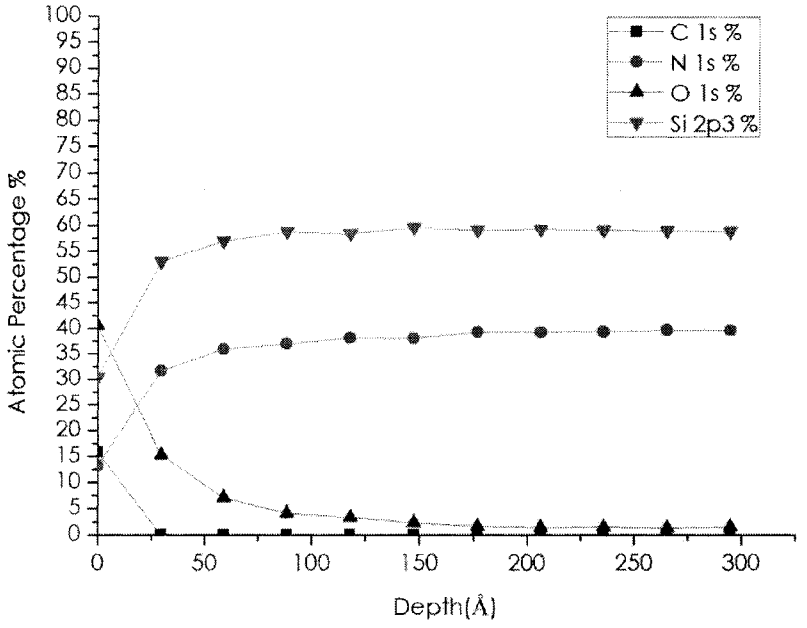

Figure 89. XPS Depth Profile of Film in Film Composition as a Function of Varied H_2 Flow Rate with SiH_4/Ar and Ammonia with H_2=300 Sccm.

Figure 84 shows that at zero sccm of H_2 flow, the film composition became approximately constant after 50Å at Si 60% N 37% O 3%. The ratio of Si: N is 1.62. Before 50Å, the oxygen decreased from 42% to 3%. The silicon increased from 30% to 60% and nitrogen decreased from 12% to 37%.

Figure 85 shows that at 15 sccm of H_2 flow, the film composition became approximately constant after 25Å at Si 37% N 3% O 60%. The ratio of Si: N is 12.3 and ratio of Si: O is 1.62. Before 25Å, the oxygen increased from 51% to 60%. The silicon increased from 25% to 37% and nitrogen decreased from 20% to 3%. This film is mostly silicon dioxide.

Figure 86 shows that at 50 sccm of H_2 flow, the film composition became approximately constant after 25Å at Si 34% N 1% O 65%. The ratio of Si: N is 34 and ratio of Si: O is 1.92. Before 25Å, the oxygen increased from 42% to 65%. The silicon increased from 22% to 34% and nitrogen decreased from 30% to 1%. This film is mostly silicon dioxide.

Figure 87 shows that at 100 sccm of H_2 flow, the film composition became approximately constant after 275Å at Si 57% N 35% O 8%. The ratio of Si: N is 1.63. Before 275Å, the oxygen increased from 63% to 8%. The silicon increased from 27% to 57% and nitrogen increased from 5% to 35%. The film composition before 275Å is mainly O 65% Si 32% N 3%. The ratio of Si: O is 1:2 and this is mainly silicon dioxide at this range.

Figure 88 shows that at 200 sccm of H_2 flow, the film composition became approximately constant after 100Å at Si 57% N 35% O 8%. The ratio of Si: N is 1.63. Before 100Å, the oxygen decreased from 47% to 8%. The silicon increased from 27% to 57% and nitrogen increased from 7% to 35%.

Figure 89 shows that at 300 sccm of H_2 flow, the film composition became approximately constant after 75Å at Si 58% N 39% O 3%. The ratio of Si: N is 1.48. Before 75Å, the oxygen decreased from 40% to 3%. The silicon increased from 30% to 58% and nitrogen increased from 15% to 39%.

H_2 Flow Rate (sccm)	Constant Film Composition	Onset of Constant Composition
0	Si 60% N 37% O 3%	50 Å
15	Si 37% N 3% O 60%	25 Å
50	Si 34% N 1% O 65%	25 Å
100	Si 57% N 35% O 8%	275 Å
200	Si 57% N 35% O 8%	100Å
300	Si 58% N 39% O 3%	75Å

Table 15. Constant Film Composition and Onset of Constant Composition of Films in Film Composition as a Function of Varied H_2 Flow Rate with SiH_4/Ar and Ammonia.

These XPS depth profile Figures show very interesting results. A decent silicon nitride film was produced with no hydrogen flow rate introduced. However, with a bit of hydrogen flow rate, mostly silicon oxide films were produced. This phenomenon was observed at both 15 sccm and 50 sccm hydrogen flow rates. There was almost 65 % of oxygen atomic percentage within deposited films. In addition, after the amount of hydrogen flow rate was increased, the silicon nitride film content increased.

Film Composition with Constant H_2 flow rate with varied silane/Argon and ammonia ratios

In previous experiments where H_2 flow was varied, very uniform of film was observed with little amounts of hydrogen flow such as 15 sccm. It led to another series that varied the ratio of silane to ammonia while kept the hydrogen flow rate was constant at 15 sccm. This silane was balanced with argon. Other conditions were those of Table 3.

$SilH_4$:NH_3	SiH_4 (sccm)	Ar (sccm)	NH_3 (sccm)	H_2 (sccm)
1:5	179	716	90	15
1:10	164	656	165	15
1:50	98.4	393.6	492	15
1:75	78.8	315.2	591	15
1:100	65.6	262.4	657	15

Table 16. Parameters of Precursors in Constant H_2 Flow Rate with Varied Silane/Argon and Ammonia Ratios Series.

The plasma was expected very homogeneous when the ratio of SiH_4: NH_3 was 1:5. After the ratio lowered to 1:10, the color of the plasma became a bit greener due to more ammonia molecules inside the plasma. With further decreased SiH_4: NH_3 ratio, the plasma became less homogeneous and the current needed to ignite the plasma was higher.

Also, more input current was needed in order to maintain the plasma. At SiH_4: NH_3 ratio 1:75, the current needed to ignite the plasma reached about 12A, and the plasma was even less homogeneous. After the SiH_4: NH_3 ratio reached 1:100, no plasma was obtained.

From this series, we could conclude that the ammonia gas in the plasma played a significant role in the homogeneity of the plasma. Less ammonia leads to better homogeneity.

In addition, the uniformity of the film decreased when the amount of ammonia gas increased. This was probably due to the homogeneity of the plasma.

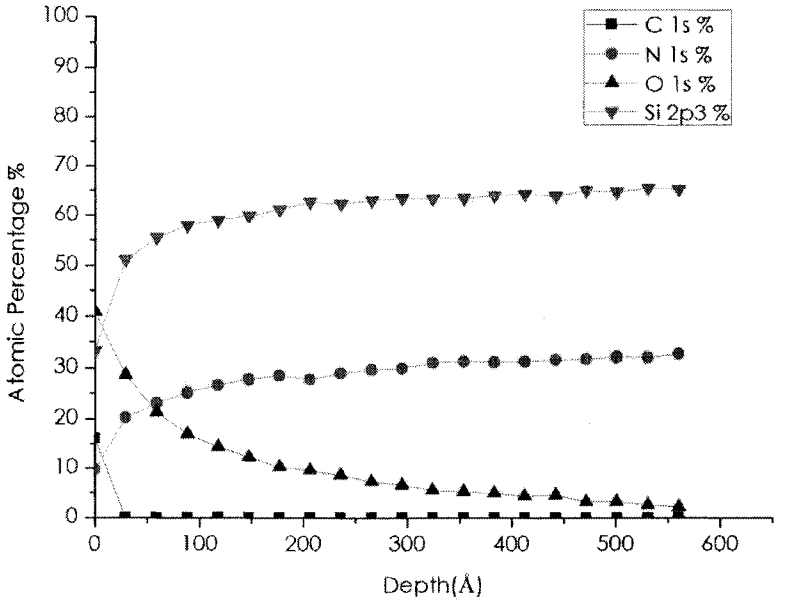

Figure 90. XPS Depth Profile of Film with Ratio of Silane to Ammonia=1:5.

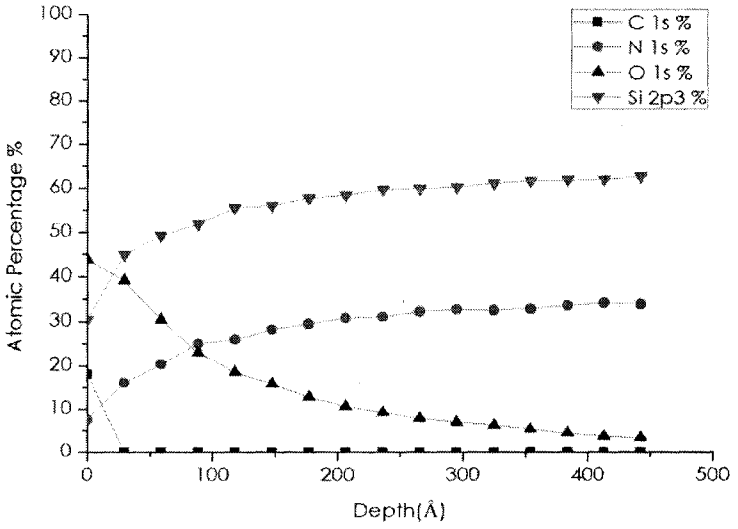

Figure 91. XPS Depth Profile of Film with Ratio of Silane to Ammonia=1:10.

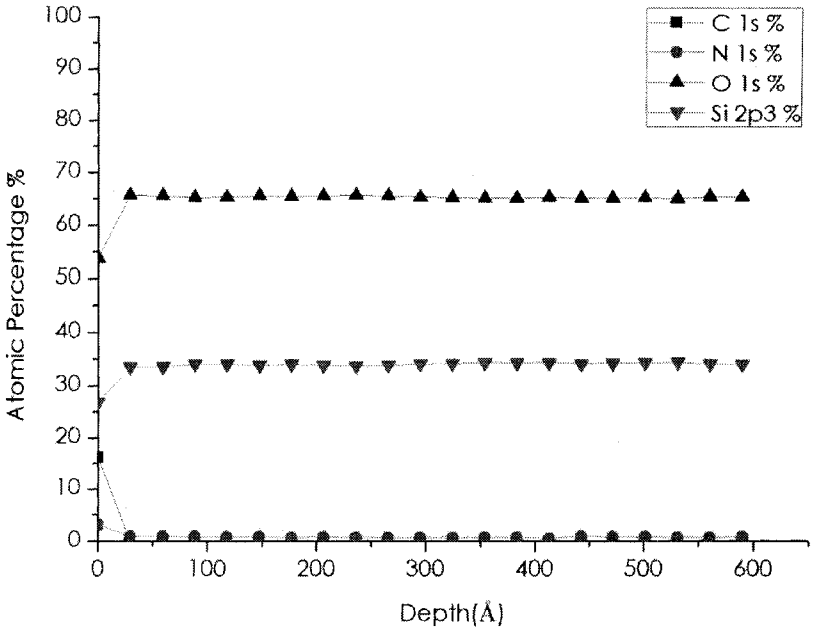

Figure 92. XPS Depth Profile Film with Ratio of Silane to Ammonia=1:50.

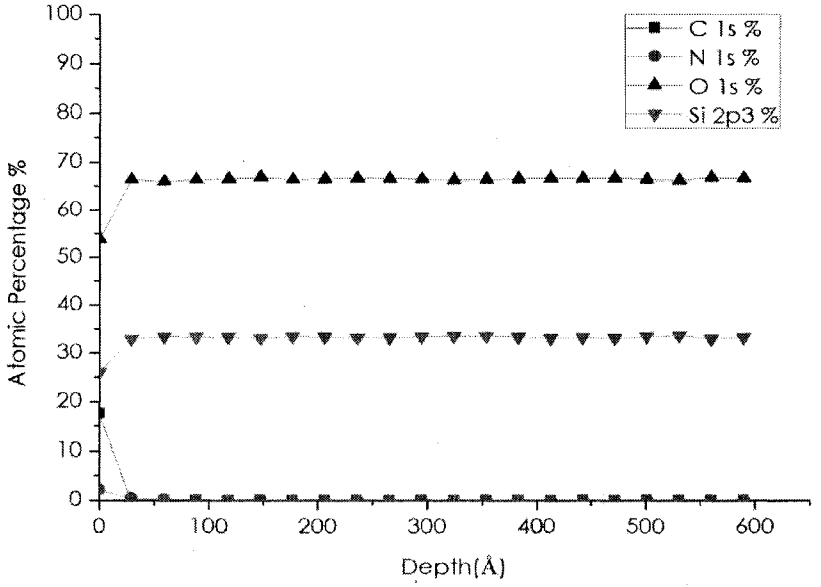

Figure 93. XPS Depth Profile Film with Ratio of Silane to Ammonia=1:75.

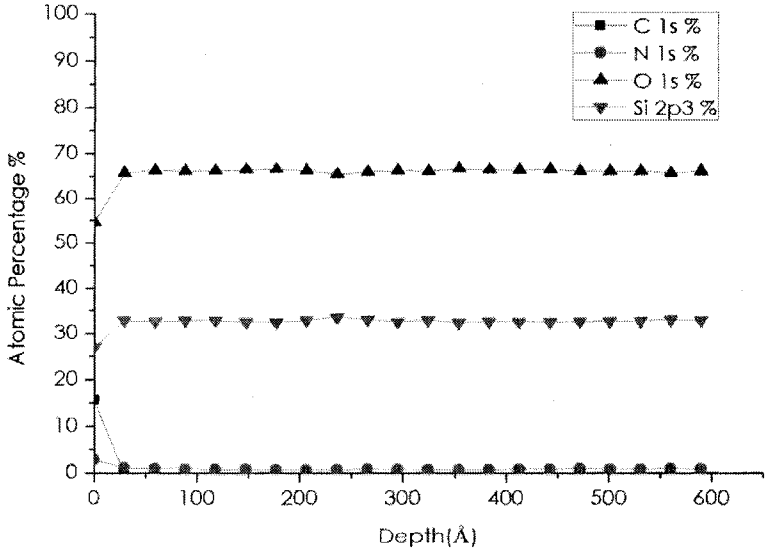

Figure 94. XPS Depth Profile with Ratio of Silane to Ammonia=1:100.

Figure 90 shows that at ratio of SiH_4:NH_3 equals 1:5; the film composition became approximately constant after 200Å at Si 63% N 29% O 8%. The ratio of Si: N is 2.17. Before 200Å, oxygen decreases from 40% to 8%. Silicon increases from 32% to 63% and nitrogen increases from 10% to 29%.

Figure 91 shows that at ratio of SiH_4:NH_3 equals 1:10; the film composition became approximately constant after 250Å at Si 60% N33% O 7%. The ratio of Si: N is 1.81. Before 250Å, oxygen decreases from 45% to 7%. Silicon increases from 31% to 60% and nitrogen increases from 7% to 33%.

Figure 92 shows that at ratio of SiH_4:NH_3 equals 1:50; the film composition became approximately constant after 25Å at Si 34% N1% O 66%. The ratio of Si: N is 34 and ratio of Si: O is 1:2. This film is silicon dioxide. Before 25Å, oxygen increases from 54% to 66%. Silicon increases from 35% to 34% and nitrogen increases from 7% to 1%.

Figure 93 shows that at ratio of SiH_4:NH_3 equals 1:75; the film composition became approximately constant after 25Å at Si 34% N1% O 66%. The ratio of Si: N is 34 and ratio of Si: O is 1:2. This film is silicon dioxide. Before 25Å, oxygen increases from 54% to 66%. Silicon increases from 27% to 34% and nitrogen increases from 19% to 1%.

Figure 94 shows that at ratio of SiH_4:NH_3 equals 1:100; the film composition became approximately constant after 25Å at Si 34% N1% O

66%. The ratio of Si: N is 34 and ratio of Si: O is 1:2. This film is silicon dioxide. Before 25Å, oxygen increases from 55% to 66%. Silicon increases from 27% to 34% and nitrogen increases from 18% to 1%.

Ratio of SiH_4:NH_3	Constant Film Composition	Onset of Constant Composition
1:5	Si 63% N 29% O 8%	200 Å
1:10	Si 60% N33% O 7%	250 Å
1:50	Si 34% N1% O 66%	25Å
1:75	Si 34% N1% O 66%	25Å
1:100	Si 34% N1% O 66%	25Å

Table 17. Constant Film Composition and Onset of Constant Composition of Films in Constant H_2 Flow Rate with Varied Silane/Argon and Ammonia Ratios Series.

As the ratio of silane to ammonia decreased, silicon nitride content in the film decreased. After the ratio of silane to ammonia achieved 1:50, the oxygen atomic percentage in the film was 66%. This is mainly silicon dioxide and there was little silicon nitride in the films.

CHAPTER V

Conclusion

In this project, silicon nitride films were successfully produced using dielectric barrier discharge at near atmospheric pressure under various conditions. Very homogeneous plasmas can be obtained by adjusting different parameters, and this is greatly related to the film uniformity. However, the uniformity of the film is still an issue due the limitation of chamber design as well as the gas delivery configuration inside the chamber.

Film Composition as a Function of Temperature

The temperature played very important role in the homogeneity of the plasma.

The plasma was very filamentary with substrate temperature 100 °C and occasionally with some electric arcs in the plasma. The plasma became more homogeneous at 200 °C and no evident filament was observed. There were no significant different between substrate temperature of 300 °C and 350 °C, and plasma were very homogeneous and even more homogeneous than 200 °C.

Based on the XPS depth profiles; Si: N decreases with increasing temperature. The oxygen atomic percentage decreases at higher temperature. The silicon and nitrogen atomic percentage increases at

higher temperature. The onset of constant composition starts at less shallow in film at higher temperature.

The incorporated hydrogen content dropped with increased substrate temperature as shown by FTIR spectrum peak area ratios. Moreover, the incorporated oxygen content in the deposited film decreased with increased substrate temperature as shown by decrease of the silicon nitride peak wavenumber from 835.5 cm-1 to 830.8 cm-1.

Films thicknesses were measured and the deposition rate decreased a bit with increased substrate temperature. They deposition rate at 200 °C was 1.6 Å/s while the deposition rate lowered to 1.3 Å/s at 350 °C. This is probably due to a denser film at higher temperature. The SEM surface pictures suggest that with higher substrate temperature, the films became denser.

The Si-N bonding was stronger at higher substrate temperature. At 200 °C, the Si-N bonding was very weak and more than 60% of oxygen atomic percentage was observed in the film. With higher substrate temperature, the Si-N bonding was stronger.

It is noticeable that 300 °C or higher substrate temperature is needed in order to produce better silicon nitride film.

Film Composition as a Function of Residence Time

There is no significant difference of plasma behavior in this series. As shown by XPS depth profiles, the ratio of Si: N only decreased a little with

increased total flow rate. The onset depth of constant composition stayed the same at 300Å. The FTIR spectrums show that the hydrogen content in the deposited films were almost the same. However, the resident time of gas flow does have a slight effect to deposition rate of silicon nitride films. The deposition rate had a slight increase with decreased residence time. However, the difference was not significant. It only has 0.1 Å/s variations.

Film Composition as a Function of Argon Dilution

The argon flow rate played an important role to the plasma. Plasma became more homogenous with increased argon flow rate. It was very filamentary when no argon flow was introduced and led to very poor uniformity of silicon nitride film. On the other hand, the Si-N bonding of deposited silicon nitride films became weaker when argon flow rates increased. At 1000 sccm of argon flow rate, the deposited silicon nitride film suggests very poor Si-N bonding as shown by XPS data and the atomic percentage of oxygen reached about 50%. The silicon atomic percentage decreased with increased argon flow rate as shown by XPS data. The XPS data also shows the onset of constant composition slightly increased with increased argon flow rate except for zero argon flow rate. It was noticeable that the deposited rate was the highest in this series when no argon flow was introduced. The deposition rate became slightly decline after more argon flow was introduced to the chamber. It is probably due to the density of excited radicals reduced by more large

argon flow rate which contributed to the slight decline of the deposition rate.

Film Composition as a Function of Stoichiometry

In this series, the plasma was significantly affected by the amount of ammonia precursors in the chamber. The plasma went weaker and more unstable when more amount of ammonia gas was introduced into the chamber. However, the plasma was very stable and homogenous at the 50 sccm of ammonia gas flow rate. But at 600 sccm of ammonia gas flow rate, the plasma was very unstable and very filamentary. The Si-N bonding of deposited silicon nitride films became weaker with increased ammonia amount in the plasma according to XPS data. At 600 sccm of ammonia gas flow, XPS data shows the incorporated oxygen was as high as 60% which indicates very poor Si-N bonding of silicon nitride. The onset of constant composition increased with increased ammonia flow rate from 45 Å to 750 Å. The best film in this series is the one with 100 sccm of ammonia flow rate. On the other side, larger deposition rate was gained with the increased ammonia gas flow rate. At 50 sccm of ammonia gas, the deposition rate of silicon nitride film was only about 0.5 Å/s showing sufficient ammonia free radicals for the deposition. The deposition rate got to 1.9 Å/s at the 600 sccm flow rate of ammonia. From this point of view, excess ammonia gas amount does play the considerable part in the deposition rate. What's more, the ammonia amount had vital effect to

the incorporated hydrogen content within silicon nitride film. The FTIR Si-N and N-H peak area ratios showed the hydrogen content decreased with increased ammonia gas flow rate.

Film Composition as a Function of Frequency

This was a very tough series in this project since several problems were met.

First, the deposited silicon nitride films showed a void area in the center of silicon wafer about ½ size of the whole wafer. No such phenomena were observed at lower frequency at 1K Hz, or 800 Hz. However, these phenomena continued with higher frequencies at 2K Hz, 3K Hz and so on. It was known due to leakage current in conductive wires and it was solved by enhanced insulation of wires. The reason of the leakage current is that due to poor insulation layer of the wires connected to the electrodes, part of current was lost to ground and cannot provide efficient current to the void area. The current for plasma goes through the surface of round electrodes, and if no current flow can reach at the center of the electrodes, the "void' will be left in wafers. The issue was solved by inserting wires into Teflon tube and using Teflon tape to wrap more than 20 layers onto the Teflon tube.

Second, another issue happened in this series. After the deposition, there was a thin layer of black power attached to deposited silicon nitride films. This also happened at higher frequency. No such issue occurred at

lower frequencies. This issue was also learned and solved by noticing the conductive carbon paint on the surface of the silicon wafer which was used to creative step for measuring film thickness. The reason why this phenomenon appeared was still not known. Probably due to the higher frequency, high vibration rates of excited radicals strike to the conductive carbon paint and caused it dissolved.

However, in this series, the plasma became more homogeneous with increased applied frequency. On the other hand, applied frequency cannot exceed 4K Hz due to limitation of equipment as well as power amplifier. So, at frequency of 3.5 KHz, plasma was very unstable and very filamentary. The best suitable range for this configuration of equipment was from 0.5 K Hz to 3 K Hz.

The deposition rate was greatly influenced by the applied frequency. The deposition rate was only about 1.3 Å/s at 1 KHz, however, nearly about 2.3 Å/s deposition rate was achieved at 3 K Hz frequency. It was a linear correlation with applied frequency. Unfortunately, the uniformity of the deposited films deteriorated with increased applied frequency.

XPS data shows that at 1.5K Hz, there is large amount of oxygen in the film, it reaches 26% which indicates poor Si-N bonding at 1.5K Hz. However, the oxygen atomic percentage is very small in 1K Hz and 3K Hz suggesting good Si-N bonding.

No significant effect to incorporated hydrogen content in the film was observed through the analysis of FTIR spectrums. The ratios of Si-H/Si-N and N-H/Si-N stayed almost the same in this series.

Film Composition as a Function of Nitrogen Precursor

Nitrogen gas was another widely used precursor to produce silicon nitride films in the industry. In this series, very homogenous plasma was obtained with ratio of silane/hydrogen to nitrogen equals 1:1. But plasma became unstable and very weak at 800 sccm gas flow rate of nitrogen.

There was a significant difference using nitrogen as the precursor compared with using of ammonia gas as precursors. As shown by FTIR spectrums, no N-H (s) and N-H (b) characteristic peaks were observed using nitrogen. However, these two peaks were very strong using ammonia as precursor. This explained that most hydrogen content incorporated in films was greatly contributed to the ammonia gas. Silicon nitride films with low hydrogen content could be produced by using nitrogen as the precursors.

The deposition rate of silicon nitride film was very much reduced using nitrogen gas as precursors. The maximum deposition rate achieved in this series was only about 0.85 Å/s which was very low compared with other series using ammonia as the precursor and it could reach about 2 Å/s.

As shown by XPS, the deposited silicon nitride films all showed very strong Si-N bonding and oxygen content was a few atomic percentages. The silicon atomic percentage in this series was very large and it reached about 80%. But the nitrogen was only about 11% which suggested only much nitrogen was broken due to stronger N-N bonding.

Film Composition as a Function of Varied Hydrogen flow rate with silane/argon and ammonia

Hydrogen flow does play an important role for dielectric barrier discharge plasma. Plasma was very homogenous when hydrogen gas was introduced and it became more homogeneous with increased hydrogen gas flow rate.

It was noticed that the deposited films showed very unique NH_2 scissor bending peak as shown by FTIR spectrum at zero sccm of hydrogen gas flow rate. This suggests that the NH_2 peak was mainly from the ammonia gas precursor. Nevertheless, this NH_2 peak became weaker after hydrogen gas flow increased and almost disappeared at hydrogen gas flow of 700 sccm. The FTIR spectrum also shows that ratios of N-H (s)/Si-N and Si-H/Si-N deceased with increased hydrogen flow rate except for 0 sccm of hydrogen flow rate.

Deposition rates in this series showed very interesting phenomena. The deposition rate was very high and reached about 2.7 Å/s with little amount of hydrogen gas flow at 15 sccm or 50 sccm. But the deposition rate dropped dramatically when hydrogen gas flow rate was increased beyond 100 sccm. It was only about 1 Å/s or even less. Thus, in order to produce high deposition rate of silicon nitride film, small amount of hydrogen gas flow rate was desirable.

It was also noticed that the uniformity of deposited silicon nitride film was better at low flow rate of hydrogen. The reason for this phenomenon was still not known. Unfortunately, the deposited films at very small amount of hydrogen all showed very poor Si-N bonding as shown by XPS data. As large as 65% of oxygen atomic percentage was observed at 15 sccm and 50 sccm. These films are mostly silicon dioxide.

REFERENCE

1. James L. Williams, "*The Coming Energy Crisis*", Oil & Gas Journal for publication February 3, 2003
2. Michael Graham Richard, "*Incredible Growth for Solar Power Industry*", Business & Politics, 04. 4.07
3. Solarbuzz, LLC, "Solar Electricity Prices-http://www.solarbuzz.com/", November, 2007
4. Energy Information Administration, "Electric power monthly-http://www.eia.doe.gov", Oct 10, 2007
5. Paul D. Maycock and Edward N. Stirewalt, *PHOTOVOLTAICS sunlight to Electricity in One Step,* Brick House Publishing Co. Andover, MA. 1981
6. Green, Martin A. *Solar Cells Operating Principles. Technology, and Systems Applications,* Prentice Hall, Englewood Cliffs, NJ 1982
7. Kasap, Safa O., *Principles of Electronic materials and Devices second edition,* McGraw-Hill, NY, NY. 2002
8. Hong, J., W.M.M. Kessels, W. J. Soppe, A. W. Weeber, W. M. Arnoldbik, and M. C. M. van de Sanden, "*Influence of the high-temperature firing step on high-rate plasma deposited silicon nitride films used as bulk passivating antireflection coatings on silicon solar cells*", J. Vac. Sci. Technol. B 21(5), Sep/Oct 2003, pp 2123-2132

9. Poortmans, J. Nijs, and R. Mertens, "*Principles of Cell Design*", Clean Electricity From Photovoltaics, Ed. Mary D. Archer and Robert Hill. Imperial College Press, London, UK, 2001, pp 91-140
10. M. Vetter, "*Surface passivation of silicon by rf magnetron-sputtered silicon nitride films*", Thin Solid Films 337 (1999) 118-122
11. J.P.Luongo, "*IR Study of Amorphous Silicon Nitride Films*", Bell Laboratories, 600 Mountain Avenue, Murray Hill, New Jersey 07974
12. Yota, J. Janani, M., "*Comparison between HDP CVD and PECVD silicon nitride for advancedinterconnect applications*",Interconnect Technology Conference, 2000. Proceedings of the IEEE 2000 International, page 76-78, 2000
13. Henning Nagel *, Armin G. Aberle, Rudolf Hezel, *Optimised "antireflection coatings for planar silicon solar cells using remote PECVD silicon nitride and porous silicon dioxide"*, Progress in Photovoltaics: Research and Applications,Volume 7, Issue 4 , Pages 245 - 260, 1 Aug 1999
14. T.N.Wittberg, J.R. Hoenigman, "*AES and XPS of silicon nitride films of varing refractive indices*", Journal of Vacuum Science and Technology -- March 1978 -- Volume 15, Issue 2, pp. 348-352
15. R.E.I. Schropp,R.H. Franken, "*Hot Wire CVDnext term for thin film triple junction cells and for ultrafast deposition of the SiN passivation layer on polycrystalline Si solar cells* ", Thin Solid Films, 2007

16. Alfred Grill, "*Cold plasma in Materials Fabrication*", IBM Research Division, T.J. Watson Research Center, Yorktown Heights, NY

17. Y. Kuo [IBM TJ Watson], "*PECVD Nitride as a Gate Dielectric for Amorphous Silicon Thin Film Transistor*", J. Electrochem. Soc. 142 186 (1995)

18. J. Osenbach and S. Voris [Bell Labs, "*Sodium diffusion in plasma-deposited amorphous oxygen-doped silicon nitride (a-SiON:H) films*", J. Appl. Phys. 63 4494 (1988)

19. D. Smith [Xerox PARC], "*Controlling the plasma chemistry of silicon nitride and oxide deposition from silane*" J. Vac. Sci. Technol, A11 1843 (1993)

20. Bogaerts, Annemie, Erik Neyts, Renaat Gijbels, Joost van der Mullen, "*Gas Discharge Plasmas and Their Applications*", Spectrochimica ACT A Part B, 57(2002) 609-658

21. Xueji Xu, "*Dielectric barrier discharge — properties and applications*", Thin Solid Films Volume 390, Issues 1-2, 30 June 2001, Pages 237-242

22. G.J. Pietsch, "*Peculiarities of Dielectric Barrier Discharges*", Contributions to Plasma Physics, Volume 41, Issue 6 , Pages 620 – 628

23. Annemie Bogaertsa, "Gas discharge plasmas and their applications", Spectrochimica Acta Part B 57 (2002) 609–658

24. A. Chirokov, A. Gutsol, "*Atmospheric pressure plasma of dielectric barrier discharges*", Pure Appl. Chem., Vol. 77, No. 2, pp. 487–495, 2005

25. W. J. M. Samaranayake, Y. Miyahara, "*Ozone Production Using Pulsed Dielectric Barrier Discharge in Oxygen*", IEEE Transactions on Dielectrics and Electrical Insulation Vol. 7"o. 6, December 2000

26. U. Kogelschatz, B. Eliasson, W. Egli, "*from ozone generators to flat television screens: history and future potential of dielectric-barrier discharges*", Pure Appl. Chem. 71 (1999) 1819–1828

27. Guido Vezzù, Reto Merz, "*Evolution of Industrial Ozone Generation", Degremont Technologies*", Stettbachstrasse , 8600 Dübendorf, Switzerland

28. Ian W. Boyd, J.Y. Zhang, "*New large area ultraviolet lamp sources and their applications*", Nuclear Instruments and Methods in Physics Research B 12 1 (1997) 349-356

29. Osram Planon (2004), "Planon Dielectric Barrier Excimer Lamp", http://www.lamptech.co.uk/Spec%20Sheets/Osram%20Planon.htm

30. O. Goossensa, "*Application of atmospheric pressure dielectric barrier discharges in deposition, cleaning and activation*", Surface and Coatings Technology 142-144(2001)474-481

31. N. Danish, "*Surface modification of Angora rabbit fibers using dielectric barrier discharge*", Applied Surface Science 253 (2007) 6915–6921

32. G. Borcia, "*Surface treatment of natural and synthetic textiles using a dielectric barrier discharge*", Surface & Coatings Technology 201 (2006) 3074–3081

33. N. De Geyter, "*Treatment of polymer films with a dielectric barrier discharge in air, helium and argon at medium pressure*", Surface and Coatings Technology Volume 201, Issues 16-17, 21 May 2007, Pages 7066-7075

34. Takezoe N., " *SIO2 thin film preparation using dielectric barrier discharge-driven excimer lamps*", Applied Surface Science, Volume 138, Number 1, January 1999 , pp. 340-343(4)

35. S. Martin, F. Massines, "*Atmospheric pressure PE-CVD of silicon based coatings using a glow dielectric barrier discharge*", Surface and Coatings Technology, Volumes 177-178, 30 January 2004, Pages 693-698

36. S. Martin, F. Massines*, N. Gherardi, C. Jimenez, "*Atmospheric pressure PE-CVD of silicon based coatings using a glow dielectric barrier*

37. Y.H. Liu, J. Li, "*Properties and deposition processes of a-C: H films from CH4/Ar dielectric barrier discharge plasmas*", Surface and

Coatings Technology, Volume 200, Issues 20-21, 22 May 2006, Pages 5819-5822

38. Wikimedia Foundation, Inc., *"Potassium bromide"*, http://en.wikipedia.org/wiki/Potassium_bromide

39. SEMATECH, *Silane Safety Improvement Project S71 Final Report*, June 30, 1994

40. Krivda, A, *"Dielectric spectroscopy of fiber-reinforced epoxy materials"*, Solid Dielectrics, 2004, Page(s): 474 - 477 Vol.1, July 2004

41. R.K. Pandey, L.S. Patil, *"Growth and characterization of silicon nitride films for optoelectronics applications"*, Optical Materials 27 (2004) 139–146

42. M. Lattemann, *"Investigation and characterisation of silicon nitride and silicon carbide thin films"*, Surface and Coatings Technology 174 –175 (2003) 365–369

43. D.V.Tsu, G.Lucovsky, *"Local atomic structure in thin film of silicon nitride and silicon diimide produced by remote plasma-enhanced chemical-vapor deposition"*, Physical Review B, Volume 33, Number 10, 15 May 1986

44. B S Sahu, A Kapoor, *"Study of thermally grown and photo-CVD deposited silicon oxide–silicon nitride stack layers"*, Semicond. Sci. Technol. 18 (2003) 670–675

45. Sergei E. Alexandrov, "*Remote Plasma-enhanced CVDof Silicon Nitride Films: Effects of DilutingNitrogen with Argon. Part I: Effect onNitrogen Plasma Parameters Studied by Emission Spectroscopy*", ADVANCED MATERIALS FOR OPTICS AND ELECTRONICS, VOL. 8: 13-22 (1998)

46. Sergei E. Alexandrov, "*Remote Plasma-enhanced CVDof Silicon Nitride Films: Effects of Diluting Nitrogenwith Argon.*

47. *Part II: Effect ofNitrogen Plasma Parameters on Layer Characteristics*", ADVANCED MATERIALS FOR OPTICS AND ELECTRONICS, VOL. 8: 23±29 (1998)

48. P. S. Nayara, "Refractive index control of silicon nitride films prepared by radio-frequency reactive sputtering", Journal of Vacuum Science & Technology A: Vacuum, Surfaces, and Films, November 2002, Volume 20, Issue 6, pp. 2137-2139

49. Barrett, P.J., "*Double-plasma instability near ion plasma frequency*", 1989 IEEE International Conference on, Volume, Issue , 22-24 May 1989 Page(s):72

50. O. V. Balachova, M. A. R. Alves, "*Influence of the substrate thickness and radio frequency on the deposition rate of amorphous hydrogenated carbon a-C:H films*", Journal of Applied Physics -- March 15, 1999 -- Volume 85, Issue 6, pp. 3345-3347

51. Zhao, A.; Bulger, J.M., "*Improvement of film uniformity stability of PECVD silicon nitride deposition process by addition of fluorine removal to the plasma clean sequence*", Advanced Semiconductor Manufacturing Conference and Workshop, 2005 IEEE/SEMI Volume , Issue , 11-12 April 2005 Page(s):143 – 148

52. Tonegawa, Akira, "*Observation of Plasma Recombination with the Negative Ions in Detached Plasma*", 42nd Annual Meeting of the APS Division of Plasma Physics combined with the 10th International Congress on Plasma Physics October 23 - 27, 2000

53. Calcote. Hartwell F, Felder. William, "*Process and apparatus for the flame preparation of ceramic powders*", United States Patent 4891339, 01/02/1990